CONTROL BASED POWER QUALITY IMPROVEMENT IN MICROGRIDS

By

Chowdhury Andalib-Bin-Karim

A thesis submitted to the

School of Graduate Studies

in partial fulfillment of the requirements for the degree of

Master of Engineering

Faculty of Engineering and Applied Science

Memorial University of Newfoundland

May, 2018

St. John's Newfoundland and Labrador Canada

Abstract

Power quality issue is one of the major concerns in modern power grids due to higher penetration of renewable energy based distributed generation sources. In this thesis, advanced inverter control mechanisms are developed to improve power quality, specifically 1) voltage and frequency regulation, and 2) reactive power sharing in microgrids. The virtual synchronous generator (VSG) control method is employed as a primary control mechanism in this research work, and several advanced control techniques are developed. The incorporation of a fuzzy secondary controller (FSC) and an adaptive virtual impedance loop in the VSG control scheme is proposed to improve voltage and frequency regulation, and reactive power sharing performance in microgrids, respectively. A systematic approach of the control system design is presented in details, and dynamic models of test microgrids are developed using MATLAB/Simulink. Extensive simulation studies are carried out to verify the effectiveness of the proposed methods through case and sensitivity studies. It is found that the proposed methods offer significantly improved performance compared to existing techniques, and dynamic characteristics of microgrids under disturbance conditions are enhanced. Furthermore, in this study a new data driven analytics approach is proposed for determination of Q-V (reactive power-voltage) curve of grid connected wind farms, which can provide useful information for voltage control action.

Acknowledgement

The author would like to convey his earnest gratitude and respect to his supervisor Dr. Xiaodong Liang for her encouragement, guidance and constructive discussions throughout the development of this thesis.

The author deeply appreciates the financial support of Research and Development Corporation (RDC) of Newfoundland and Labrador (recently RDC was combined with another organization to form InnovateNL) and the Graduate Fellowship from Memorial University. Without their support, this work could not have been possible.

The author would like to thank Memorial University of Newfoundland for all kind of support to this research.

Finally, the author would like to give special thanks to his family members, for their unconditional love and mental supports.

Table of Contents

List of Tables

List of Figures

List of Abbreviations

DG	Distributed generation
VSG	Virtual synchronous generator
POI	Point of interconnection
VSI	Voltage source inverters
SG	Synchronous generator
VSM	Virtual synchronous machine
PLL	Phase-locked loop
PCC	Point of common coupling
PV	Photovoltaic
THD	Total harmonic distortion
PWM	Pulse width modulation
VSC	Voltage source converter
APF	Active power filters
SVPWM	Space Vector Pulse Width Modulation
RMS	Root mean square
RMSE	Root mean squared error
SSE	Sum of squares due to error
SSR	Sum of squares of the regression
SST	Total sum of squares
FSC	Fuzzy secondary controller
LPF	Low pass filter

List of symbols

I_{ref_f}	Fundamental current reference
I_{ref_h}	Harmonic current reference
$H_D(s)$	Harmonic detector
V_{ref_f}	Fundamental voltage reference signal
V_{PCC_h}	Harmonic component of the PCC voltage
Q_{ref}	Reactive power reference
Q	Reactive power
V	Voltage
P	Active power
f	Frequency
J	Rotor inertia
ω_g	Angular frequency of the utility grid
D	Damping coefficient
T_m	Mechanical torque
T_e	Electrical torque
R_s	Stator resistance
L_s	Stator inductance
δ	Phase angle
Zv	Virtual impedance
Rv	Virtual resistance
Lv	Virtual inductor
ω_C	cut-off frequency of LPF

X_v virtual reactance

Note: Other symbols not mentioned are defined in the text.

Chapter 1

Introduction

1.1 Background

Conventional fossil fuels based power generation leads to serious environmental pollution problems. With the degradation of fossil fuel reserves all over the world and the increase of public awareness about environmental impacts of traditional energy sources, renewable energy resources such as solar, wind, and biomass, based distributed generation (DG) is being considered as an attractive way of satisfying future energy demand. Therefore, in a modern power grid, DG units are implemented rapidly and new technologies are being developed to integrate these renewable energy sources without disturbing satisfactory operation of the main power grid [1], [2].

Renewable energy resources are intermittent in nature due to meteorological factors, therefore integration of renewable power generation directly into utility power grids in a conventional way can lead to deterioration of system stability and reliability [1], [3]. The microgrid concept has emerged as a prospective solution to problems associated with integration of renewable DG units. A microgrid is defined as a local distribution system, which integrates distributed generators, energy storage, dispersed loads, data acquisition, communication, protection and supervisory control devices etc. It can operate being connected or disconnected from the main power grid in an organized and coordinated fashion [1], [3], [4], [5].

The microgrid allows increased penetration of small capacity DG units, where the generation is mainly localized at the customer end. It increases power generation capacity, reduces the pressure on existing transmission system as some loads are supplied by the microgrid, and load congestion

of the conventional utility grid is also reduced [2], [3]. Moreover, a microgrid offers increased flexibility in control to satisfy power quality requirements and improve reliability of the system [3]. Recent development of power electronic devices and advancement of control technologies facilitate integration of renewable based DG units to great extent.

As a microgrid can be operated in an islanded mode or a grid-connected mode, it is susceptible to power quality problems originated from both DG and power grid sides. For example, non-controllable variability of renewable energy resources and grid side disturbances such as voltage sags can lead to voltage and frequency fluctuations in microgrids. The high speed switching of the interfacing inverters can result in harmonic distortions [6], [7]. Moreover, the presence of nonlinear, unbalanced and reactive local loads can also cause deterioration of power quality [5]. The microgrid can be operated in islanded mode when the power quality is not satisfactory due to grid side disturbances. However, according to modern grid codes, the distributed generation such as solar photovoltaic (PV) power plants must have the capability to ride through specific disturbances without disconnecting from power grids [7]. Therefore, switching to an islanded mode as soon as the grid side disturbance occurs is not always an option. Poor power quality can cause economic losses as the price of electricity is directly related to the quality of power delivered by DGs and microgrids; additional loss and overheating occurs in different power equipment; and stability of the system is also influenced by poor power quality at the grid interconnection point [5]. Therefore, it is very important to ensure that good power quality is achieved by DG units.

When a microgrid is tied to a utility grid, any internal disturbance in the microgrid may cause power quality problems in the utility grid and vice versa. A power quality conditioner needs to be used between the microgrid and the utility grid to ensure that disturbances occurred in one side does not initiate power quality problems in other side [4]. Different passive power quality

conditioners such as, harmonic filters and capacitors are conventionally used, which have lower cost and are easy to maintain. The active power quality conditioners such as active power filter (APF), dynamic voltage regulator (DVR), power factor correction (PFC), unified power quality conditioner (UPQC) etc. can offer superior performance and better flexibility compared to passive devices, and thus, being utilized more recently [5]. However, no matter what mechanism is used, an additional device for power conditioning will involve installation and maintenance cost, and also require additional spaces. Such devices may also adversely impact stability and reliability of microgrids [5]. One preferable solution to this problem is to utilize advanced control technologies through the inverter, which is interfaced between a DG unit and a microgrid, to provide power quality improvement. The DG units are often integrated to microgrids with the aid of a power electronic converter, if a proper control strategy is employed for the interfacing converter, it can take part in ancillary services such as voltage and frequency regulation, harmonic suppression etc. and can effectively compensate power quality problems, along with maintaining its primary role which is control of power injection [4]. This is possible because there is a similarity exists between the DC/AC stage of the power quality conditioner and the grid interfacing inverter [5]. Thus, the inverter can be utilized effectively to provide multiple functionalities through employing proper control strategies, and the necessity of using additional device for power quality conditioning can be avoided. For instance, droop control is widely used as the interfacing inverter control mechanism in microgrids to coordinate operation of each DG unit connected to the system.

From operation point of view, a microgrid can be operated in either an islanded mode or a grid connected mode. In the grid-connected mode, voltage and frequency are determined by the power grid [2], an important control objective in this mode is proper regulation of active and reactive power, which has substantial influence on power quality [6]. In the islanded mode, voltage and

frequency need to be established by the microgrid itself, and accurate power sharing also needs to be ensured. The power sharing feature is necessary to ensure that, each DG unit supplies power according to its rated capacity and available generation [3]. Additionally, good power quality needs to be maintained, for instance DG units must be controlled in an appropriate way to ensure adequate active and reactive power supply at the wake of power quality events such as, voltage sags, frequency variations etc. [2]. The desired operation is that each DG unit must have the ability to operate effectively without requiring any communication or measurement from external sources. In this thesis, the main focus is to develop advanced inverter control mechanisms for power quality enhancement for DG units in microgrids.

1.2 Thesis Outline

This thesis consists of five manuscripts, four of them are published and one will be submitted for publication.

Chapter 1

In Chapter 1, the importance of the research topic is introduced, the objectives of the research work are described.

Chapter 2

In Chapter 2, a literature review for the research work is conducted. The main objective of this thesis is to develop advanced inverter control mechanisms for power quality improvement in microgrids. Virtual synchronous generator (VSG) control and virtual impedance method are two major control approaches investigated in this thesis. The VSG control is also compared with conventional droop control. In this chapter, firstly, literatures are reviewed to introduce virtual

synchronous generator (VSG) method, which has been used recently to reduce voltage and frequency fluctuations in microgrids by controlling grid interfacing inverters. The fundamental principle of VSG control and the state of art VSG control techniques in renewable energy grid integration are explained. Secondly, literature review on advanced control methods specially, virtual impedance control for reactive power sharing and harmonic mitigation are presented. This portion of the review facilitates better understanding of reactive power sharing, harmonic generation sources, and state of art techniques to mitigate harmonics in renewable energy based DG system. This chapter consists of two manuscripts; which are published in the proceedings of the following two conferences: 1) *IEEE PES Asia-Pacific Power and Energy Engineering Conference, 2016, Xi'an, China*, 2) *IEEE Industry Application Society Annual Meeting, 2017, Cincinnati, OH, USA.*

Chapter 3

In Chapter 3, a data driven analytics approach is proposed based on the curve fitting procedure to determine the Q-V characteristic curve at the point of interconnection (POI) of large wind farms utilizing measurement data recorded at the POI. In this chapter, different curve fitting models are evaluated and the best fit is determined based on different graphical and numerical evaluation metrics. Case studies are conducted using field measurement data at two grid connected wind farms currently in operation in Newfoundland and Labrador, Canada. The Q-V curve and associated functions developed in this chapter can be readily used for the voltage controllers design in order to reduce voltage fluctuations or for voltage stability evaluation at the POI of a grid-connected wind farm. The research work undertaken in this chapter is consistent with the overall objective of this thesis, as it contributes to the advancement of controller design for power quality

improvement in grid integrated renewable energy system. This chapter has been published in the *IEEE Transactions on Industry Applications, September/October 2017*.

Chapter 4

In Chapter 4, a fuzzy secondary controller based VSG control scheme to improve voltage and frequency regulation and dynamic performance of a microgrid is developed. In this chapter, several case and sensitivity studies are carried out in Matlab/Simulink environment to evaluate the effectiveness and robustness of the proposed method. The performance of proposed control scheme is also compared with that of conventional droop control and conventional VSG control. It is found that the proposed method can effectively regulate voltage and frequency, and shows significantly improved dynamic performance under various disturbance conditions when compared with existing techniques. This chapter has been published in the proceeding of *IEEE Industry Application Society Annual Meeting, 2017, Cincinnati, OH, USA*. A version of this chapter has been published in the *IEEE Transactions on Industry Applications, March/April 2018*.

Chapter 5

In Chapter 5, an adaptive virtual impedance method for improvement of reactive power sharing performance in a Fuzzy secondary controller based VSG controlled microgrid is proposed. Accurate reactive power sharing feature is essential to ensure that each DG unit supplies power according to its rated capacity. In a real system, reactive power sharing among DG units become inaccurate due to feeder impedance mismatch and difference in rated capacity. In this chapter, an innovative approach of implementing adaptive virtual impedance method is proposed to deal with this practical situation. An adaptive virtual impedance loop is incorporated in the VSG control to accurately regulate reactive power supply of DG units under variation of operating points of

microgrids. Several case and sensitivity studies are carried out in Matlab/Simulink environment to evaluate the effectiveness and robustness of the proposed method. A significant improvement in reactive power sharing has been achieved using the proposed method. This chapter is prepared for submission to a Special Issue on Grid-Connected Power Electronics Systems: Stability, Power Quality, and Protection for *IEEE Transactions on Industry Applications.*

Chapter 6

In Chapter 6, the research outcomes are summarized. The potential future work is addressed.

References

[1] E. Planas, A. Gil-de-Muro, J. Andreu, I. Kortabarria, and I. M. Alegría, "General aspects, hierarchical controls and droop methods in microgrids: A review," *Renewable and Sustainable Energy Reviews [Elsevier]*, vol. 17, pp. 147-159, 2013.

[2] P. Basak, S. Chowdhury, S. H. Dey, and S. P. Chowdhury, "A literature review on integration of distributed energy resources in the perspective of control, protection and stability of microgrid," *Renewable and Sustainable Energy Reviews [Elsevier]*, vol. 16, no. 8, pp. 5545-5556, 2012.

[3] T. L. Vandoorn, J. D. M. De Kooning, B. Meersman, and L. Vandevelde, "Review of primary control strategies for islanded microgrids with power-electronic interfaces," *Renewable and Sustainable Energy Reviews [Elsevier]*, vol. 19, pp. 613-628, 2013.

[4] J. M. Guerrero, P. C. Loh, T. Lee, and M. Chandorkar, "Advanced control architectures for intelligent microgrids—Part II: Power quality, energy storage, and AC/DC microgrids," *IEEE Trans. Industrial Electronics*, vol. 60, no. 4, pp. 1263-1270, 2013.

[5] Z. Zeng, H. Yang, R. Zhao, and C. Cheng, "Topologies and control strategies of multi-functional grid-connected inverters for power quality enhancement: A comprehensive review," *Renewable and Sustainable Energy Reviews [Elsevier]*, vol. 24, pp. 223-270, 2013.

[6] W. A. B. Al-Saedi, "Optimal control of power quality in microgrids using particle swarm optimisation," 2013.

[7] X. Liang, "Emerging power quality challenges due to integration of renewable energy sources," *IEEE Trans. Industry Applications*, vol. 53, no. 2, pp. 855-866, 2017.

Chapter 2

Literature Review

In a microgrid comprising DG interfacing inverters, the output voltage amplitude and frequency are mainly determined by the inverter control strategy [1]. Control strategies adopted in a microgrid can be classified into two main types: 1) Central/Master-slave control strategy, 2) peer to peer control strategy [2]. In the master-slave strategy, one DG unit contains the master controller which is responsible for regulation of voltage (V) and frequency (f) through *V/f* control in an islanded mode, while other DG units present in the system contain slave controllers which follow the regulation command received from the master controller through communication infrastructure [1]. In the peer to peer strategy, each DG unit controller can operate independently without requiring any communication from other DG units and can effectively respond to system changes. Moreover, in this strategy, DG units in a microgrid can achieve 'plug and play' feature, which means a new DG unit can be added to the system without requiring to change the control strategy and parameters of existing DG units [1], [2]. In the peer to peer strategy, no communication links among DG units need to be established, which improves the system reliability and reduces costs to great extent. Therefore, the peer to peer strategy is being utilized widely in the microgrid control recently. This strategy is also adopted in this thesis.

When a microgrid is connected to a utility grid through intertie breakers, the system maintains a desired level of voltage and frequency at the point of interconnection. In this situation, no frequency regulation in microgrids is required, and constant power transfer control can be adopted which actually allows control of active and reactive power flow from the utility grid to the microgrid [2], [3]. As a consequence, the microgrid becomes part of the distribution system and

acts as a constant load when viewed from the grid side. When a microgrid is subjected to unintentional islanding and disconnected from the utility grid, the deficiencies in power supply need to be fulfilled by DG units according to load demand [3]. In the peer to peer strategy, droop control is considered to be one of the most effective control approaches which can adjust power output from each DG unit instantly according to droop coefficients and also provides voltage and frequency support to the system [2], [3]. Recently, majority of the research work undertaken to improve voltage and frequency regulation in microgrids mostly involves utilization of droop characteristics of the system [4]. In the conventional droop control, the reactive power and voltage (*Q/V*) droop control is realized for voltage control, where the DG output voltage amplitude reference is produced according to the measured output reactive power, utilizing the existence of linear relationship between the DG output reactive power and the voltage [2], [4]. Similarly, the frequency control is realized by the active power and frequency (*P/f*) droop control. In a highly resistive microgrid, where strong linkage exists between the DG output active power and the voltage, the active power and voltage (*P/V*) droop control can be considered for voltage regulation purpose [4].

In [5], [6], a droop controller is utilized to regulate voltage and frequency in an islanded microgrid with parallel connected DG units, and a real power and reactive power (*PQ*) controller is adopted for controlling power supply to the grid in the grid connected operation. Using such an approach, where different sets of controllers are employed in different microgrid operation modes, fast switching between controllers is required when the mode transition is detected, thus the microgrid dynamic performance becomes highly dependent on the accuracy of islanding detection and switching schemes [7]. To eliminate the necessity of islanding detection scheme in a microgrid operation, a unified control strategy is proposed in [8] which is suitable for operating a microgrid

in both modes. Using this approach, the active part of the controller regulates power flow during the grid connected operation, while in an islanded mode, active compensators becomes saturated and the controller enables power sharing between DG units according to droop characteristics. A similar unified control approach is adopted in [9] for a solar PV microgrid operation, where proportional–integral (PI) regulators are incorporated in active and reactive power loop of the droop controller, which remains unsaturated during grid connected operation allowing voltage source inverters (VSIs) to supply power according to power set command, it becomes saturated in an islanded mode to follow typical power sharing and voltage, frequency regulation characteristics of droop control mechanism. The effectiveness of conventional *P/f* droop controller to regulate active power flow in grid connected operation is confirmed in [10], however a limitation is found to be imposed by droop coefficients on the dynamic performance of the controller. The performance of droop controller in grid connected microgrid operation is also studied in [11], where an impact of the grid fluctuation on the accuracy of power control is reported. To eliminate such impacts, a feedforward control for grid frequency and voltage magnitude is proposed. In [12], the limitation of conventional droop controller to share power accurately in a microgrid containing parallel connected DG units with unequal network impedances is reported and an active power-reactive power-frequency-derivative (PQFD) droop control is proposed to reduce the error in power sharing.

With the inclusion of large number of DG units, the total system inertia becomes less compared to the conventional synchronous generator (SG) based system. Droop controller is unable to provide inertia support in such systems and cannot contribute in primary frequency control during disturbance conditions. To overcome this limitation and enhance the power system stability, the VSG control strategy, also known as virtual synchronous machine (VSM), was proposed in

renewable energy integration. In this thesis, VSG control is adopted as a primary control strategy in microgrids and several enhancement is proposed to improve certain power quality features. In this chapter, the literature review is mainly focused on VSG control technique and its application in renewable energy integration. Moreover, some literatures are reviewed which discuss advanced control approaches to mitigate harmonics generated by renewable energy sources, which is also an important power quality concern in modern power grids.

Virtual Synchronous Machine Method in Renewable Energy Integration

Xiaodong Liang, *Senior Member, IEEE* and Chowdhury Andalib-Bin-Karim, *Student Member, IEEE.*

Faculty of Engineering and Applied Science, Memorial University of Newfoundland, St. John's, Newfoundland, Canada.

A version of this work has been published in the proceeding of *IEEE PES Asia-Pacific Power and Energy Engineering Conference, 2016, Xi'an, China*. The paper was written by Dr. Xiaodong Liang, and the co-author Chowdhury Andalib-Bin-Karim participated in preparing this paper. Mr. Karim conducted some related literature survey to support the paper writing. Dr. Liang provided continuous technical guidance and necessary instructions during the literature review process. In this chapter, the manuscript is presented with altered figure numbers, table numbers, section numbers and reference formats in order to match the thesis formatting guidelines set out by Memorial University of Newfoundland.

Abstract- The virtual synchronous machine (VSM) method is a power electronics based approach which was first introduced by Beck and Hesse in 2007 for renewable energy integration modeling. This method controls grid-connected renewable energy sources as electromechanical synchronous machines, which makes renewable energy sources behave as conventional power generation stations if viewed from the power grid. During the last decade, some developments have been made to operate power electronic converters as VSMs, which offers a promising way to design advanced control systems for renewable energy integration. Most publications on this topic actually occurred within the past two years. As an emerging new method with huge potential, the VSM method has been used to reduce voltage and frequency fluctuation of renewable energy sources, and improve power system stability. In this paper, a comprehensive literature review is conducted for the VSM method. The principle, and current state of the art control techniques to implement this method are reviewed and summarized in the paper.

Keywords- Power Electronic Converters, Power Quality, Renewable Energy Integration, Virtual Synchronous Machine Method.

2.1 Introduction

The power grid infrastructure experiences a gradual transition from centralized traditional power generation to decentralized distributed power generation due to increasing penetration of renewable energy sources [13, 14]. The distributed renewable energy is usually connected to consumer sites as close as possible, which offers advantages such as reduced losses in transmission system, and local reactive power support [14]. Most renewable energy sources are interfaced with power grid through a power electronic converter/inverter. Digitally controlled power electric converters/inverters offer optimal utilization of renewable energy resources, and they can further enhance power system controllability due to their fast dynamic response capability to system disturbances, voltage and frequency deviations [15]. However, it does pose power system transient stability and power quality concerns when penetration level of renewable generation become larger [13, 16].

Conventional electric machine based power plants can maintain voltage and frequency during disturbances due to large inertia and proper control of synchronous generators. A synchronous generator stores huge amount of kinetic energy due to inertia. This kinetic energy is used to compensate imbalance in electrical and mechanical power of the generator. The system voltage and frequency are well regulated through the control of speed governors and exciters of synchronous generators. The speed governor adjusts the mechanical power input, so the system frequency is stabilized; the exciter controls field voltage to maintain the system voltage [16]. When a frequency variation occurs in the system, the inertial reserve of power system counter-acts the initial frequency deviation before the primary reserve brings the frequency back to a steady state value. In conventional power grid, large rotational masses of synchronous generators can provide

significant amount of inertia to large power systems. Synchronous generators release or absorb kinetic energy during grid frequency variation [17, 18].

On the other hand, power electronic converters/inverters as interface between renewable energy and utility power grid are static without any rotational energy, this results in negligible inertia. Extensive usage of static power electronic converters/inverters can considerably reduce the equivalent rotational inertia of power grid. Low moment of inertia degrades frequency stability of power grid because power system frequency is inversely proportional to the system's inertia, could cause large frequency oscillations when subjected to severe disturbances [16, 19].

To solve this problem and enhance power system stability, virtual synchronous machine (VSM) method was first introduced by Beck and Hesse in 2007 in order to allow renewable energy integration. As a new power electronics based approach, the VSM method models and controls grid-connected renewable energy generation as electromechanical synchronous machines. Using this method, renewable energy sources such as wind and solar photovoltaic systems can behave as conventional power generation stations if viewed from power grid. The virtual inertia will be created in the virtual synchronous machine to improve transient stability of the system [13, 19]. In the literature, this method is also called virtual synchronous generator (VSG) [19-21].

During the last decade, some developments have been made to operate power electronic converters as VSMs, which offers a promising way to design advanced control systems for renewable energy integration. Most publications on this topic actually occurred within the past two years. As an emerging new method with huge potential, the VSM method has been used to reduce voltage and frequency fluctuation of renewable energy sources by controlling power electronic converters/ inverters and electric energy storage. This method can also be combined with other method such as reactive power compensation to achieve better power quality.

In this paper, a comprehensive literature review is conducted for the VSM method. The paper is arranged as follows: The principle of the VSM method is presented in Section 2.2; current state of art control techniques of implementing the VSM method in renewable energy integration are summarized in Section 2.3. Conclusions are drawn in Section 2.4.

2.2 Fundamental Principle of Virtual Synchronous Machines Method

The VSM control method is a combination of advanced inverter technology and electromechanical synchronous machine. The properties of an inverter can be specified to make it act like a synchronous machine between renewable generation, energy storage, and power grid. The fundamental concept of the VSM method is shown in Figure 2.1 (a) [13].

As shown in Figure 2.1 (a), the energy storage is connected to the renewable energy generation side of the VSM and can change voltage, and thus, the combination of renewable energy and energy storage correspond to the stator output of the virtual synchronous machine [13].

The rotational virtual inertia is a critical aspect of the VSM. Reference [13] did not advise how to create the virtual inertia. It is recommended in [19, 20] that the virtual inertia can be attained by adding a short-term energy storage to any distributed generation unit together with an intelligent control of the interface to the grid.

As a conventional synchronous generator, the VSM should be able to handle active and reactive power flow effectively in both directions as shown in Figure 2.1 (b). Such power flow can be either caused by variations on the renewable energy generation side or by demands/disturbances on the grid side. Renewable energy generation is intermittent and variable depending on weather condition; the power grid could have voltage and frequency variation due to remote dispatch or short circuit fault disturbances [13].

Although the mechanical component of a VSM only exists as a logical concept, the VSM is electrically fully effective when viewed from a grid because it is modelled mathematically in real time by the control system, and have a physical direct voltage supply circuit. The full analogy of a VSM with the electromechanical synchronous machine is established on the basis of virtual values of torque and excitation voltage combined with an intermediate circuit [13].

The VSM model is based on the two-axis frame model of a synchronous machine, which can be fully described electrically by impedances at direct (d)-axis and quadrature (q)-axis of the machine: the stator impedance (L_d, R_d, L_q, R_q), the damper impedance (L_D, R_D, L_Q, R_Q), the exciter impedance (L_e, R_e), the magnetically coupling impedances and the mass inertia of the virtual rotor. Because of this modeling method, the VSM has both static and dynamic properties [13].

In practical applications, the virtual synchronous machine/generator is an engineering device that is developed using the VSM control method. It consists of a power electronic converter, a short term energy storage, and an advanced VSM control algorithm. This device can be connected between the renewable energy source and the power grid. The sizes of a VSM device should be chosen properly to fit in a particular application. It is reported that 10 prototypes of 5 kW VSM were demonstrated in Netherland [19], and 1 prototype of 100 kW VSM was demonstrated in Romania [22] through the VSYNC project [23].

A high level block diagram of VSM/VSG implementation in a power grid is provided in [24] as shown in Figure 2.2.

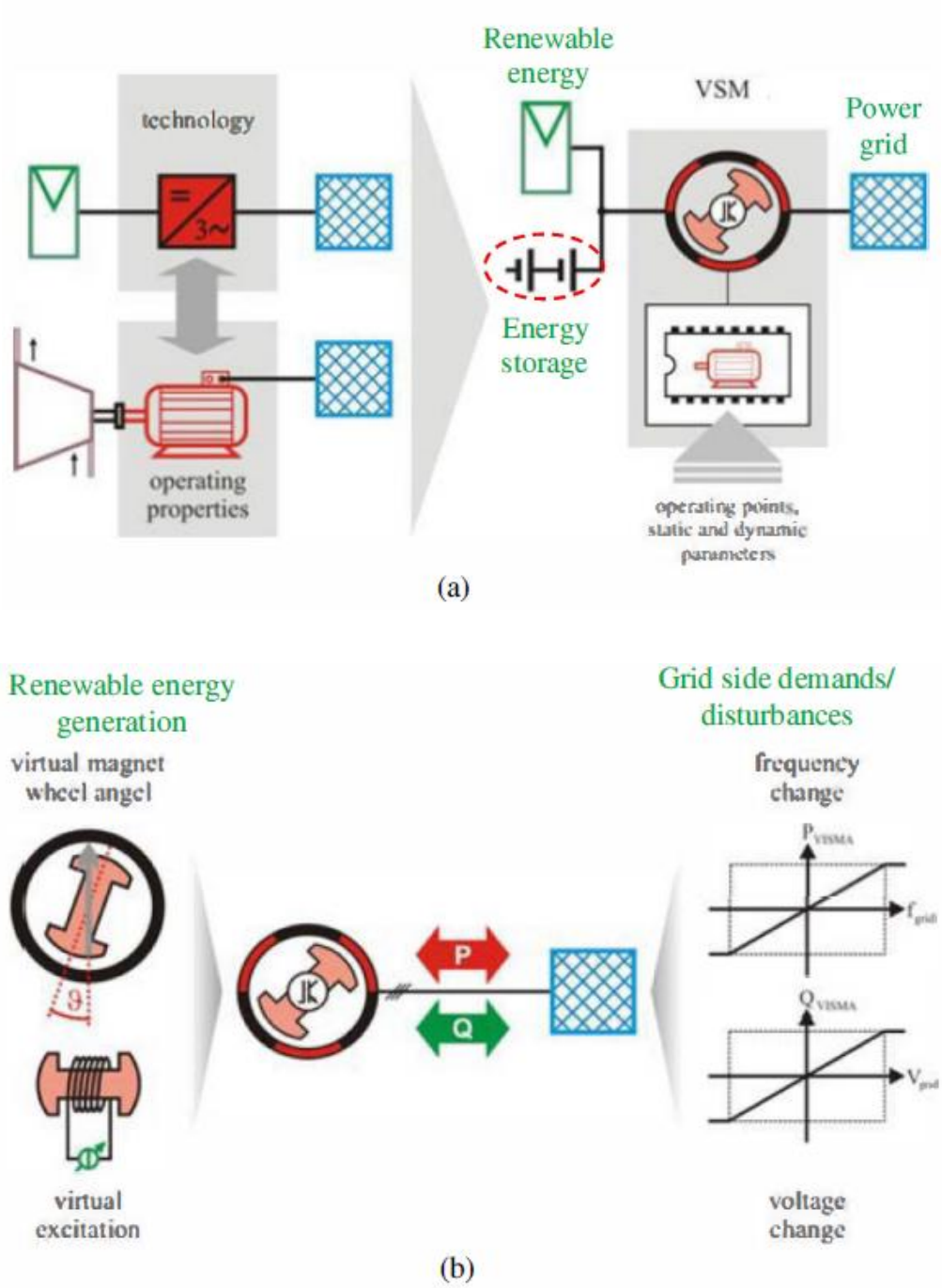

Figure 2. 1: The VSM method: (a) fundamental concept. (b) active and reactive power flow due to variations on local induced renewable generation side (left) and voltage and frequency variation on the grid side (right) [13]

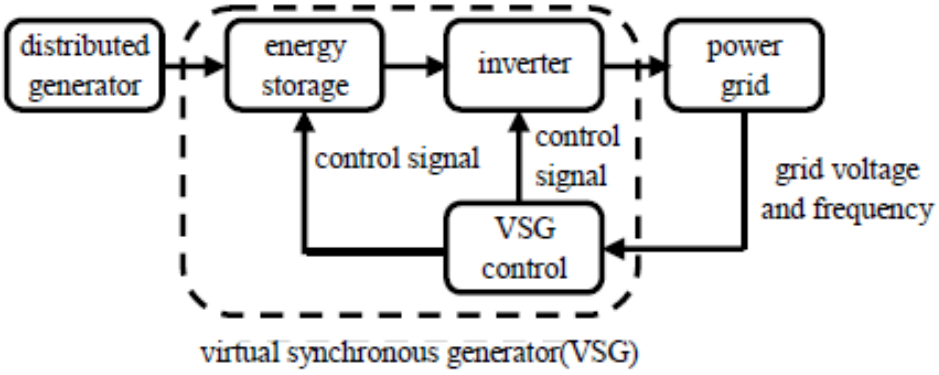

Figure 2. 2: The block diagram of a VSM/VSG implementation [24]

The characteristics that can be implemented in a VSM device are listed as follows: 1) Prevent grid instability and blackouts due to large frequency variations caused by decentralized generation; 2) Retain safety in fault situations of the grid with decentralized generation; 3) Setup a basis for intentionally islanding of low voltage areas with decentralized generation [20]. These characteristics are critical to improve security, stability and power quality of the power grid with renewable energy integration.

2.3 Control Schemes in VSM

The control schemes are the brain of a VSM. The development of an innovative and intelligent control system is the most challenging aspect for VSM devices [25-45].

Distributed renewable generation interfacing power grid are voltage source inverters (VSI). The main control scheme for the grid-connected VSIs is a current-regulated control, which requires a d-q frame phase-locked loop (PLL) to achieve power balance-based synchronization with frequency and phase of the power grid. The frequency of the inverter follows the frequency determined by other synchronous generators in the system, which is detected by PLL. If the PLL loses the locked situation due to power system disturbances, the converter might stop operation

due to over current of ac side or over voltage of dc side. The PLL may also be affected by the power injected by various distributed generations, which has a negative impact on power system stability. This problem is especially significant in a weak grid [25-28].

To overcome the issues associated with PLL, several voltage source inverter control methods have been proposed. The droop control is a well-developed VSI control method, which focuses on stand-alone operation and power sharing of synchronous generators under stable state, but no effort is done for transient state in droop control, therefore, distributed generation with droop control are still lack of inertia, which is prone to cause frequency instability. The VSM is another voltage source inverter control method, which imitates not only droop characteristics but also the swing equation of synchronous generators. A VSM has a virtual inertia and similar dynamic characteristics as a synchronous generator [29].

The relationship between the VSM and droop control is investigated [30-32]. It is proved that the small-signal response of inertia emulation characteristics of the VSM control is equivalent to conventional droop control for standalone and microgrid operation of converters in [30]. Thus, the droop gain and the filter time constant of the power feedback in a droop controller can be directly associated with the damping factor and inertia constant of a VSM. This provides additional physics-based insight into operation and tuning of both types of controllers [30]. The conclusion drawn in [30] is not against the statement in [29] as the small signal response does not represent a transient state.

Ref [31] compares the frequency-droop-based control schemes with VSMs. These two approaches have been developed in two separate contexts, but present strong similarities, they are equivalent under certain conditions [31].

A frequency-droop based VSM control method is proposed by adding a distributed frequency controller to the emulated swing equation of the VSM. This controller uses line frequency as a feedback signal that produces an embedded transient active power droop with improved closed-loop dynamic performance. A generalized model for power generation is built to illustrate similarities and differences between conventional droop control and the proposed control method. It is found that a faster transient response and better dynamic performance are achieved by the proposed controller [32].

There are three main functions for a VSM: oscillation damping [25, 33], frequency control, and voltage control [34]. VSMs add virtual inertia to power systems. The energy storage can be utilized to realize virtual inertia creation through an advanced control system. Since the inertia is closely related to the frequency, a VSM shows significantly improved performance on power system stability and oscillation damping.

The oscillation damping using VSM is investigated in [25]. The virtual inertia can be created from energy storage during a short operation time, and the active power can be produced by a VSM similar to a synchronous generator. The VSM control block diagram is shown in Figure 2.3. To improve power grid stability due to high penetration of inverter-based distributed generation, a novel linearizing technique for VSG-based control scheme is proposed. This new damping control approach is developed by linearizing the system equation and decoupling the voltage deviation and damping factor, and using a linear control theory [25].

Ref [33] proposes an alternating moment of inertia method to achieve power system stabilization using VSM. The alternating inertia scheme adopts a suitable value of the moment of inertia of the VSM considering its virtual angular velocity and acceleration/deceleration in each phase of oscillation. During acceleration, a big value of the moment of inertia is chosen; while during

deceleration, a small value of the moment of inertia is adopted to increase the deceleration effect. This method is verified to be effective by the transient energy analysis. Compared to normal damping factor *D*, the damping exerted by alternating inertia is considerably more effective [33].

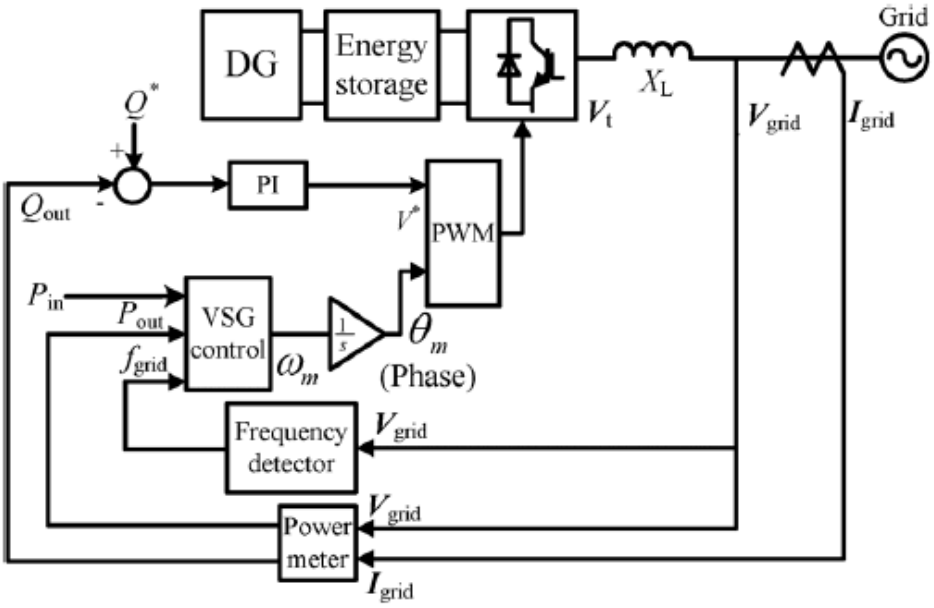

Figure 2. 3: The VSM control block diagram [25]

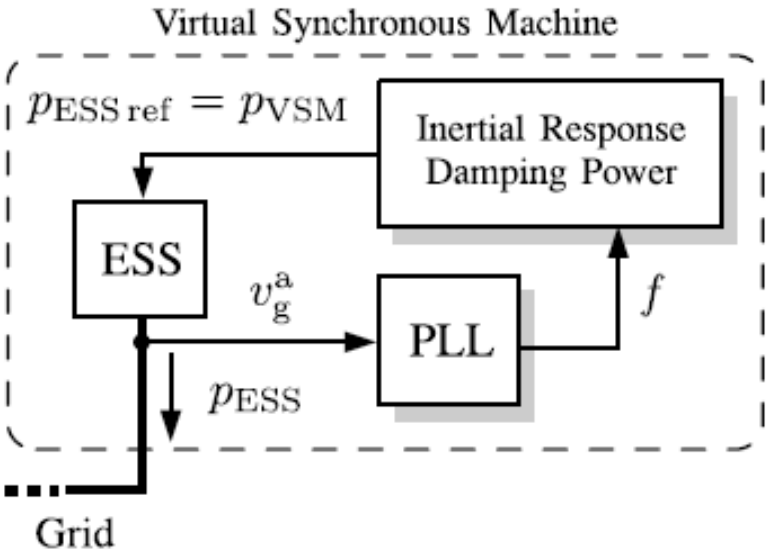

Figure 2. 4: The VSM control block diagram used in [34]

Extensive research work have been done on frequency control in [14, 18, 31, 32, 34, 35]. Ref [34] investigates the use of a VSM to support dynamic frequency control in a diesel-hybrid autonomous power system. The proposed VSM controls the grid-interface converter and an energy storage system to emulate the inertial response and damping power of a synchronous generator. The self-tuning algorithms are used to continuously search for optimal parameters during the operation of the VSM in order to minimize the amplitude and rate of change of the frequency variations, and the power flow through the energy storage system. Compared to a constant-parameters based VSM, the proposed self-tuning based VSM achieved a similar performance, while reduced the power flow in the energy storage system up to 58%. The proposed VSM method was also found to be more efficient than the constant parameter based VSM method in attenuating frequency variations [34]. Fig. 2.4 shows the VSM control block diagram in [34].

The voltage control using VSM is investigated in [27, 28, 36, 37] by combining with STATCOM. STATCOMs are typically installed at the point of common coupling (PCC) to regulate the PCC voltage using reactive power compensation. A wind farm with a STATCOM at the PCC is shown in Figure 2.5 [36]. Ref [36] combines the VSM concept into the design of a STATCOM controller. The VSM based STATCOM controller behaves like a fully-adjustable synchronous condenser, including the adjustment of its virtual inertia and impedance. Compared to the existing d-q frame STATCOM control strategies, the proposed VSM based STATCOM controller can achieve better synchronization, an improved voltage regulation performance at the PCC (due to its virtual impedance), and a lower sensitivity to system disturbances (due to its virtual inertia). Fig. 2.6 shows the control block diagram of the VSM based STATCOM controller [36].

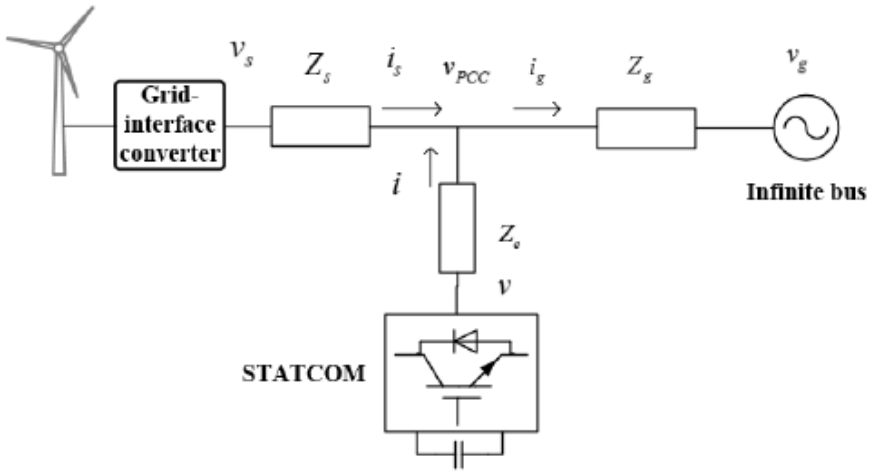

Figure 2. 5: A wind farm with a STATCOM connected at the PCC [36]

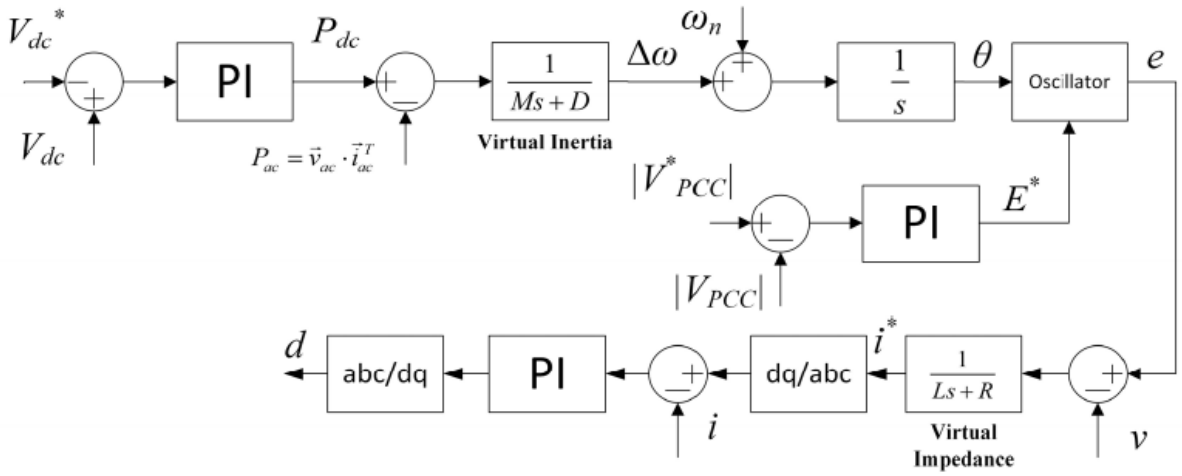

Figure 2. 6: The control block diagram of a VSM based STATCOM controller [36]

2.4 Conclusions

As a new emerging method first introduced in 2007, the VSM method has been widely recognized due to its promising research potential. There are three main streams of work utilizing VSMs: 1) oscillation damping to improve power system stability; 2) frequency control; 3) voltage control.

In this paper, an extensive literature review is conducted on the VSM method in renewable energy integration. The principle of the VSM is first introduced in the paper, current state of art control schemes used in VSMs are reviewed and summarized. Due to advancement of renewable energy and their increasing penetration in power grid, the VSM method will remain to be an active research area.

Harmonic Mitigation through Advanced Control Methods for Grid-Connected Renewable Energy Sources

Xiaodong Liang, *Senior Member, IEEE* and Chowdhury Andalib-Bin-Karim, *Student Member, IEEE.*

Faculty of Engineering and Applied Science, Memorial University of Newfoundland, St. John's, Newfoundland, Canada.

A version of this work has been published in the proceeding of *IEEE Industry Application Society Annual Meeting, 2017, Cincinnati, OH, USA*. The co-author of this manuscript Chowdhury Andalib-Bin-Karim participated in this work under the supervision of Dr. Xiaodong Liang. Mr. Karim performed literature review, and wrote some content of the paper. Dr. Xiaodong Liang provided continuous technical guidance, wrote some content of the paper, and modified the final version of the paper. In this chapter, the manuscript is presented with altered figure numbers, table numbers, section numbers and reference formats in order to match the thesis formatting guidelines set out by Memorial University of Newfoundland.

Abstract- With increasing renewable distributed generation (DG) units connected to utility power grids, deterioration of power quality at the point of common coupling (PCC) becomes a major concern. Power electronic devices in DG units generate harmonics, these harmonics along with harmonics from other nonlinear load in the system might cause excessive harmonic distortion at the PCC. In this paper, an extensive literature review is conducted focusing on harmonic mitigation techniques through advanced control methods for grid-interfacing inverter. Harmonics generated by solar photovoltaic (PV) system are firstly reviewed, potential resonance due to LCL filter is discussed. Then various control methods for harmonics mitigation are reviewed and summarized. This systematic review can facilitate better understanding of harmonics and develop more advanced control schemes to mitigate harmonics in renewable energy system.

Keywords- Active filtering, distributed generation, harmonics mitigation, power quality, virtual impedance.

2.5 Introduction

With increasing interest on power generation in an environmental friendly way, the development of renewable energy based distributed generation (DG) has received great attention in recent years as renewable energy resources are pollution free and abundant in nature. Among all renewable energy sources, the solar photovoltaic (PV) system has experienced rapid growth both in residential and commercial sectors mainly due to the recent advancement of the PV generation technology and various support programs introduced by governments and utility companies to encourage grid-connected PV generation.

In a grid-connected renewable energy system, grid connection is generally achieved through an interfacing power electronic inverter. The switching of power electronic inverter will generate harmonics at its output. Also, a PV inverter may experience high frequency switching during low irradiance level of solar energy, resulting in an injection of highly distorted current to the distribution network [46].

To ensure a good quality of power supplied to the consumers, utility companies need to maintain harmonics level within an acceptable limit as indicated in different grid codes. For example, according to IEEE std. 519, the acceptable limit of the voltage total harmonic distortion (THD) at the PCC with each consumer is 5% [47]. To mitigate harmonic distortions, passive LCL or LC filters are traditionally used with the grid-interfacing inverters, however, such filters have disadvantages such as the fixed compensation capability, creation of resonance problem etc.

To overcome the limitations of passive filters, the DG interfacing converters can be utilized to operate as power conditioners for power quality improvement. Although, the primary function of the interfacing converter is to supply real power to the grid, it can also provide auxiliary harmonic

compensation service upon the availability of sufficient apparent power rating. With proper design and control, the DG interfacing converters can improve the system efficiency and ensure reliable harmonic compensation performance.

In this paper, an extensive literature review of harmonic mitigation methods based on the control of grid interfacing converters for DG units is conducted. Based on the review results, a classification of control methods used for harmonic mitigation is presented in Fig. 2.7. There are two main streams of harmonic mitigation methods: 1) virtual impedance based control method; and 2) active harmonic filtering method. They will be summarized in detail in this paper.

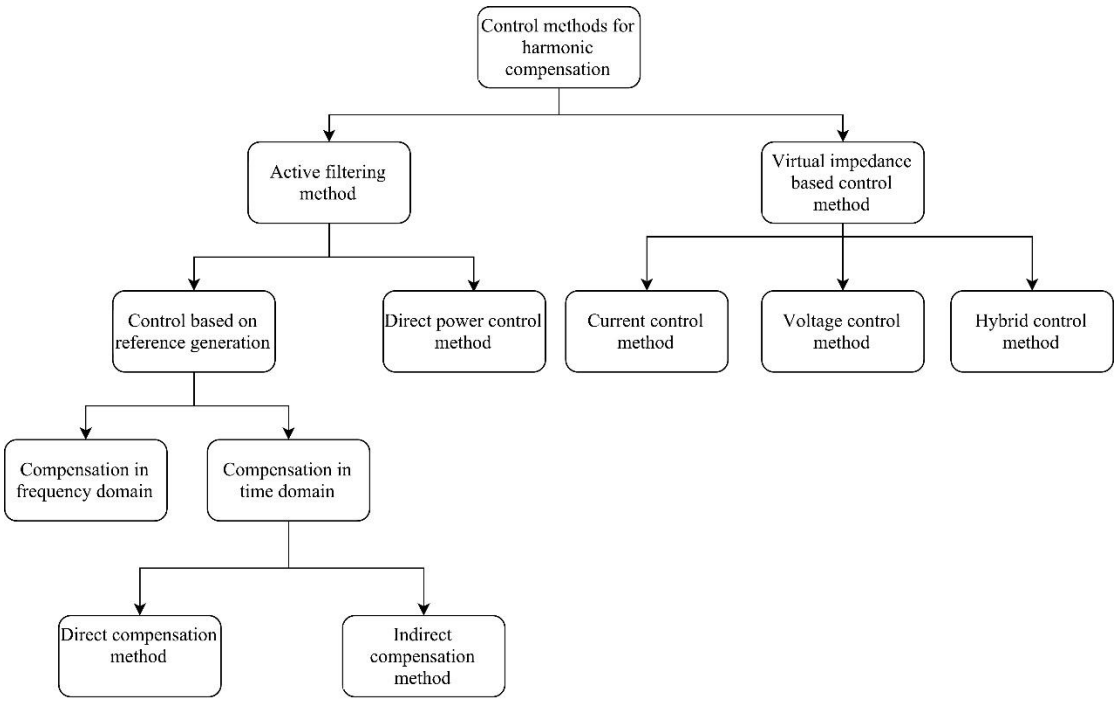

Figure 2. 7: Classification of control methods for harmonics mitigation

The paper is arranged as follows: in Section 2.6, harmonics experienced in renewable power generation systems are reviewed, and the potential resonance in the system due to LCL filter is discussed; harmonic compensation using virtual impedance based control methods is reviewed in Section 2.7; Active harmonic filtering method is presented, and a topology based classification of

active power filters is provided in Section 2.8; This is continued by a discussion of different control techniques for active power filters and current control techniques for the generation of gating signal to the converters in Sections 2.9 and 2.10, respectively; the conclusion is drawn in Section 2.11.

2.6 Harmonics in Renewable Generation Systems

Power electronic inverters utilized at renewable DG units and their interface with the utility power grid pose harmonic concern at the PCC as the penetration of DG units increases. Harmonics come from two sources in renewable energy system: 1) power electronic devices at renewable energy sources, and 2) harmonics from other nonlinear loads in the system.

2.6.1 Harmonics Generated by Renewable Energy Sources

Solar PV systems use large amount of power electronic inverters to get connected with the distribution system. The typical system configuration for a solar PV power plant is shown in Fig. 2.8, for a residential solar PV system is shown in Fig. 2.9 [48].

These power electronic inverters will generate harmonics during operation. The characteristics of harmonics are affected by the system impedance, the control system, and the LCL or LC filter implemented in the inverters. Several papers have reported harmonics generated by solar PV systems through lab experiments or field testing [49]-[52].

A laboratory experiment using a 3 kW rated single-phase inverter for solar panels is conducted in [49], the active power of the inverter is varied between 500 W and 2500 W in steps of 500 W during the experiment, and measurements are taken at each loading point. The recorded voltage total harmonic distortion (THD) is always within the 5% recommended IEEE limit, while the recorded current THD has a higher value close to 30% at a light load, and approaches the IEEE

standard limit with an increased loading. The paper concludes that the distribution network under the impact of solar panels is within IEEE standard limits [49]. In this study, voltage and current harmonic spectrums are not measured.

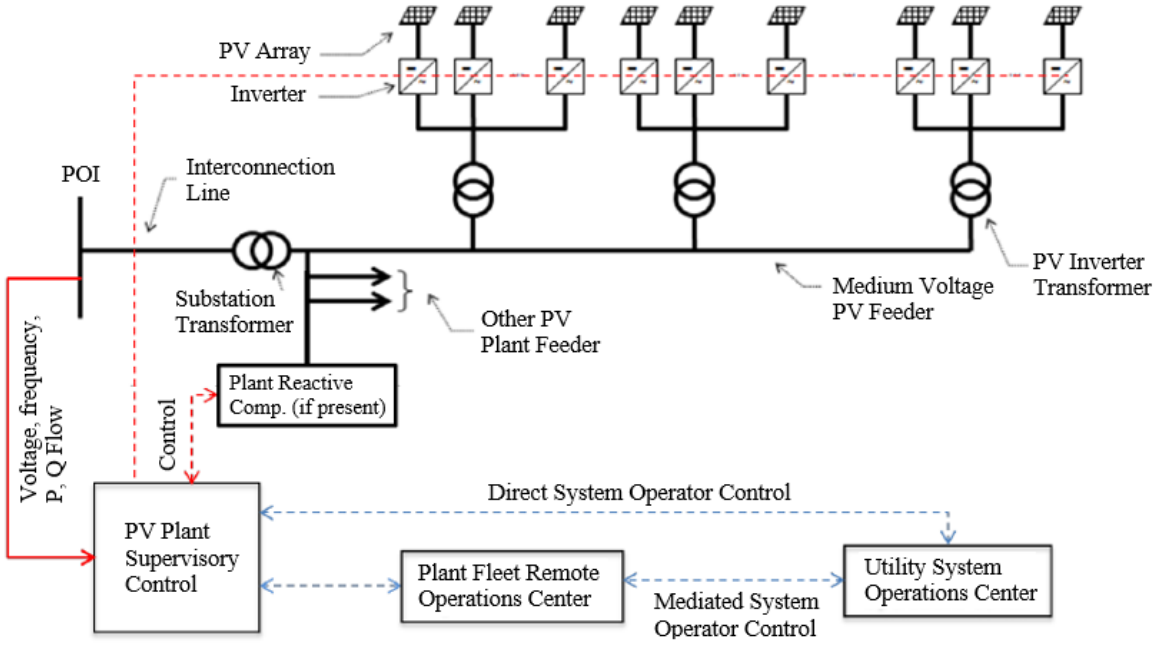

Figure 2. 8: Typical system configuration for a solar PV power plant [48]

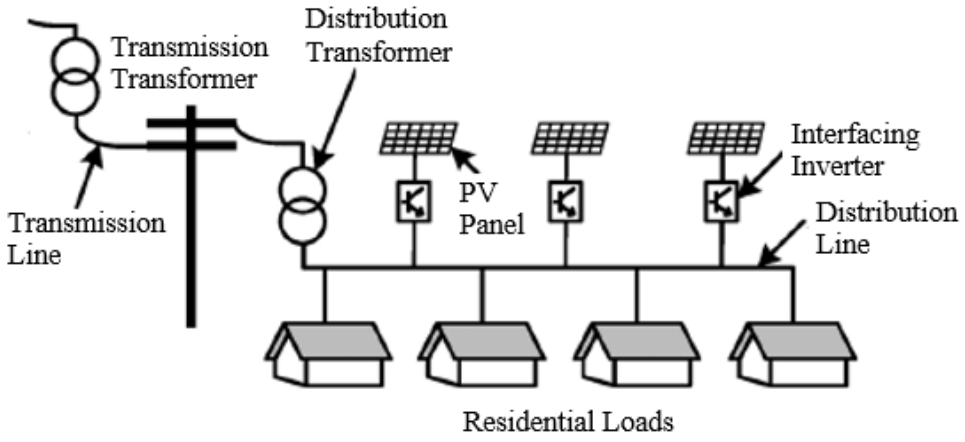

Figure 2. 9: Typical system configuration for a residential solar PV system [48]

However, as mentioned in [53], although each inverter associated with a set of solar panels may generate harmonics which are within acceptable standard limits recommended by IEEE standard 519, the harmonics at the PCC of a large scale connection of many inverters in a realistic solar farm may exceed these limits [53]. Harmonic distortion level for large scale solar farms should be carefully evaluated.

Reference [50] reports field measurements data for two 10 MW solar farms at a 27.6 kV main feeder. The harmonic data were recorded for several months by the transmission utility at the two solar farms and at the main feeder. The feeder consists of a 7.8 km of overhead distribution line and two small segments of three phase underground cable. Two 10 MW solar farms located about 6.2 km away are connected to this feeder. The feeder is equipped with two 20 MVar capacitor banks (SC1 and SC2) for voltage support. A set of 1.2 MVar power factor correction capacitors is located close to the 2 MW customer site. The system configuration is shown in Fig. 2.10 [50].

With many long lines and capacitors involved, the system harmonic resonance condition must be analyzed. Reference [50] did perform the harmonic resonance analysis as shown in Fig. 2.11. It is found that for this base case analysis, the harmonic resonance frequencies are located around 3^{rd} order and 25^{th} order. The field measurements show large 3^{rd} harmonic current content in some days, which matches the resonance response characteristics. The recorded harmonic current spectrums provided by Hydro One during June 2012 are shown in Fig. 2.12. Fig. 2.12 (a) shows a harmonic current spectrum recorded on a day with high 3^{rd} harmonic current content, Fig. 2.12 (b) shows a harmonic current spectrum on a sunny day, and Fig. 2.12(c) shows a harmonic current spectrum on a cloudy day [50].

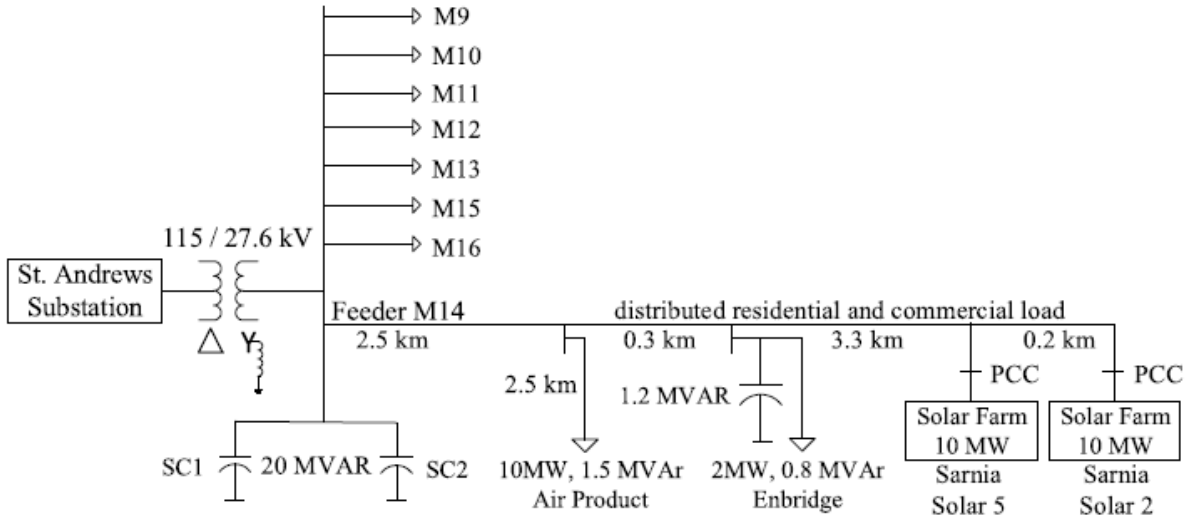

Figure 2. 10: The electrical single line diagram for the main feeder [50]

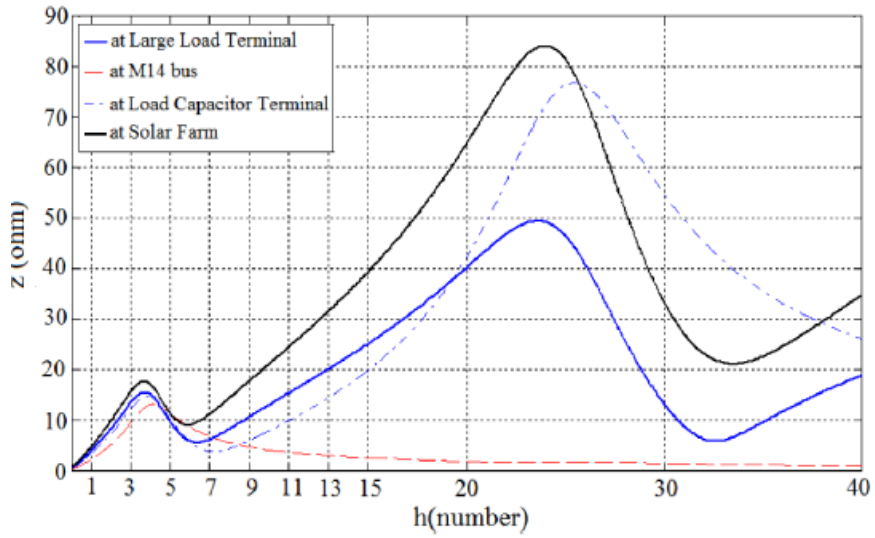

Figure 2. 11: The network harmonic resonance response showing impedance versus the order of harmonics for a base operating case with one 20 Mvar station capacitor and 1.2 Mvar load capacitor in operation [50]

It is concluded in [50] that the steady state voltage THDs at the two solar farms and at the main feeder were well within the 5% limit based on IEEE Standard 519. Note this study did not consider harmonics from the rest of the system.

By examining measured harmonic current spectrums in Fig. 2.12, it appears that the highest order harmonics shown is only 25th, which poses some concerns about harmonic measurement accuracy. Because the pulse width modulation (PWM) based voltage source inverter output will generate characteristic harmonics at the multiple of the carrier/switching frequency of the inverter [54], which are usually much higher than 25th harmonic order shown in this case. For example, if the switching frequency of the inverter is 2200 Hz, the characteristic harmonic bands will be located around 2200 Hz, 4400 Hz, 6600Hz etc. A 2200 Hz harmonic band corresponds to 37th order harmonics. However, this higher order harmonic is not recorded in [50], and their effect is not included in THD calculation.

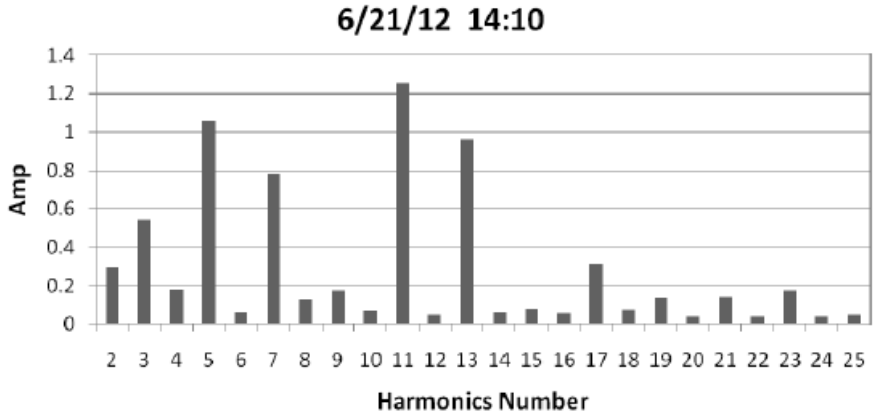

(a)

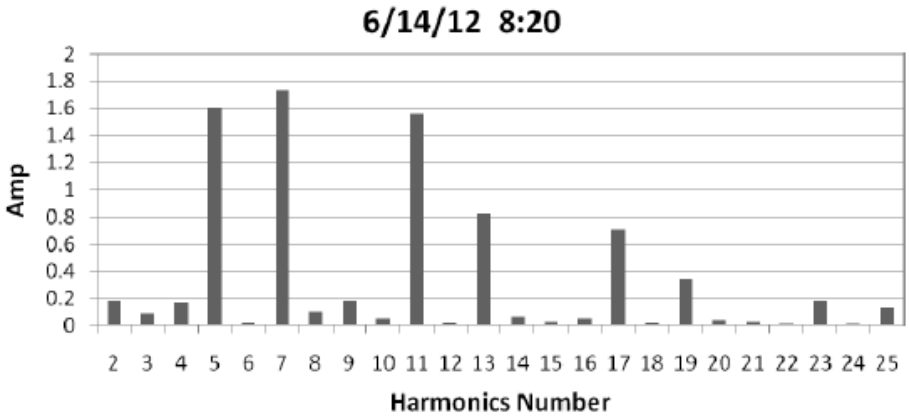

(b)

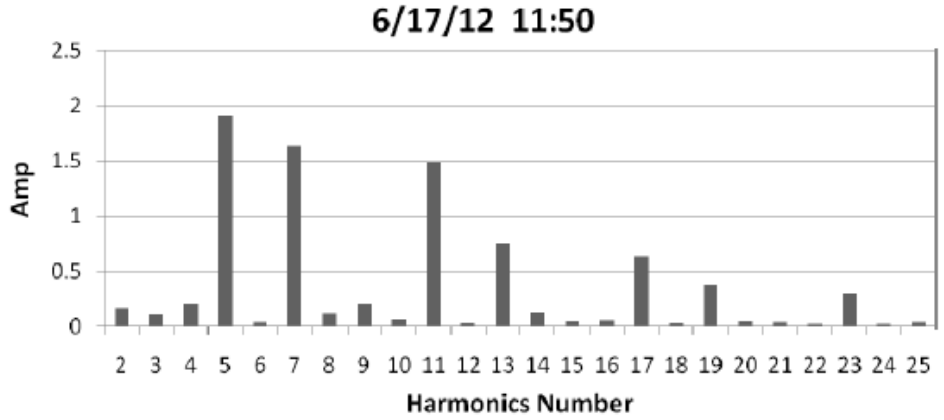

(c)

Figure 2. 12: The recorded harmonic current spectrum at the solar farm by Hydro One in June 2012: (a) a day with a high 3rd harmonic current; (b) a sunny day; (c) a cloudy day [50].

In Reference [51], a comprehensive testing is conducted to evaluate harmonics and inter-harmonics generated by solar PV inverters. One conclusion is drawn in [51], which matches the authors' concern about Reference [50] measurements discussed earlier, is that some PV inverters might have strong high frequency component emission in low-power modes and/or at rated and higher power mode. Accordingly, it is suggested that tests of PV inverters include high frequency range and suitable high frequency distortion indices be used [51]. Another interesting discovery in [51] is that the maximum power point tracking control might be a possible origin of the interharmonic distortion.

A field test of inverters installed in a Brazilian solar farm was conducted in [52]. Measurements were performed on three different commercial inverters, with 15 kVA rated capacity each. It is found that high frequency harmonic current distortions may reach up to 2% of the fundamental frequency current, but high frequency harmonic voltages remain below 0.2% of the fundamental frequency voltage. Fig. 2.13 shows the measured sample harmonic voltage and current spectrums, the dominant harmonic frequency is at 16.5 kHz. A conclusion is drawn in [52] based on the findings that these specific PV inverters are unlikely to cause significant problems to the utility.

By examining the solar farm set-up, there is no long distribution lines or cables involved. If there is a long line connected to the solar farm, which can potentially causes harmonic resonance at 16.5 kHz frequency, the conclusion drawn in [52] might have to be changed. In a case of resonance, the harmonics at the PCC will be amplified, and might exceed the IEEE limit.

Although some field tests and lab experiments have been conducted, harmonics generated by solar PV systems are still not well understood. More field tests are needed in the future.

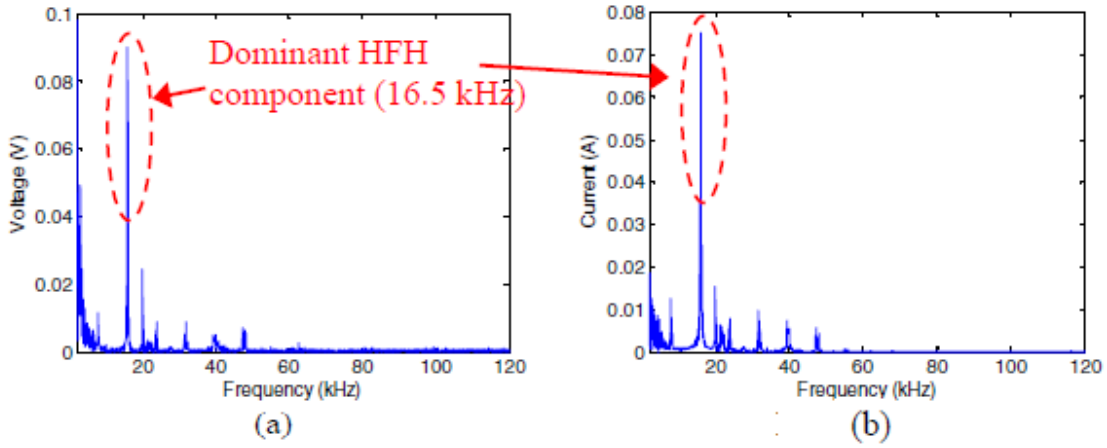

Figure 2. 13: The sample recorded harmonic current spectrums: (a) high frequency harmonic (HFH) voltage; (b) high frequency harmonic current [52].

2.6.2 Harmonic Resonance Caused by LCL Filters

The *LCL* and *LC* filters are widely applied in PV inverters to mitigate high-order harmonics generated by the inverters. The possibility that these filters excite harmonic resonance by interacting with the system impedance is evaluated in [55], [56]. The general configuration of a voltage source converter (VSC) system is shown in Fig. 2.14. A LCL filter with a damping resistor R_d in series with the capacitor is shown in Fig. 2.15 [55].

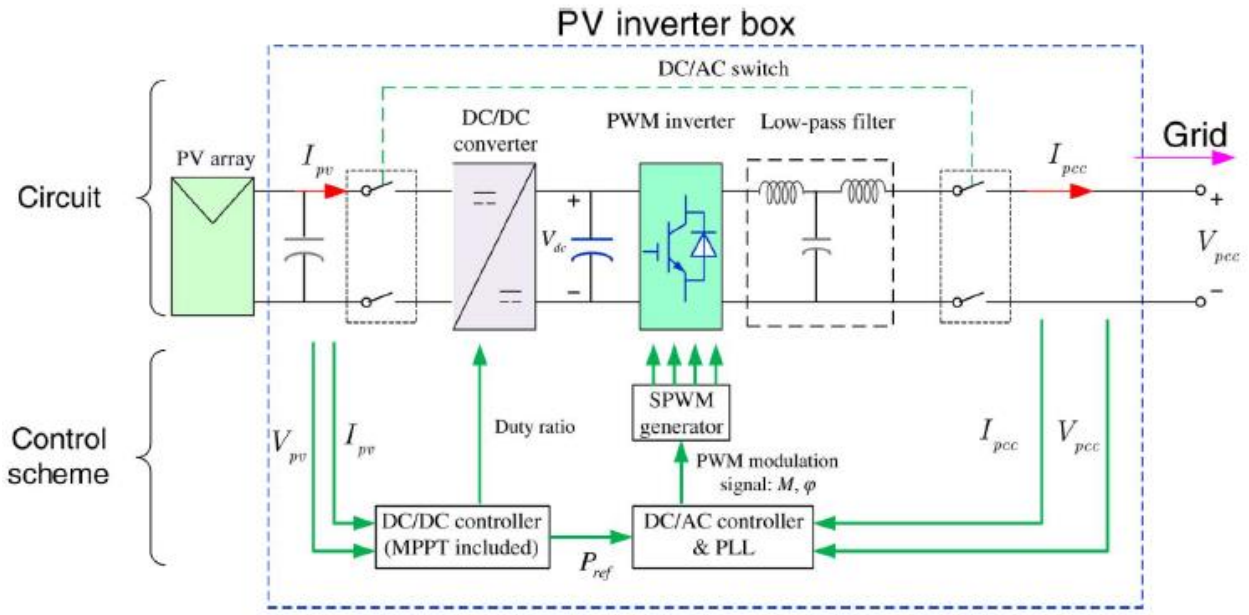

Figure 2. 14: A general configuration of a voltage source converter (VSC) system [55].

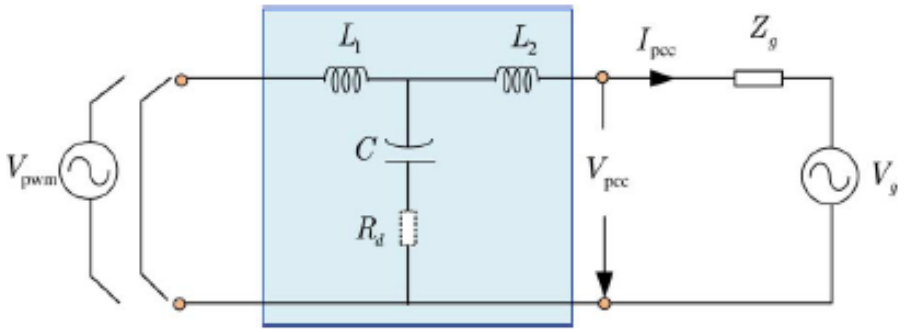

Figure 2. 15: The proposed model of individual PV with a damping resistor R_d at the LCL filter [55].

It is concluded in [55] that: 1) the damping resistance R_d has a significant damping impact on the resonance, an individual PV inverter will excite harmful resonance as long as the passive damping impedance is below 2 Ω; 2) The supply system impedance is not the dominant factor contributing to resonance amplification; 3) the number of PVs affects the resonance magnitude and frequency, and a large number of PV installations in a distribution system is not of concern.

Fig. 2.16 shows the system resonance with different damping resistor values [56]. Reference [56] also shows similar effect using a 6 Ω damping resistor (Fig. 2.17).

The harmonic content at the PCC for a case study (a residential system with 10 houses) in [56] is shown in Fig. 2.18. The harmonics amplified at the switching frequency can be observed, which match the discussion in previous sections.

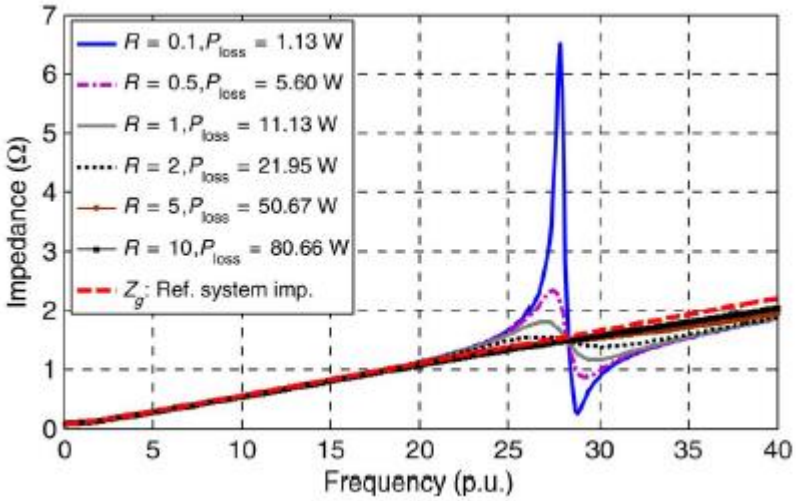

Figure 2. 16: The system resonance with different damping resistors [55].

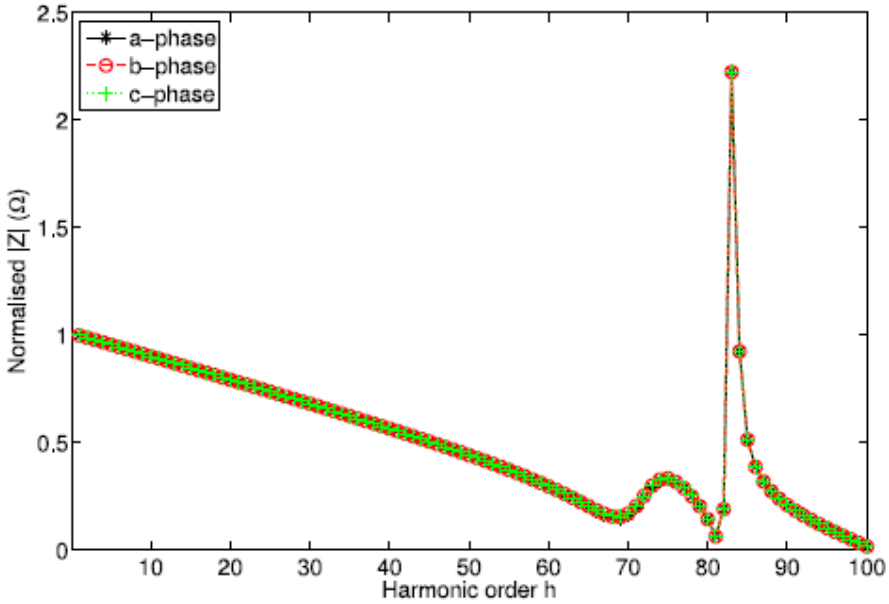

(a)

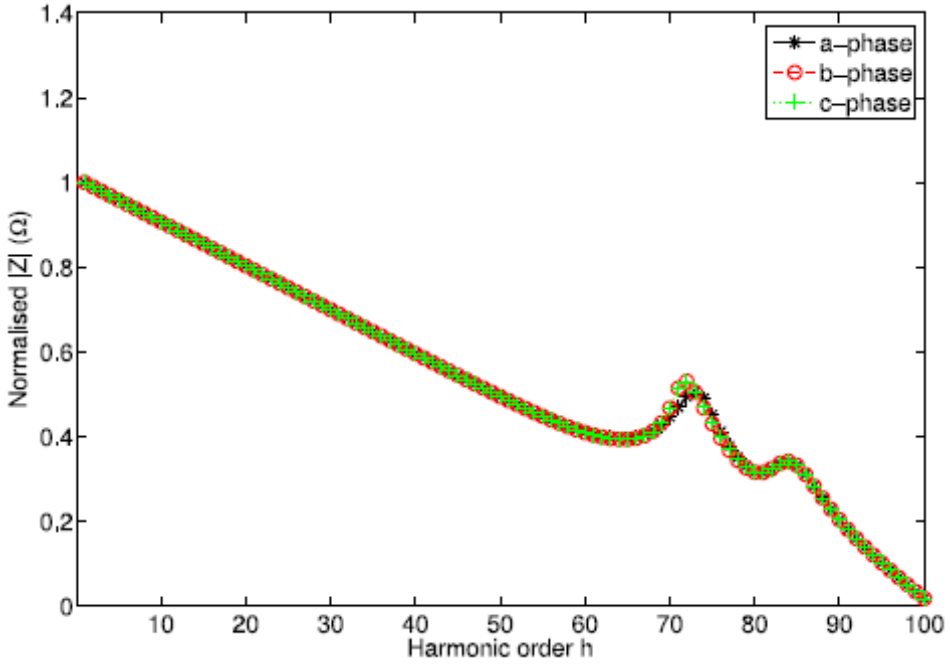

(b)

Figure 2. 17: PV system frequency response at the PCC: (a) without a damping resistance R_d; (b) with a damping resistor R_d = 6Ω [56].

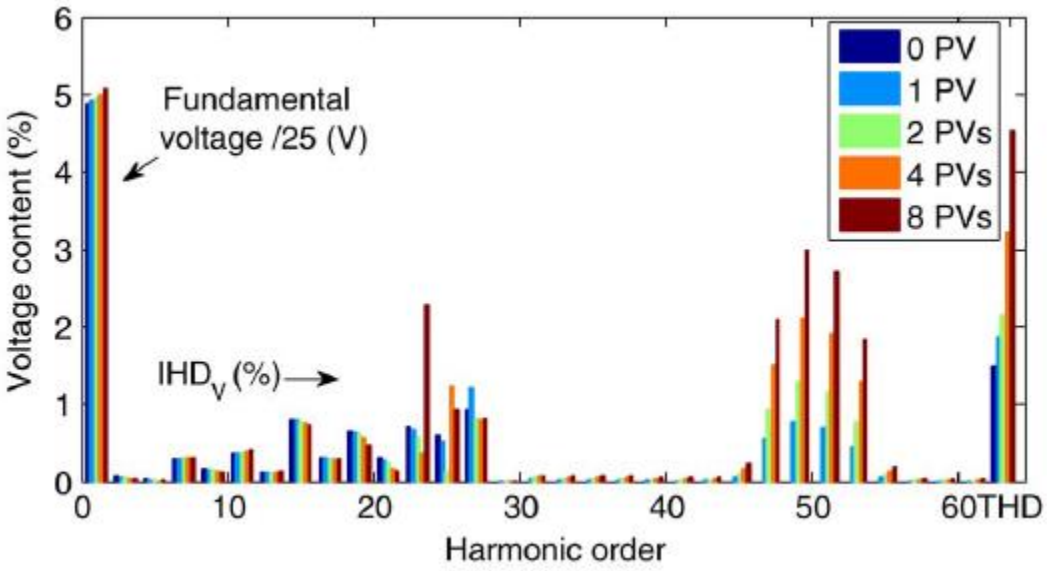

Figure 2. 18: Harmonic contents of secondary PCC voltage [expect for fundamental voltage/25 (*V*), rated voltage is 120 V] [55].

2.7 Harmonic Compensation by Virtual Impedance based Control Method

The grid interfacing inverters can be controlled as virtual impedance at harmonic frequencies for system harmonics mitigation. The virtual impedance can be realized by modifying the current or voltage reference signal according to the harmonic compensation requirement. Different control schemes based on virtual impedance are discussed in the following subsections.

2.7.1 Current Control Method (CCM)

The harmonic compensation in a DG unit can be effectively realized by using the current control method. In this method, the DG line current is controlled according to a modified current reference. The current reference is modified based on the system harmonic compensation requirement and available power rating of DG interfacing inverter. The main idea of this control method is to make the DG unit (i.e. grid tied PV generation unit) behave like a small damping resistor at the selected harmonic frequencies, when viewed from power distribution system level. As a result, more harmonic current from non-linear loads will flow to the DG unit, resulting in an undistorted current supply at the PCC. Consequently, the PCC voltage waveform is also improved as there is no harmonic voltage drop on the grid impedance [57], [58].

In the current control method, the current reference is modified by adding a harmonic current reference term (I_{ref_h}) to the fundamental current reference term (I_{ref_f}) derived from the power control branch, as follows,

$$I_{ref} = I_{ref\_f} + I_{ref\_h} \tag{2.1}$$

$$I_{ref\_h} = \left(-\frac{1}{R_v}\right).(H_D(s).V_{PCC}) \tag{2.2}$$

where R_v is the virtual harmonic damping resistor and the harmonic component of the PCC voltage (V_{PCC}) is extracted using a harmonic detector ($H_D(s)$). The stability range of the virtual impedance is to be taken into consideration while determining the value of R_v. The proportional and parallel multiple resonant controllers (PR controller) at fundamental and harmonic frequencies are adopted to ensure accurate control of DG line current [59]. The PR controller can achieve very high gain at resonant frequencies with narrow bandwidth. The desired bandwidth can be obtained by appropriate tuning of the integral gain of the controller [60], [61].

The fundamental reference current is computed based on the power reference in order to control DG unit real and reactive power generation. In conventional CCM based compensation technique, the grid voltage is assumed to be stiff while computing the fundamental reference current, and the synchronization of current reference with the grid is achieved using a Phase Locked Loop (PLL). But, during the occurrence of distribution system power fluctuation and variation of grid voltage in a weak grid, the conventionally used open loop power control algorithm cannot guarantee accurate power control. Moreover, the interaction between the distorted DG current and PCC harmonic voltage may give rise to some DC power offset. In order to avoid such power control difficulties, a closed loop power control method with PI controller in power control loop to regulate the fundamental reference current has been proposed in [59], which can ensure compensation of power control errors during reference current generation.

In the conventional current control method, the use of a harmonic extraction block is required, which significantly increases the computational burden, as well as leads to some inaccuracy in harmonic compensation performance by introducing magnitude and phase error in the harmonic component of the signal extracted by filtering [62]. In order to avoid the use of harmonic extraction block, an improved current controller with separate current control branches for fundamental and

harmonic current control has been proposed in [63], where the PCC voltage can be directly used as the input of the controller without any harmonic extraction, also maintaining harmonic compensation accuracy of the DG unit. The block diagram of CCM based harmonic compensation is depicted in Fig. 2.19.

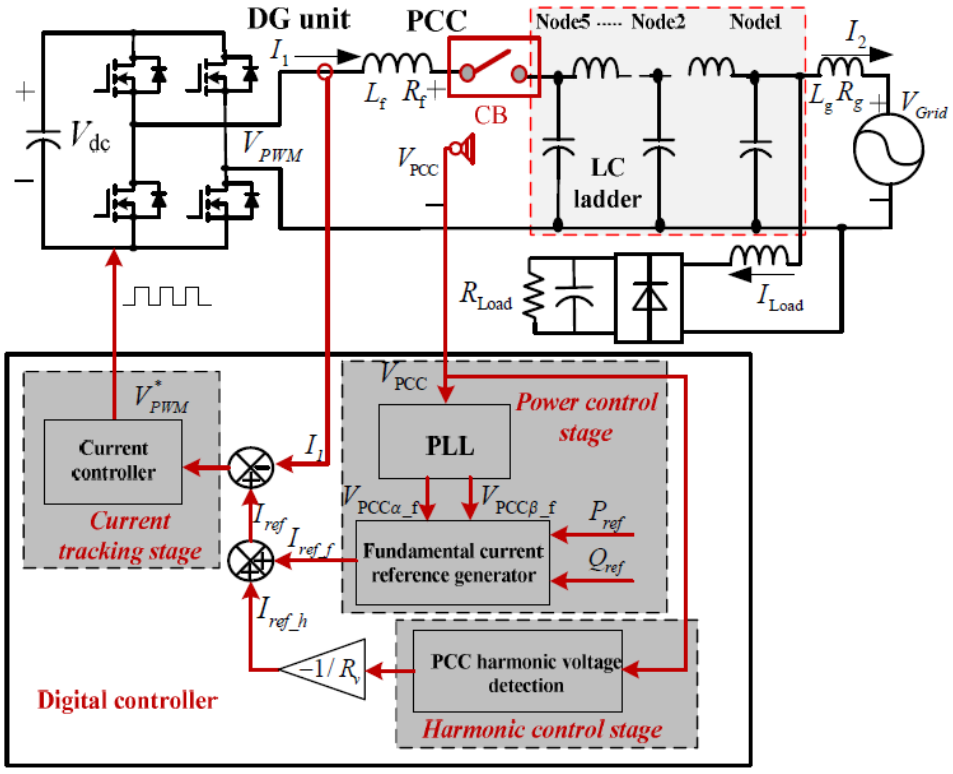

Figure 2. 19: Block diagram of CCM based harmonic compensation [59]

2.7.2 Voltage Control Method (VCM)

When grid connection is not available and the DG unit needs to maintain continuous supply to local loads, the CCM based control technique is not particularly suitable, as it cannot provide direct voltage support to the loads. The voltage control method (VCM) is suitable for harmonic compensation in such islanded mode of operation. The voltage control method cannot directly control DG unit line current as in CCM, but it can ensure reliable PCC harmonic compensation performance using virtual harmonic impedance control [58]. Moreover, when multiple DG units

are connected to the system, VCM can utilize the droop control method (real power-frequency *P-f* droop and reactive power-voltage *Q-V* magnitude droop) to derive the fundamental voltage reference signal (V_{ref_f}), thus facilitating the sharing of load demands among DG units, without any direct communication between them [57]. A double loop voltage controller is generally incorporated in the voltage tracking stage, with a proportional-resonant controller in the outer loop, to control the filter capacitor voltage. The voltage reference is modified by adding a harmonic voltage reference feed forward term (V_{ref_h}) as follows [62]:

$$V_{ref} = V_{ref\_f} + V_{ref\_h} \tag{2.3}$$

$$V_{ref\_h} = (-G).V_{PCC\_h} \tag{2.4}$$

where, *G* is the gain value of the feed forward term and V_{PCC_h} is the harmonic component of the PCC voltage which is extracted using a harmonic detector. The main idea of this control method is to operate the DG unit as a controlled voltage source (V_{DG_h}) with output series impedance, Z_{DG_h} [64]. The equivalent impedance of DG unit at harmonic frequencies can be expressed as, $Z_{DG\_h} / (1 + G)$. So, by controlling the DG harmonic voltage with proper selection of the gain value, the equivalent harmonic impedance of the DG unit can be made lower compared to the grid side. As a result, the DG unit will absorb more harmonic current contributed by non-linear loads and consequently, the waveform of grid current and PCC voltage get improved. The over modulation problem and system instability problem associated with high gain value should be taken into consideration while choosing the value of *G* [65]. The block diagram of VCM based harmonic compensation is depicted in Fig. 2.20.

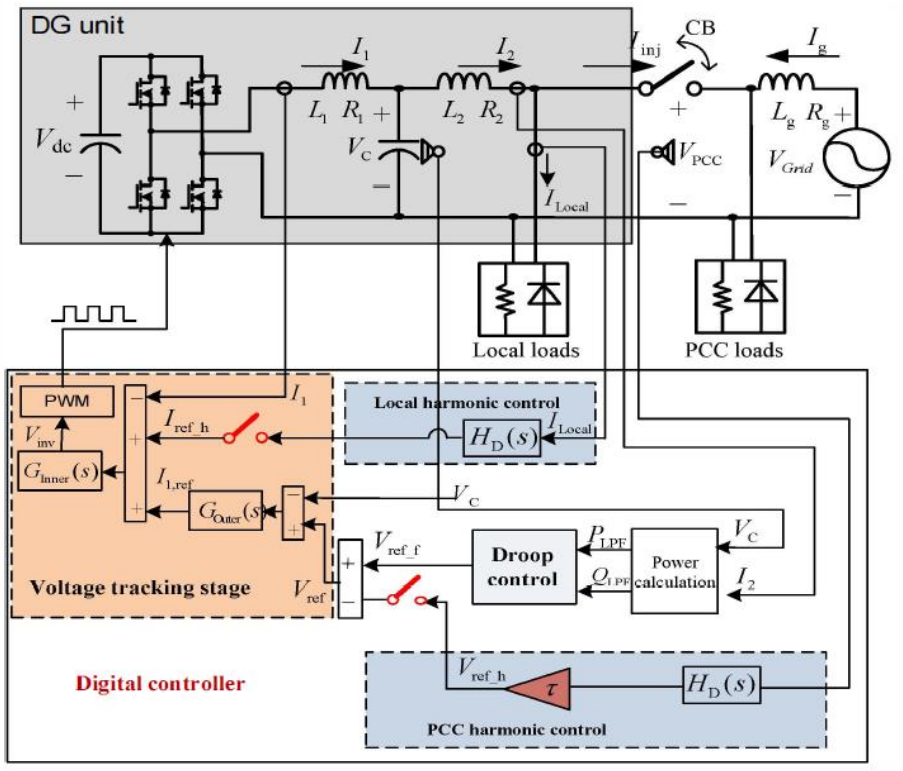

Figure 2. 20: Block diagram of VCM based harmonic compensation [57]

2.7.3 Hybrid Control Method (HCM)

As discussed in the previous sections, the CCM cannot provide direct voltage support to loads during the islanded mode of operation, while VCM cannot directly control DG unit line current for compensating local load harmonics. To address these limitations of traditional CCM and VCM, an innovative control approach, called the Hybrid Control Method (HCM) has been proposed in [66], [67], where the required real and reactive power can be generated by controlling the filter capacitor voltage as in VCM, while line current harmonics can be mitigated by regulation of DG unit line current. In this method, a resonant controller with frequency selective nature is adopted in the current control loop, which having a high gain at selected frequencies, allows accurate control of filter capacitor voltage and line current at different frequencies without

affecting each other. Moreover, in HCM, smooth transition between grid connected and islanded operation mode can be realized without generating any transient currents [66]. For the HCM, a single loop control structure with three separate parallel control branches can be adopted as follows [57],

$$V_{INV} = G_{Power}(s).(V_{ref_f} - V_c) + G_{harmonic}(s).(I_{ref_h} - I_2) + G_{damping}(s).I_1 \quad (2.5)$$

where, the first term realizes the closed loop control of filter capacitor voltage (V_c) by adopting a fundamental frequency resonant controller ($G_{power}(s)$) in the control loop, the second term realizes proper regulation of line harmonic current (I_2) in a closed loop manner by incorporating harmonic frequency resonant controller ($G_{harmonic}(s)$) in the control loop, while the third term provides necessary damping to filter resonance through a damping controller ($G_{damping}(s)$). The HCM based compensation technique can be used for reliable compensation of both the PCC voltage and local load current harmonics.

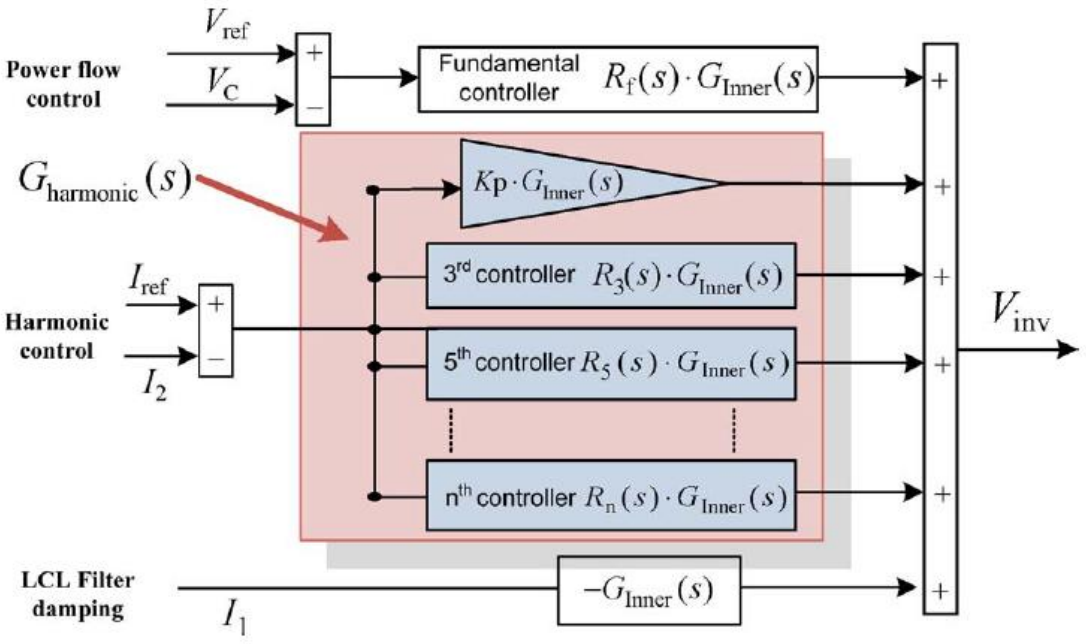

Figure 2. 21: Block diagram of HCM based harmonic compensation [66]

Another attractive feature of HCM is that, harmonic compensation is done without involving any harmonic extraction block which is particularly suitable for DG unit with low power rating and limited computational capabilities [66], [67]. The block diagram of HCM based harmonic compensation is depicted in Fig. 2.21.

2.8 Harmonic Compensation by Active Filtering Method

Active power filters (APF) are electronic devices that are mostly used in electrical power system to improve power quality as well as to compensate power unbalance. In a grid connected renewable energy system, the grid interfacing converter can be operated as active power filter which allows the improvement of power quality in the system by effective use of compensation characteristic of APF [68]. For this purpose, the converter is connected in parallel to non-linear load. The converter detects non-linear load current, which contains harmonic components of current along with the fundamental frequency current component. Due to the phase difference between harmonic current and source voltage, reactive component of power is generated and the shunt converter injects a compensating current out of phase to the non-linear load current in order to ensure unity load power factor and to make the source current from grid to be free from harmonic current [69], [70]. The compensating current is produced by comparing the load current with a pre-determined reference current. An error signal is generated by comparing the required compensating current with the actual shunt current flowing through the converter, which is used to generate appropriate gating signals for switching of converter switches. Different current control methods can be applied to track the compensating current to be injected. A shunt APF integrated with distributed generation unit is depicted in Fig. 2.22.

Active power filters can be classified mainly as shunt or series active filter based on the topology used. Shunt APFs are generally used in the load end to mitigate the current harmonics generated by the non-linear load. The applications of shunt connected APF also include reactive power and unbalanced current compensation. Series APFs are usually connected before the load in series with the ac grid, through a matching transformer. Primary applications of series APFs include elimination of voltage harmonics, compensation of grid voltage disturbances and regulation of terminal voltage of the load or line [71].

The topology, in which a combination of shunt and series APF is used, is called Unified Power Quality Conditioner (UPQC). In the UPQC topology, the parallel connected converter supplies active power to the load along with compensating current harmonics and reactive power for a solar PV system, when the sunlight is available. During the time when the sunlight is not available, the parallel connected converter only operates as reactive power and harmonic current compensator. On the other hand, the series connected converter is responsible for reduction of supply voltage fluctuation [72]. The UPQC topology can ensure high functionality but at the same time, due to incorporating large number of solid state devices, it involves high cost and complexity in control technique. Another topology, in which a combination of a series APF and a shunt passive filter is used, is called the hybrid filter. The hybrid filter can ensure reliable harmonic compensation performance in reduced cost as it involves less number of solid state devices in the active part and also of reduced size, whereas the shunt passive filter mainly takes part in eliminating lower order harmonics [73].

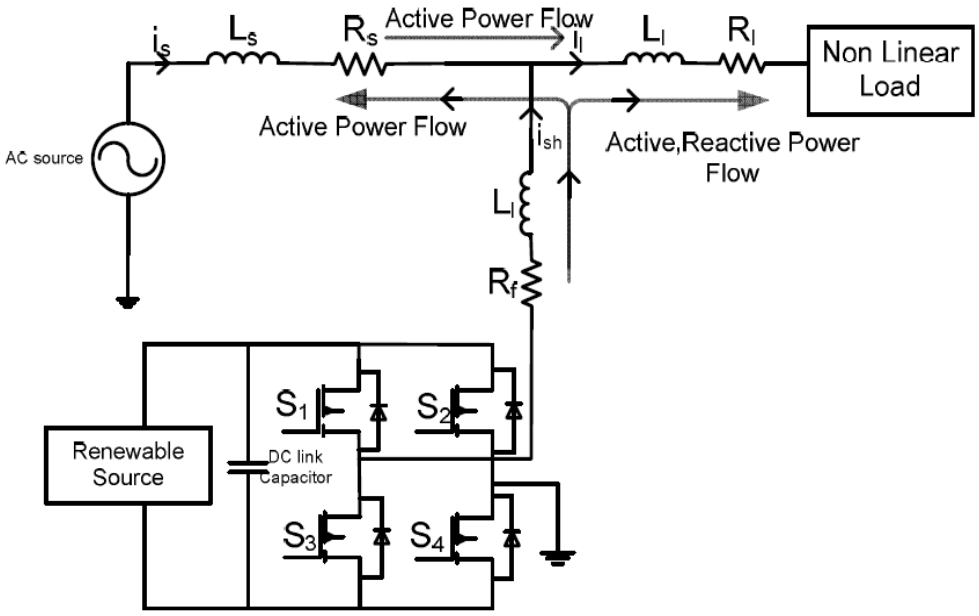

Figure 2. 22: Shunt APF integrated with distributed generation unit [69]

2.9 Control Strategies Applied to APFs

The main aim of the control strategies applied to APF is to generate an appropriate compensating current in order to cancel harmonic components of load current, which consequently makes the source current sinusoidal. For this purpose, at first the necessary voltage and current signals are sensed from different locations of the system and then, using the gathered system information, appropriate compensating signals are generated in terms of current or voltage quantity based on applied control strategy. Finally, the gating signal for converter switching is generated based on different current control techniques.

2.9.1 Control Method based on Reference Generation Techniques

Derivation of appropriate compensating signal is the most important stage of APF control and the performance of the APF mainly depends on the selection of reference generation scheme. Many

reference generation schemes either in frequency domain or in time domain are presented in different literatures for generating appropriate compensating signals.

2.9.1.1 Compensation in Frequency Domain

In the frequency domain compensation technique, Fourier Transformation of distorted voltage or current signal is done and the compensating harmonic component is extracted to generate appropriate compensating signals. To ensure a good compensation performance, the switching frequency of solid state devices in APF is to be kept at least twice the highest compensating harmonic frequency [73]. A high computation time is required for online application of Fourier transformation, which is even increased with the increase of the harmonic order to be eliminated [74]. The large response time is the main disadvantage of the frequency domain compensation technique.

2.9.1.2 Compensation in Time Domain

In the time domain compensation technique, instantaneous derivation of compensating signals is done from the harmonic polluted current or voltage signals. The time domain compensation techniques are easy to implement and requires less computation time compared to the frequency domain compensation methods.

The instantaneous active and reactive power (p-q) theory based control method is the mostly used control method for APFs in time domain. In this method, the reference current is generated such that, it ensures to maintain the required value real (p) and reactive power (q) for compensating the network. In normal operating condition of SAPF, it only compensates the alternating component of p and both the average and alternating component of q. But when sunlight is available, the load is partly supplied by the PV generator. In this case, the real power contribution of grid to load is reduced, whereas the reactive power contribution remains same, which makes

the power factor to decrease. In such situation, the average component of real power is also to be managed by the SAPF. Moreover, with the variation of sunlight amount, the active power generated by the PV generator varies, which consequently affects the power factor. Thus the compensation requirement through SAPF varies throughout the day [68]. The required p and q value to be compensated into the network can be expressed as, $P = \bar{P}_{solar} + \tilde{P}_{load}$, $q = \bar{q}_{load} + \tilde{q}_{load}$. Based on the knowledge of required power to be compensated and measured phase voltage value in *'α-β'* reference frame, the compensating current in '*α-β*' reference frame can be computed. The inverse transformation is to be done to obtain the phase current to be injected by the inverter to ensure required value of *p* and *q* for compensation. In this method, zero sequence component is neglected, so this method cannot guarantee accurate performance when the three phase system is unbalanced.

The synchronous *d-q* reference frame based method can also be applied to control the APF integrated with the PV generator as presented in [70]. In this method, the non-linear load current is considered as input signal and transformed from a-b-c frame to *d-q-0* frame by Park's transformation. The whole current in *q*-axis and AC component of *d*-axis current extracted by filtering method, are used to generate reference current for compensating harmonic current and reactive power. The phase angle value required for grid synchronization can be obtained from the phase locked loop (*PLL*). In this method, the reference generation is not affected by voltage unbalance. So, this method demonstrates reliable compensation performance also in unbalanced voltage condition [70], [75]. A block diagram of SRF based compensation algorithm is depicted in Fig. 2.23.

Several indirect methods of reference generation are presented in [76]. The main idea of indirect method is to balance system parameters, such as inductor current or capacitor voltage using

different types of controllers. Some of the literatures also suggested the use of PLL for reference generation.

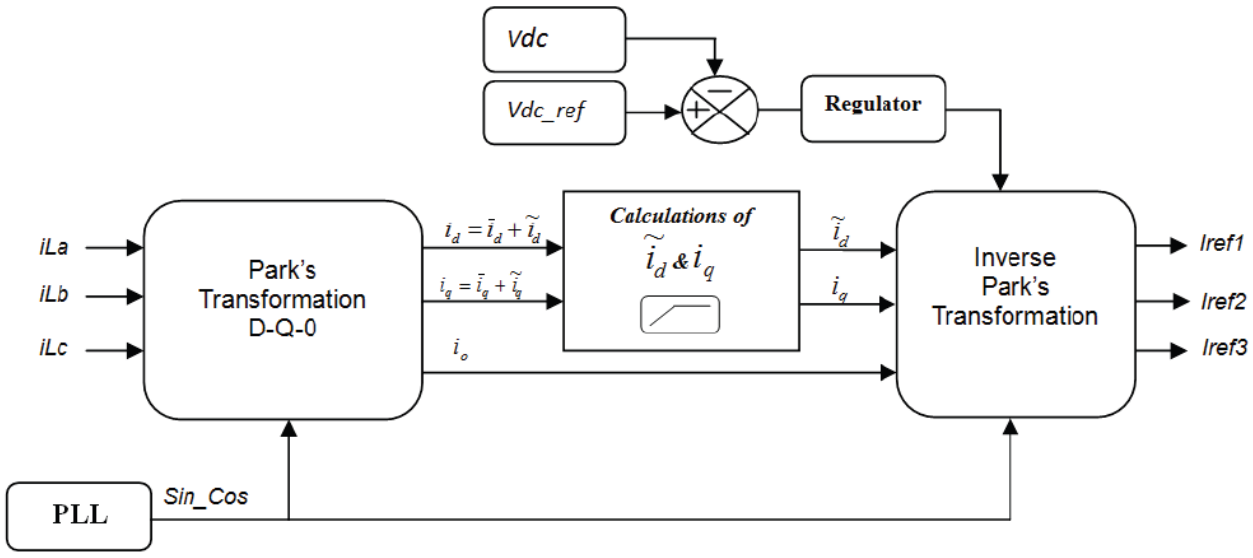

Figure 2. 23: Block diagram of SRF based compensation algorithm [70]

2.9.2 Direct Power Control Method

The Direct Power Control (DPC) method can be successfully applied in an APF based grid connected solar PV system for harmonic current and reactive power compensation as presented in [77],[78],[79]. In this method, the instantaneous values of active power (P_s) and reactive power (Q_s) can be computed using the sensed voltage and current values of the source and then compared with the reference values of active (P_{ref}) and reactive power (Q_{ref}) in hysteresis controllers. The digitized error signals generated at the output of the hysteresis controllers and line voltage vector position are used to select the appropriate voltage vector, which is then utilized as the input of the switching table, in which all the switching states of the converter is stored. By utilizing the switching table and based on the values of digitized variables, optimum switching state of the

converter can be determined. The active power reference should be generated in such a way that, it maintains a power balance between the power supplied by the source and filter and consumed by the load. To ensure a reliable harmonic current and reactive power compensation performance, the APF should supply the oscillatory component of active power and the whole reactive power to the load. For the reference generation purpose in an appropriate manner, an outer integral proportional (IP) controller is incorporated in the system, which also ensures the regulation of dc link voltage during steady state and limits the variability during transient state [77], [78]. The reference value of reactive power is set to zero for unity power factor.

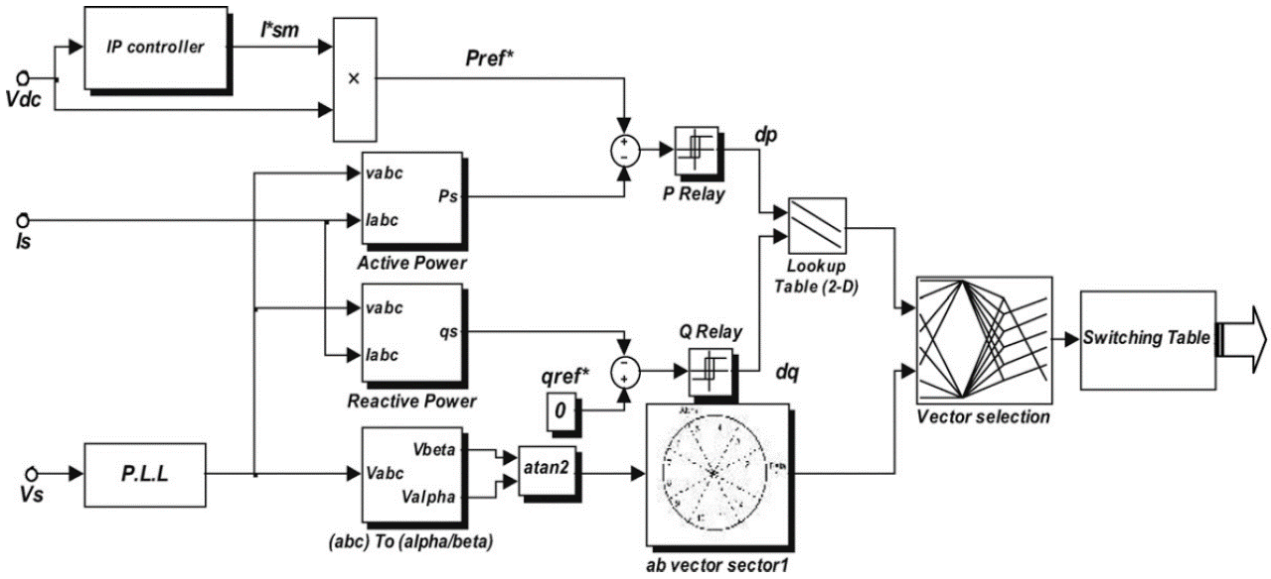

Figure 2. 24: Block scheme of DPC with source voltage sensor [78]

The DPC control algorithm is simple and easy to implement as it does not require any internal control loop of controlled variables, coordinate transformations or decoupling between active and reactive current. This control method also shows excellent performance in terms of dynamic response and harmonic and reactive power compensation. The main disadvantage of this method, which is the dependency of switching frequency on various factors, can also be overcome by

introducing space vector modulation (SVM) technique as discussed in [80]. A block diagram of DPC with voltage sensor is depicted in Fig. 2.24.

2.10 Current Control Techniques for Generation of Gating Signal to Converter for APFs

In order to obtain appropriate gating signals for switching devices of APFs based on the derived compensating commands, numerous current control techniques can be applied. The current control technique must have good tracking capability of time varying reference signal.

The Pulse Width Modulation (PWM) control technique is a widely used current control technique, which is also called linear current control technique. In this technique, a modulating signal is derived from a current regulator, which is compared to a triangular wave of same frequency, to obtain the appropriate pulse signal to control the switching pattern of the converter. This method is easy to implement and also requires small response time [74], [81].

In the hysteresis current control technique, which is suitable for medium and low voltage utility application, the inverter line current is made to track a specific sinusoidal reference current within specific error margin. By comparing the line current to the reference current, an appropriate switching signal of converter is generated. When the reference current change, the inverter line current needs to remain within the specified range of error signal. The amount of ripple present in the current injected from the inverter is directly dependent on the hysteresis band. The hysteresis current control technique is robust in nature and also has good transient response. The main disadvantage of this technique is the generation of variable switching frequency which makes it difficult to design the input filter with varying load [82]. The switching frequency can be reduced by reducing the bandwidth of the hysteresis band with the cost of increased distortion in output

current. To overcome this limitation, a variable hysteresis band constant switching frequency hysteresis controller is proposed in [76].

The Space Vector Pulse Width Modulation (*SVPWM*) based current control applied to three phase voltage source inverter (*VSI*) can also offer constant switching frequency. In *SVPWM* technique, an output voltage vector in *d-q* reference frame is generated based on which an appropriate switching combination of converter switches is determined. For a three phase VSI, there are total eight switching pattern is possible associated with a specific voltage space vector for each pattern, which divides the complex plane into six sectors as presented in Fig. 2.25. Based on the knowledge of phase angle of reference voltage vector and grid angle, the location of the reference voltage vector in complex plane and the adjacent switching state vectors can easily be determined. Using the SVPWM technique, reduction in loss and stress in switching devices is possible due to its generation of quasi optimal switching pattern [83]. The main disadvantage of this technique is its slow response due to huge computational burden.

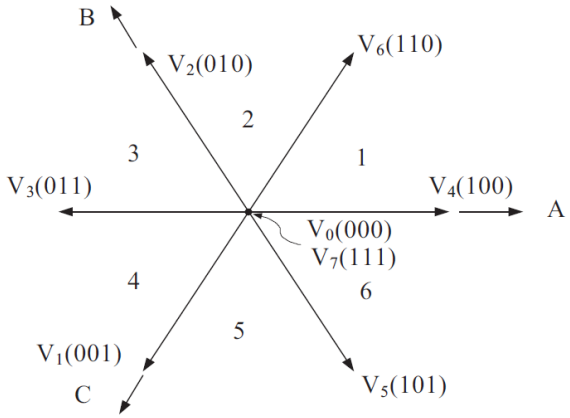

Figure 2. 25: Voltage space vectors for three phase VSI [75]

Some other useful current control techniques such as, sliding mode control, dead-beat control, fuzzy logic based control etc. are reported in different literatures [84].

2.11 Conclusion

In this paper, harmonics generated by a solar PV system are reviewed through reported field measurements and lab experiments in the literature, and the potential resonance related to LCL filter is discussed. It is found that some field testing did not allow measuring high order harmonics, the switching frequency is usually quite high for inverters, characteristic harmonics at the output of the inverters are around multiple of the switching frequency. Therefore, high order harmonic measurements must be allowed for solar PV system. More field and lab testing are needed for harmonics generated by large solar farms and small residential PV panels to facilitate better understanding of harmonics in renewable energy systems.

The control of DG interfacing converters in appropriate manner can offer an effective solution to harmonic mitigation. The advantage of this technology is cost effective, does not require any additional devices to ensure harmonic current or reactive power compensation, rather the available power rating of interfacing converters are properly utilized to provide such auxiliary services. This paper presents the state of the art of control methods for harmonic mitigation in grid connected PV system with a hope to facilitate development of more advanced control schemes in the future.

References

[1] W. Huang, M. Lu, and L. Zhang, "Survey on microgrid control strategies," *Energy Procedia [Elsevier]*, vol. 12, pp. 206-212, 2011.

[2] S. Baudoin, I. Vechiu, and H. Camblong, "A review of voltage and frequency control strategies for islanded microgrid," in *Proc. IEEE 16th Int. Conf. System theory, control and computing*, 2012, pp. 1-5.

[3] I. Chung, W. Liu, D. A. Cartes, E. G. Collins, and S. Moon, "Control methods of inverter-interfaced distributed generators in a microgrid system," *IEEE Trans. Industry Applications*, vol. 46, no. 3, pp. 1078-1088, 2010.

[4] H. Bevrani, and S. Shokoohi, "An intelligent droop control for simultaneous voltage and frequency regulation in islanded microgrids," *IEEE Trans. Smart Grid*, vol. 4, no. 3, pp. 1505-1513, 2013.

[5] W. Bai, M. R. Abedi, and K. Y. Lee, "Distributed generation system control strategies with PV and fuel cell in microgrid operation," *Control Engineering Practice [Elsevier]*, vol. 53, pp. 184-193, Feb 2016.

[6] L. Su, G. Li, and Z. Jin, "Modeling, control and testing of a voltage-source-inverter-based microgrid," in *Proc. IEEE 4th Int. Conf. Electric Utility Deregulation and Restructuring and Power Technologies*, 2011, pp. 724-729.

[7] N. Merritt, C. Chakraborty, and P. Bajpai, "New voltage control strategies for VSC based DG units in an unbalanced microgrid," *IEEE Trans. Sustainable Energy*, to be published.

[8] B. M. Delghavi and A. Yazdani, "A unified control strategy for electronically interfaced distributed energy resources," *IEEE Trans. Power Delivery*, vol. 27, no. 2, pp. 803-812, Apr 2012.

[9] M. Mao, Z. Dong, Y. Dong, H. Huang, and L. Chang, "Parameters sensitivity analysis of the controller based on unified control strategy in a photovoltaic microgrid," in *Proc. IEEE 5th Int. Symposium Power Electronics for Distributed Generation System*, 2014, pp. 1-8.

[10] Y. Li, D. M. Vilathgamuwa, and P. C. Loh, "Design, analysis, and real-time testing of a controller for multibus microgrid system," *IEEE Trans. power electronics*, vol.19, no. 5, pp. 1195-1204, Sept 2004.

[11] Y. Deng, Y. Tao, G. Chen, G. Li, and X. He, "Enhanced power flow control for grid-connected droop-controlled inverters with improved stability," *IEEE Trans. Industrial Electronics*, to be published.

[12] S. Bhattacharya and S. Mishra, "Efficient power sharing approach for photovoltaic generation based microgrids," *IET Renewable Power Generation*, vol. 10, no. 7, pp. 973-987, Jul 2016.

[13] Hans-Peter Beck, and Ralf Hesse, "Virtual Synchronous Machine" 2007 9th International Conference on Electrical Power Quality and Utilisation, pp. 1-6, 2007.

[14] Pablo F. Frack, Pedro E. Mercado, and Marcelo G. Molina, “Extending the VISMA Concept to Improve the Frequency Stability in Microgrids”, 2015 18th International Conference on Intelligent System Application to Power Systems (ISAP), pp. 1-6, 2015.

[15] Igor Cvetkovic, Dushan Boroyevich, Rolando Burgos, Chi Li, Marko Jaksic, and Paolo Mattavelli, “Modeling of a Virtual Synchronous Machine-Based Grid-Interface Converter for Renewable Energy Systems Integration”, 2014 IEEE 15th Workshop on Control and Modeling for Power Electronics (COMPEL), pp. 1-7, 2014.

[16] Y. V. Pavan Kumar, and Ravikumar Bhimasingu, “Improving Resiliency in Renewable Energy Based Green Microgrids Using Virtual Synchronous Machines Controlled Inverter”, 2015 IEEE Innovative Smart Grid Technologies - Asia (ISGT ASIA), pp. 1-6, 2015.

[17] Ujjwol Tamrakar, David Galipeau, Reinaldo Tonkoski, and Indraman Tamrakar, “Improving Transient Stability of Photovoltaic-Hydro Microgrids Using Virtual Synchronous Machines”, IEEE Eindhoven PowerTech, 2015, pp. 1-6, 2015.

[18] G. Delille, B. Francois, and G. Malarange, “Dynamic frequency control support by energy storage to reduce the impact of wind and solar generation on isolated power system's inertia”, IEEE Transactions on Sustainable Energy, vol. 3, pp. 931-939, 2012.

[19] Vu Van Thong, Achim Woyte, Mihaela Albu, Marcel Van Hest, Jan Bozelie, Javier Diaz, Tom Loix, Dan Stanculescu, and Klaas Visscher, “Virtual Synchronous Generator: Laboratory Scale Results and Field Demonstration”, 2009 IEEE Bucharest PowerTech, pp. 1-6, 2009.

[20] J. Driesen, and K. Visscher, “Virtual Synchronous Generators”, 2008 IEEE Power and Energy Society General Meeting - Conversion and Delivery of Electrical Energy in the 21st Century, pp. 1-3, 2008.

[21] Miguel Torres, and Luiz A. C. Lopes, “Virtual Synchronous Generator Control in Autonomous Wind-Diesel Power Systems”, 2009 IEEE Electrical Power & Energy Conference (EPEC), pp. 1-6, 2009.

[22] M. Albu, J. Diaz, V. Thong, R. Neurohr, D. Federenciuc, M. Popa, and M. Calin, “Measurement and Remote Monitoring for Virtual Synchronous Generator Design”, 2010 IEEE International Workshop on Applied Measurements For Power Systems (AMPS), pp. 7-11, 2010.

[23] VSYNC Project, “Virtual Synchronous Machines (VSG's) For Frequency Stabilisation In Future Grids With A Significant Share Of Decentralized Generation”. http://www.vsync.eu/ , visited at 1:25 pm on July 30, 2016.

[24] K. Sakimoto, Y. Miura, and T. Ise, “Stabilization of a Power System with a Distributed Generator by a Virtual Synchronous Generator Function”, 2011 IEEE 8th International Conference on Power Electronics and ECCE Asia (ICPE & ECCE), pp. 1498 – 1505, 2011.

[25] Toshinobu Shintai, Yushi Miura, and Toshifumi Ise, “Oscillation Damping of a Distributed Generator Using a Virtual Synchronous Generator”, IEEE Transactions on Power Delivery, Vol. 29, No. 2, pp. 668 – 676, 2014.

[26] Jinhua Wang, Yuxiang Wang, Yunjie Gu, Wuhua Li, and Xiangning He, “Synchronous Frequency Resonance of Virtual Synchronous Generators and Damping Control”, 2015 9th International Conference on Power Electronics and ECCE Asia (ICPE-ECCE Asia), pp. 1011 – 1016, 2015.

[27] Chi Li, Rolando Burgos, Igor Cvetkovic, Dushan Boroyevich, Lamine Mili, and Pedro Rodriguez, “Analysis and Design of Virtual Synchronous Machine Based STATCOM Controller”, 2014 IEEE 15th Workshop on Control and Modeling for Power Electronics (COMPEL), pp. 1-6, 2014.

[28] Chi Li, Rolando Burgos, Igor Cvetkovic, Dushan Boroyevich, and Lamine Mili, “Design, Analysis and Experimental Evaluation of a Virtual-Synchronous-Machine-Based STATCOM with LCL Filter”, 2015 IEEE Energy Conversion Congress and Exposition (ECCE), pp. 5771 – 5778, 2015.

[29] Jia Liu, Yushi Miura, and Toshifumi Ise, “Dynamic Characteristics and Stability Comparisons between Virtual Synchronous Generator and Droop Control in Inverter-Based

Distributed Generators", 2014 International Power Electronics Conference (IPEC-Hiroshima 2014 - ECCE ASIA), pp. 1536 – 1543, 2014.

[30] Salvatore D'Arco, and Jon Are Suul, "Virtual Synchronous Machines — Classification of Implementations and Analysis of Equivalence to Droop Controllers for Microgrids", 2013 IEEE Grenoble PowerTech (POWERTECH), pp. 1-7, 2013.

[31] Salvatore D'Arco, and Jon Are Suul, "Equivalence of Virtual Synchronous Machines and Frequency-Droops for Converter-Based MicroGrids", IEEE Transactions on Smart Grid, Vol. 5, No. 1, pp. 394-395, 2014.

[32] Yan Du, J. M. Guerrero, Liuchen Chang, Jianhui Su, and Meiqin Mao, "Modeling, Analysis, and Design of a Frequency-Droop-Based Virtual Synchronous Generator for Microgrid Applications", 2013 IEEE ECCE Asia Downunder (ECCE Asia), pp. 643 – 649, 2013.

[33] Jaber Alipoor, Yushi Miura, and Toshifumi Ise, "Power System Stabilization Using Virtual Synchronous Generator With Alternating Moment of Inertia", IEEE Journal of Emerging and Selected Topics in Power Electronics, Vol. 3, No. 2, pp. 451 – 458, 2015.

[34] Miguel A. Torres L., Luiz A. C. Lopes, Luis A. Morán T., and José R. Espinoza C, "Self-Tuning Virtual Synchronous Machine: A Control Strategy for Energy Storage Systems to Support Dynamic Frequency Control", IEEE Transactions on Energy Conversion, Vol. 29, No. 4, pp. 833 – 840, 2014.

[35] K. Visscher, and S. W. H. De Haan, "Virtual Synchronous Machines (VSG's) for Frequency Stabilisation in Future Grids with a Significant Share of Decentralized Generation", 2008 SmartGrids for Distribution, IET-CIRED, CIRED Seminar, pp 1-4, 2008.

[36] Chi Li, Rolando Burgos, Igor Cvetkovic, Dushan Boroyevich, Lamine Mili, and Pedro Rodriguez, “Evaluation and Control Design of Virtual-Synchronous-Machine-Based STATCOM for Grids with High Penetration of Renewable Energy”, 2014 IEEE Energy Conversion Congress and Exposition (ECCE), pp. 5652 – 5658, 2014.

[37] Chi Li, Rolando Burgos, Igor Cvetkovic, and Dushan Boroyevich, “Active and Reactive Power Flow Analysis of a STATCOM with Virtual Synchronous Machine Control”, 2015 IEEE 16th Workshop on Control and Modeling for Power Electronics (COMPEL), pp. 1-8, 2015.

[38] Anastasios Tzavellas, Phuong Nguyen, Paulo Ribeiro, and Wil Kling, “A Game Theory Approach for Coordinating Multiple Virtual Synchronous Generators”, 2013 IEEE Grenoble PowerTech (POWERTECH), pp. 1-6, 2013.

[39] Yong Chen, Ralf Hesse, Dirk Turschner, and Hans-Peter Beck, “Improving the Grid Power Quality Using Virtual Synchronous Machines”, 2011 International Conference on Power Engineering, Energy and Electrical Drives (POWERENG), pp. 1-6, 2011.

[40] Yong Chen, Ralf Hesse, Dirk Turschner, and Hans-Peter Beck, “Investigation of the Virtual Synchronous Machine in the Island Mode”, 2012 3rd IEEE PES Innovative Smart Grid Technologies Europe (ISGT Europe), pp. 1-6, 2012.

[41] Jaber Alipoor, Yushi Miura, and Toshifumi Ise, “Voltage Sag Ride-Through Performance of Virtual Synchronous Generator”, 2014 International Power Electronics Conference (IPEC-Hiroshima 2014 - ECCE ASIA), pp. 3298 – 3305, 2014.

[42] Salvatore D'Arco, Jon Are Suul, and Olav B. Fosso, “Small-signal modelling and parametric sensitivity of a Virtual Synchronous Machine”, 2014 Power Systems Computation Conference (PSCC), pp. 1-9, 2014.

[43] Salvatore D'Arco, and Jon Are Suul, “A Synchronization Controller for Grid Reconnection of Islanded Virtual Synchronous Machines”, 2015 IEEE 6th International Symposium on Power Electronics for Distributed Generation Systems (PEDG), pp. 1-8, 2015.

[44] Rafael Pena-Alzola, David Campos-Gaona, and Martin Ordonez, “Control of Flywheel Energy Storage Systems as Virtual Synchronous Machines for Microgrids”, 2015 IEEE 16th Workshop on Control and Modeling for Power Electronics (COMPEL), pp. 1-7, 2015.

[45] Y. Hirase, O. Noro, K. Sugimoto, K. Sakimoto, Y. Shindo, and T. Ise Osaka, “Effects and Analysis of Suppressing Frequency Fluctuations in Microgrids Using Virtual Synchronous Generator Control”, 41st Annual Conference of the IEEE Industrial Electronics Society, IECON 2015, pp. 43-49, 2015.

[46] A. Chidurala, T. K. Saha, N. Mithulananthan, and R. C. Bansal, "Harmonic emissions in grid connected PV systems: A case study on a large scale rooftop PV site," in *Proc. IEEE PES General Meeting, Conference & Exposition,* 2014, pp. 1-5.

[47] J. He, M. S. Munir, and Y. W. Li, "Opportunities for power quality improvement through DG-grid interfacing converters," in *Proc. IEEE Int. Power Electronics Conference,* 2010, pp. 1657-1664.

[48] X. Liang, “Emerging power quality challenges due to integration of renewable energy sources”, *IEEE Trans. Industry Applications,* vol. 53, no. 2, pp. 855-866, 2017.

[49] M. A. Awadallah, B. Venkatesh, and B. N. Singh, “Impact of solar panels on power quality of distribution networks and transformers”, *Canadian Journal of Electrical and Computer Engineering,* vol. 38, no. 1, pp. 45-51, 2015.

[50] R. K. Varma, S. A. Rahman, T. Vanderheide, and M. D. N. DANG, “Harmonic impact of a 20-MW PV solar farm on a utility distribution network”, *IEEE Power and Energy Technology Systems Journal,* vol. 3, no. 3, pp. 89-98, 2016.

[51] R. Langella, A. Testa, J. Meyer, F. Möller, R. Stiegler, and S. Z. Djokic, “Experimental-based evaluation of PV inverter harmonic and interharmonic distortion due to different operating conditions”, *IEEE Trans. Instrumentation and Measurement,* vol. 65, no. 10, pp. 2221-2233, 2016.

[52] R. Torquato, W. Freitas, G. R. T. Hax, A. R. Donadon, and R. Moya, “High frequency harmonic distortions measured in a Brazilian solar farm”, *2016 17th International Conference on Harmonics and Quality of Power (ICHQP),* pp. 623 – 627, 2016.

[53] R. K. Varma, and M. Salama, “Large-Scale Photovoltaic Solar Power Integration in Transmission and Distribution Networks”, *2011 IEEE Power and Energy Society General Meeting*, pp. 1-4, 2011.

[54] X. Liang, and R. Adedun, “Load harmonics analysis and mitigation”, 48th IEEE Industrial & Commercial Power Systems Conference, pp. 1-8, 2012.

[55] H. Hu, Q. Shi, Z. He, J. He, and S. Gao, “Potential harmonic resonance impacts of PV inverter filters on distribution systems”, *IEEE Trans. Sustainable Energy*, vol. 6, no. 1, pp. 151-161, 2015.

[56] O. S. Nduka, and B. C. Pal, “Harmonic Domain Modeling of PV System for the Assessment of Grid Integration Impact”, *IEEE Trans. Sustainable Energy,* vol. 8, no. 3, pp. 1154-1165, 2017.

[57] J. He and Y. W. Li, "Generalized microgrid harmonic compensation strategies using DG unit interfacing converters," in *Proc. IEEE Industrial Electronics Society Annual Conference,* 2012, pp. 3419-3424.

[58] Y. W. Li and J. He, "Distribution system harmonic compensation methods: An overview of DG-interfacing inverters," *IEEE Industrial Electronics Magazine*, vol. 8, no. 4, pp. 18-31, Dec 2014.

[59] J. He, Y. W. Li, X. Wang, and F. Blaabjerg, "An improved current control scheme for grid-connected DG unit based distribution system harmonic compensation," in *Proc. IEEE 28th Annual Applied Power Electronics Conference and Exposition,* 2013, pp. 986-991.

[60] R. Teodorescu, F. Blaabjerg, and M. Liserre, "Proportional-resonant controllers. A new breed of controllers suitable for grid-connected voltage-source converters," in *Proc. OPTIM,* 2004, pp. 9-14.

[61] F. Blaabjerg, R. Teodorescu, M. Liserre, and A. V. Timbus. "Overview of control and grid synchronization for distributed power generation systems," *IEEE Trans. Industrial Electronics,* vol. 53, no. 5, pp. 1398-1409, Oct 2006.

[62] J. He, Y. W. Li, and M. S. Munir, "A flexible harmonic control approach through voltage-controlled DG–grid interfacing converters," *IEEE Trans. Industrial Electronics,* vol. 59, no. 1, pp. 444-455, Jan 2012.

[63] J. He, Y. W. Li, F. Blaabjerg, and X. Wang, "Active harmonic filtering using current-controlled, grid-connected DG units with closed-loop power control," *IEEE Trans. Power Electronics,* vol.29, no. 2, pp. 642-653, Feb 2014.

[64] S. Munir and Y. W. Li, "Residential distribution system harmonic compensation using PV interfacing inverter," *IEEE Trans. Smart Grid,* vol. 4, no. 2, pp. 816-827, Jun 2013.

[65] M. S. Munir, and Y. W. Li, "Harmonic compensation using residential PV interfacing inverter," in *Proc. IEEE Industrial Electronics Society 38th Annual Conference,* 2012, pp. 5324-5329.

[66] J. He and Y. W. Li, "Hybrid voltage and current control approach for DG-grid interfacing converters with LCL filters," *IEEE Trans. Industrial Electronics,* vol. 60, no. 5, pp. 1797-1809, May 2013.

[67] J. He, Y. W. Li, and F. Blaabjerg, "Flexible microgrid power quality enhancement using adaptive hybrid voltage and current controller," *IEEE Trans. Industrial Electronics,* vol. 61, no. 6, pp. 2784-2794, Jun 2014.

[68] D. H. Pontoriero and P. E. Mercado, "Network compensation with active power filters integrated to PV generation," in *Proc. IEEE Porto Power Tech,* 2001, pp. 1-6.

[69] P. Agarwal and R. Gupta, "Grid integration of solar PV power using shunt connected VSC," in *Proc. IEEE Conf. Engineering and Systems*, 2013, pp. 1-6.

[70] R. Belaidi, M. Hatti, A. Haddouche, and M. Mghezzi Larafi, "Shunt active power filter connected to a photovoltaic array for compensating harmonics and reactive power simultaneously," in *Proc. IEEE 4th Int. Conf. Power Engineering, Energy and Electrical Drives,* 2013, pp. 1482-1486.

[71] R. A. Mastromauro, M. Liserre, and A. Dell'Aquila, "Single-phase grid-connected photovoltaic systems with power quality conditioner functionality," in *Proc. IEEE European Conf. Power Electronics and Applications*, 2007, pp. 1-11.

[72] M. C. Cavalcanti, G. M. S. Azevedo, B. A. Amaral, and F. A. S. Neves, "A photovoltaic generation system with unified power quality conditioner function," in *Proc. IEEE 31st Industrial Electronics Society Annual Conference,* 2005, pp. 1-6.

[73] B. Singh, K. A. Haddad, and A. Chandra, "A review of active filters for power quality improvement," *IEEE Trans. Industrial Electronics,* vol. 46, no.5, pp. 960-971, Oct 1999.

[74] D. Chen and S. Xie, "Review of the control strategies applied to active power filters," in *Proc. IEEE Int. Conf. Electric Utility Deregulation, Restructuring and Power Technologies*, 2004, pp. 666-670.

[75] N. Mendalek and K. A. Haddad, "Modeling and nonlinear control of shunt active power filter in the synchronous reference frame," in *Proc. IEEE 9th Int. Conf. Harmonics and Quality of Power,* 2000, pp. 30-35.

[76] Q. Yao and D. G. Holmes, "A simple, novel method for variable-hysteresis-band current control of a three phase inverter with constant switching frequency," in *Proc. IEEE Industry Applications Society 28th Annual Meeting,* 1993, pp. 1122-1129.

[77] A. Chaoui, F. Krim, J. Gaubert, and L. Rambault, "DPC controlled three-phase active filter for power quality improvement," *Int. Journ. Electrical Power & Energy Systems,* vol. 30, no. 8, pp. 476-485, Oct 2008.

[78] A. Chaoui, J. Gaubert, and F. Krim, "Power quality improvement using DPC controlled three-phase shunt active filter," *Electric Power Systems Research*, vol. 80, no. 6, pp. 657-666, Jun 2010.

[79] A. Boukezata, A. Chaoui, J. P. Gaubert, and M. Hachemi, "Improving the quality of energy in grid connected photovoltaic systems," in *Proc. IEEE 3rd Int. Conf. Systems and Control,* 2013, pp. 1122-1126.

[80] S. Saidi, R. Abbassi, and S. Chebbi, "Power quality improvement using VF-DPC-SVM controlled three-phase shunt active filter," in *Proc. IEEE 12th Int. Conf. Systems, Signals & Devices,* 2015, pp. 1-5.

[81] H. A. Kazem, “Harmonic Mitigation Techniques Applied to Power Distribution Networks,” *Advances in Power Electronics*, vol. 2013, pp. 1-10, Jan 2013.

[82] R. Sunny and R. Anto, "Harmonics control and performance analysis of a grid connected photovoltaic system," in *Proc. IEEE Int. Conf. Advanced Computing and Communication Systems*, 2013, pp. 1-6.

[83] H. Zhang, H. Zhou, J. Ren, W. Liu, S. Ruan, and Y. Gao, "Three-phase grid-connected photovoltaic system with SVPWM current controller," in *Proc. IEEE 6th Int. Power Electronics and Motion Control Conference*, 2009, pp. 2161-2164.

[84] M. Hojabri, A. Z. Ahmad, A. Toudeshki, and M. Soheilirad, "An overview on current control techniques for grid connected renewable energy systems," *Int. Proceedings Computer Science and Information Technology*, vol. 56, pp. 119-126, 2012.

Chapter 3

Determine Q-V Characteristics of Grid Connected Wind Farms for Voltage Control Using Data Driven Analytics Approach

[1]Chowdhury Andalib-Bin-Karim, *Student Member, IEEE*, [1]Xiaodong Liang, *Senior Member, IEEE*, [2]Nahidul Khan, [3]Huaguang Zhang, *Fellow, IEEE*

[1]Faculty of Engineering and Applied Science, Memorial University of Newfoundland, St. John's, Newfoundland, Canada.

[2]System Operation & Planning, Energy Control Center, Newfoundland and Labrador Hydro, St. John's, Newfoundland, Canada.

[3]College of Information Science and Engineering, Northeastern University, Shenyang, Liaoning, China.

A version of this chapter has been published in the *IEEE Transactions on Industry Applications, September/October 2017*. The author of this manuscript Chowdhury Andalib-Bin-Karim developed this work under the supervision of Dr. Xiaodong Liang. Mr. Karim's contribution to this paper is as follows:

- Performed all literature searches required for background information.
- Developed all the codes and performed analysis in MATLAB.
- Analyzed the results.
- Wrote the paper.

Dr. Xiaodong Liang provided continuous technical guidance, checked the results, reviewed the manuscript, provided important suggestions to accomplish the work, and modified final version of the manuscript. Dr. N. Khan provided with the data used for the analysis, Dr. H. Zhang reviewed the manuscript and provided expert opinion to improve the work. In this chapter, the manuscript is presented with altered figure numbers, table numbers and reference formats in order to match the thesis formatting guidelines set out by Memorial University of Newfoundland.

Abstract- Due to varying and intermittent nature of wind resource, grid connected wind farms pose significant technical challenges to power grid on power quality and voltage stability. Wind farm Q-V characteristic curve at the point of interconnection (POI) can offer valuable information for voltage control actions and provide essential indication about voltage stability. Data driven analytics is a promising approach to determine characteristics of a large complex system, physical model of which is difficult to obtain. In this paper, the data driven analytics is used to determine Q-V curve of grid connected wind farms based on measurement data recorded at the POI. Different curve fitting models, such as Polynomial, Gaussian and Rational, are evaluated and best fit is determined based on different graphical and numerical evaluation metrics. A case study is conducted using field measurement data at two grid connected wind farms currently in operation in Newfoundland and Labrador, Canada. It is found that the Gaussian (degree 2) model describes the Q-V relationship most accurately for the two wind farms. The obtained functions and processed data can be used in the voltage controller design. The plotted Q-V curve can also be used to determine the reactive margin at the POI for voltage stability evaluation. As a generic method, the proposed approach can be employed to determine Q-V characteristic curve of any grid connected large wind farms.

Keywords- Curve fitting, data driven analytics, power quality, Q-V curve, voltage fluctuation, voltage stability, wind farms

3.1 Introduction

With the increasing desire to achieve electricity generation in an environmental friendly way, the development of renewable energy has received great attention in recent years as renewable resources are pollution free and abundant in nature. Among all renewable power generation, grid connected high capacity wind farms have experienced rapid growth mainly due to technological advancement of large wind turbine generators and high capacity power converters. The increased amount of wind energy integration into power grid can cause deterioration of grid power quality and system stability [1, 2].

The power quality issues can be categorized into two basic categories: disturbances and steady state variations. The transient and RMS voltage variations under short circuit faults fall into the disturbance category. The RMS voltage variation, frequency deviation, and harmonic distortion under normal operating conditions, which are usually measured based on sampling of current and/or voltage over time, belong to the steady state variations category [3].

Power quality indices include voltage unbalance, voltage harmonics, voltage fluctuation, and flicker. Voltage fluctuation for grid connected wind farms under normal operating condition belongs to the long duration steady state voltage variation category, which can be harmful for sensitive loads. This type of variation is a common phenomenon usually caused by continuous change of loads in a power system. For wind power generation, wind speed variation throughout the day leads to output power fluctuation of the wind turbine and voltage fluctuation at the POI [4].

For large grid connected wind farms, to keep the voltage fluctuation within the acceptable range defined by utility grid code, voltage regulation is typically employed [5]. The voltage regulation can be achieved by decentralized control of reactive power in each distributed generation unit. The voltage droop control method can be employed in grid interfacing converters to control reactive power flow to the grid [6]. To implement such control mechanism, a slope in droop characteristics is needed to be set which governs the relation between the system voltage and reactive power output variation. A proportional control mechanism for grid interfacing inverters is reported in [7], and it consists of four control modes, each control mode utilizes a set of piecewise linear relationships between reactive power and voltage to realize reactive power control. The prior knowledge of the configuration and parameters of wind farms is essential to accurately estimate the relationship between the injected power to the grid and voltage fluctuation at the POI [8]. However, with the increased system complexity level, obtaining such prior knowledge of wind farms sometimes can be difficult.

The data driven analytics has become a popular approach for a complex large scale system modeling, where the physical model is difficult to obtain [9-12]. Using this approach, the system performance can be assessed accurately under different operating conditions, and the proper decision making for the system's operation and control becomes possible [9]. In [10], a data driven framework has been developed to assess the performance of a residential PV system with the variation of weather conditions and other environmental factors. This approach is beneficial to the PV users for characterizing PV system's performance as the users don't have to rely on the benchmarked PV system results, which are obtained under standard testing conditions and largely vary under practical conditions. In [11], a data analytics based control mechanism has been

proposed, where a neuro-fuzzy controller is employed to regulate the frequency of a diesel-PV based AC micro-grid system in both grid connected and off grid modes of operation.

Among various reported voltage control schemes for wind farms, using the Q-V characteristic curve for the controller design appears to be a new and effective approach [13, 14]. It is well known that a Q-V curve serves as a voltage stability evaluation tool in conventional power systems [15, 16]. Therefore, a Q-V curve at the POI of wind farms can also be used to evaluate power system stability.

In literatures, different ways of determining Q-V characteristic curve are utilized for different purposes. In [17], the desired busbar static Q-V characteristic of a steam power plant (SPP) is used to define static performance of a coordinated Q-V controller for the SPP. The natural Q-V static characteristic of SPP is defined as a straight line with slope equal to the natural droop characteristic (X_{droop}), which is calculated based on an equivalent circuit model of SPP incorporating both the equivalent droop reactance and the step-up transformer leakage reactance. The desired Q-V static characteristic based on which the Q-V controller is implemented is expressed as follows [17]:

$$V_{HV} = V_{HVref} - X_{droopSPP} * \sum Q_i \tag{3.1}$$

where, V_{HV} is the HV busbar voltage, V_{HVref} is the reference value of the busbar voltage, $X_{droopSPP}$ is the desired HV busbar droop preset in the controller and $\sum Q_i$ is the total reactive power delivered to the HV busbar. In [18], voltage stability issue of grid connected wind farm is discussed, which is largely dependent on the type of wind generator used. The Q-V characteristic of grid connected wind farm is reported to vary as well depending on the type of wind generator. For example, the reactive power drawn by the squirrel cage induction generator (SCIG) from grid varies with the square of voltage according to Equation (3.2), where, X_{m} and X_{l} are the magnetising and leakage

reactance, respectively. *V* and *I* are terminal voltage and current of the SCIG. However, the reactive power drawn by a doubly fed induction generator (DFIG) does not follow above Q-V characteristic [18]. The rotor side converter (RSC) magnetizes the DFIG, the reactive power (Q_m) required for magnetization can be expressed as Equation (3.3), where, V_S is the stator terminal voltage and X_m is the magnetizing reactance. The RSC supplies reactive power according to its rated capacity to meet the voltage regulation requirement. The reactive power supplied by the stator (Q_s) and rotor of DFIG (Q_r) can be expressed as Equation (3.4), where, *S* is the slip of the generator.

$$Q_{gen} = {V^2}/{X_m} + 3I^2X_l \tag{3.2}$$

$$Q_m = 3V_s^2/2X_m \tag{3.3}$$

$$Q_s = Q_m + Q_r/s \tag{3.4}$$

An adaptive Q-V scheme is proposed in [13] for voltage control in DFIG based wind power plant (WPP). In this control scheme, an adaptive Q-V characteristics is adopted in the WPP controller which allows the DFIG with higher reactive power capability to inject more reactive power, thus improving the transient voltage recovery performance of the WPP. Different localized and centralized reactive power control methods for PV inverter are discussed in [19]. The localized methods are applied based on droop control mechanism for reactive power management of PV inverters and utilizes Q-V characteristic at PV connection point. In this method, the PV inverter absorbs reactive power when voltage at PV connection point exceeds the value specified according to the Q-V characteristic curve. Mainly deterministic approaches are adopted in different literatures to ascertain Q-V characteristic curve. As per authors' knowledge, there exists no literature which adopts data analytics approach to determine Q-V characteristic curve for grid connected wind farms.

Although the Q-V characteristic curve at the POI of a wind farm can provide valuable information for voltage control actions and voltage stability evaluation, only very limited research has been conducted on utilizing Q-V curve in wind farm's operation and control. The first question needs to be answered in order to implement Q-V curve to improve power quality and voltage stability is: how to determine a Q-V curve at the POI of a grid-connected wind farm. To answer this question, a data driven analytics approach based on the curve fitting procedure is employed to determine a Q-V curve of wind farms in this paper. The curve fitting method is adopted to derive a Q-V curve using field measurement data recorded at the POI. Different curve fitting models are evaluated and the best fitted model is determined based on different graphical and numerical evaluation metrics.

The paper is arranged as follows: potential applications of the developed Q-V curves at the POI of grid-connected wind farms are discussed in Section 3.2; curve fitting procedure and goodness of fit evaluation to determine the Q-V curve are presented in Sections 3.3 and 3.4, respectively; in Section 3.5, two case studies are conducted to create Q-V curves for two wind farms currently in operation in Newfoundland; conclusions are drawn in Section 3.6.

3.2 Applications of Q-V Characteristic Curve - Voltage Control and Voltage Stability

The developed Q-V curve in this paper can be used for 1) voltage control scheme design; and 2) voltage stability evaluation.

3.2.1 Voltage Control

Reference [13] utilizes a fixed Q–V characteristic curve for a wind farm controller design, and the Q-V curve is used to generate the reactive power reference, Q_{ref}, for voltage control purpose. This curve has the maximum and minimum reactive power capabilities of 33% of the rated power, and the slope of the Q–V characteristics was set to a fixed value of 6.6 as shown in Fig. 3.1. However, it is not very accurate to use a fixed Q-V characteristic to design voltage controller for any wind farm, the adaptive Q–V characteristic is proposed in the control scheme in [13].

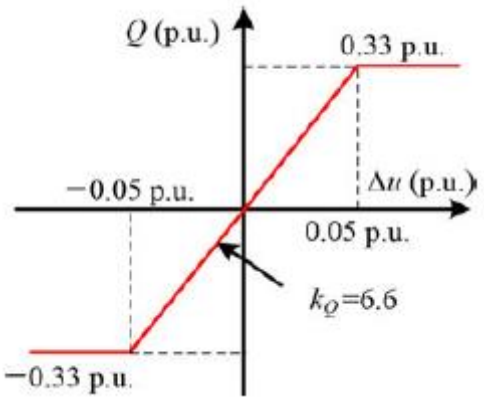

Figure 3. 1: The fixed Q-V characteristic curve used in the voltage controller to generate the reactive power reference, Qref [13].

To further advance this research direction, a method to determine a Q-V characteristic curve for a particular wind farm using the data driven analytics approach is proposed in this paper. The developed Q-V curve can be used to generate a more accurate reactive power reference for the voltage controller design.

The Q-V curve can be developed using measured data during various time windows. For example, monthly Q-V curves over a year can be created using historical measurement data to reflect seasonable changes.

3.2.2 Voltage Stability

The developed Q-V curve reveals important information about the system voltage stability. For a given Q-V curve, the sensitivity, $\partial Q/\partial V$, of reactive power with respect to bus voltage is the slope of the Q-V curve at the operating point, which indicates the voltage stability [15].

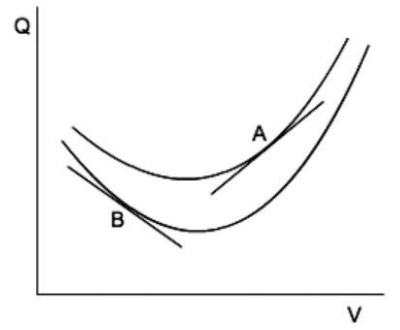

(a)

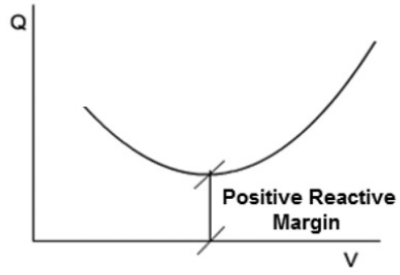

(b)

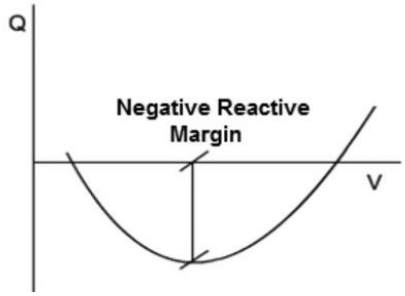

(c)

Figure 3. 2: The Q-V curve: (a) unstable and stable regions associated with a Q-V curve [16]; (b) the positive reactive margin [16]; (c) the negative reactive margin [16].

As shown in Fig. 3.2, the stable operating region is located to the right ($\partial Q/\partial V > 0$) of the minimal point (which is also called the nose of the Q-V curve, where $\partial Q/\partial V = 0$), while the

unstable region is located to the left ($\partial Q/\partial V < 0$) of the minimal point. For example, the point A is in the stable region, and the point B is in the unstable region. The reactive margin is the distance between the minimal point and the V-axis in the Q-V curve, and it can be either positive (Fig. 3.2 (b)), or negative (Fig. 3.2(c)). Contingencies close to buses with a positive reactive margin are severe, and tend to drive the system to instability; while a negative reactive margin leads to a more stable system [16].

When using a Q-V curve for voltage stability evaluation, each curve should correspond to a fixed real power *P* (load level). The higher the load (real power *P* value), the smaller is the negative reactive margin. The Q-V curve moves up as the load level increases [15, 16].

In the case study of this paper, the developed Q-V curve is not for a fixed load because the duration is a month, but this Q-V curve can be easily modified for a fixed load using a much shorter measurement duration, where the real power remains constant.

3.3 Curve Fitting Procedure to Obtain a Q-V Curve

The curve fitting procedure is employed in this paper to determine a mathematical relationship between the measured values of reactive power (*Q*) and the generated voltage (*V*) at the POI of a wind farm. A curve fitting method helps to understand the relation between data variables by fitting an appropriate curve to measured data points. A mathematical function representing the reactive power *Q* as a function of the generated voltage *V*, $Q = f(V)$, can be derived from the fitted curve.

There are different curve fitting models available such as Linear, Exponential, Polynomial, Gaussian. The model parameters should be determined such that, the residual value (difference between measured value and calculated value using the function) is close to zero. The Least Square method is a very common and popular method to determine the model parameters with a minimum

residual error. Other than data extrapolation, there are some other application of curve fitting method can be seen such as, data smoothing, interpolation, noise reduction, error compensation etc [20, 21].

In this paper, different curve fitting methods available in MATLAB are evaluated and the best fitted model is determined to correctly represent the relation between the reactive power and voltage. Three curve fitting models considered in this paper are described below.

3.3.1 Polynomial Model

Polynomial curve fitting process is suitable to establish a simple empirical model. The model can be useful for both data interpolation and extrapolation. The polynomial curve fitting model can be expressed as,

$$y = a_1 x^n + a_2 x^{n-1} + \cdots + a_{n+1}, \qquad 1 \leq n \leq 9 \tag{3.5}$$

Where, *n* is the degree of the polynomial, *n+1* is the order of the polynomial, and a_1 to a_{n+1} are the parameters to be fitted.

The number of parameters needed to define the model depends on the order of the model. Polynomial is a simple curve fitting process, disadvantages of this method include: 1) it may become unstable when the degree of the model is high, and 2) it is unable to ensure a good fit outside the data range [22]. In this paper, up to fifth degree of polynomial models are evaluated for curve fitting, beyond that significant improvement in fitting cannot be observed.

3.3.2 Gaussian Model

The Gaussian curve fitting model is particularly suitable for fitting peaks encountered in diverse areas of science and engineering. The model can be described by the equation below [23],

$$y = a_1 e^{-\frac{(x-b_1)^2}{{c_1}^2}} + \cdots + a_n e^{-\frac{(x-b_n)^2}{{c_n}^2}}, \quad 1 \leq n \leq 8 \tag{3.6}$$

Where, a_1-a_n, b_1-b_n, and c_1-c_n are parameters to be fitted. The symbols *a* denotes the amplitude, *b* denotes the centroid, *c* denotes the parameter defining the peak width, and *n* defines the number of peaks in the model [22].

In this paper, the measurement data sets are large enough for high order curve fitting. However, only the 2nd and 3rd order Gaussian models are evaluated because higher order models do not show significant improvement and seem to overfit the data.

3.3.3 Rational Model

The rational model can be expressed as the ratio of two polynomial functions. The model can be described by equation below,

$$y = \frac{\sum_{i=1}^{n+1} p_i x^{n+1-i}}{x^m + \sum_{i=1}^{m} q_i x^{m-i}} \tag{3.7}$$

Where, *n* is the degree of polynomial function in the numerator and $1 \leq n \leq 5$, while *m* is the degree of polynomial function in the denominator and $1 \leq m \leq 5$ [22, 24]. When, the degrees of the numerator and denominator are the same, the functions of the numerator and denominator become identical, as the coefficient associated with x^m always remains 1.

The rational models are suitable for establishing simple empirical models and they provide flexibility while working with complex structured data. However, rational models cannot ensure stability when the denominator becomes zero [22].

3.4 Goodness of Fit Evaluation

After obtaining fitting curves, it is necessary to evaluate the goodness of fit to determine the best fitted model. Different graphical and numerical measures are available in the MATLAB curve fitting toolbox to evaluate the goodness of fit of both linear and nonlinear parametric fits. The graphical measures include residuals, and prediction bounds. The numerical measures include goodness of fit statistics, and confidence bounds. It is not always possible to determine the best fit using graphical measures only, although they help to understand wide range of relationships between data and fitted models by enabling to view the entire data set at once. In such cases, the numerical measures become useful to determine the best fitted model. The evaluation metrics are discussed below.

3.4.1 Residuals

The residual is a graphical measure that illustrates the difference between the measured data and the fitted curve at each predictor value. Mathematically it can be expressed as,

$$r = y - \hat{y} \tag{3.8}$$

Where, y is the response value and $\hat{y}$ is the predicted response value for a specific predictor value. The error values approximated by the residuals are always random in nature if the model fits the data in a correct manner. Therefore, if the residuals are observed to follow a systematic pattern, it indicates that the model is a poor fit for the data set [25].

3.4.2 Goodness of Fit Statistics

Different numerical evaluation metrics are available to evaluate goodness of fit for parametric models such as, R-square, adjusted R-square, root mean squared error (RMSE), the sum of squares due to error (SSE) etc.

The sum of squares due to error (SSE) represents the total deviation from the observed values to the estimated values determined by the curve fitting model. The SSE can be computed as the sum of square of residuals between the observed and predicted value using the following formula,

$$SSE = \sum_{i=1}^{n} w_i \, (y_i - \hat{y}_i)^2 \tag{3.9}$$

Where, w_i are the weights. The weights determine how much each response value influences the final parameter estimates. The SSE is a way to measure the goodness of fit, with a value closer to zero indicates a better fit and higher accuracy of prediction [20, 25].

The R-square value represents how successfully a fit can explain the variance of measured data. The R-square can also be defined as the square of the correlation between measured and predicted values. Mathematically, R-square can be expressed as the ratio of the sum of squares of the regression (*SSR*) and the total sum of squares (*SST*), which are defined by the equations below,

$$SSR = \sum_{i=1}^{n} w_i \, (\hat{y}_i - \bar{y})^2 \tag{3.10}$$

$$SST = \sum_{i=1}^{n} w_i \, (y_i - \bar{y})^2 \tag{3.11}$$

$$R - square = \frac{SSR}{SST} \tag{3.12}$$

The R-square value always remains within 0 to 1 and a better fit possesses a value closer to 1. However, the increment of R-square value with the increment of the number of model parameters cannot always guarantee an improvement of fit. The degree of freedom adjusted R-square statistic can be useful to avoid such a situation.

The R-square value becomes negative during the cases when the fit is worse than just fitting a horizontal line. In this case, R-square value cannot successfully represent the square of the correlation, and adding a constant trend to the model can be a solution [25, 26].

The root mean squared error (RMSE) statistic is useful to measure the standard error of the random data noise component. An RMSE value closer to zero indicates a better fit similar to the SSE.

3.4.3 Confidence and Prediction Bounds

The confidence and prediction bounds are useful measures to determine goodness of fit. The prediction bound defines an upper and lower boundary of the fit such that, all the future observation values will fall within this boundary. The width of interval defined by prediction bounds is an effective way to measure the uncertainty of the fitted coefficients, the predicted fit, or the predicted observation etc. For example, a narrower interval indicates higher accuracy of the fitted coefficients. The accuracy of the fitted coefficients also de-pends on the certainty level specified for the prediction interval. Generally, a 95% prediction interval is specified, which indicates that, there lies a 95% chance for the new observation values to fall within the range of defined boundaries and only a 5% chance for the new observation values to be predicted incorrectly [25].

3.5 Case Studies

In order to obtain an accurate *Q* vs. *V* relation using the proposed curve fitting procedure based on the measurement data, two case studies are conducted to create Q-V curves using the measured reactive power and the generated voltage data with respect to time during January 2016 at the POIs of two wind farms currently in operation in Newfoundland and Labrador, Canada. The understanding of the underlying nature of reactive power variation with voltage for a particular wind farm is useful to develop a control mechanism to reduce voltage fluctuations at the POI, it can also be used for voltage stability assessment at the POI.

The two wind farms are located at St. Lawrence and Fermuse, each is rated at 27 MW, and connected to provincial grid by 66 kV transmission lines. Each of these wind farms consists of nine wind turbines each rated at 3 MW [27]. The measured parameters include the voltage, real and reactive power at the 66 kV rated POI. The measurement is recorded in every fifteen minutes interval for the whole month.

The voltage variation measured at wind farms 1 and 2 are shown in Figs. 3.3 and 3.5, respectively. From the figures, the voltage at both wind farms fluctuates significantly over time. The main reason of such voltage fluctuation is the variation of active power injection to the grid. The fluctuation in wind speed causes active power injection to vary, which results in a variation of the generated voltage [28]. Additionally, the reactive power consumption from power grid can cause reduction in the generated voltage [29]. The strength of the network to which the wind farms are connected also has some impact on the degree of voltage variation [30]. The highest voltage fluctuations for wind farms 1 and 2 are found to be ± 3.05% and ± 1.86%, respectively.

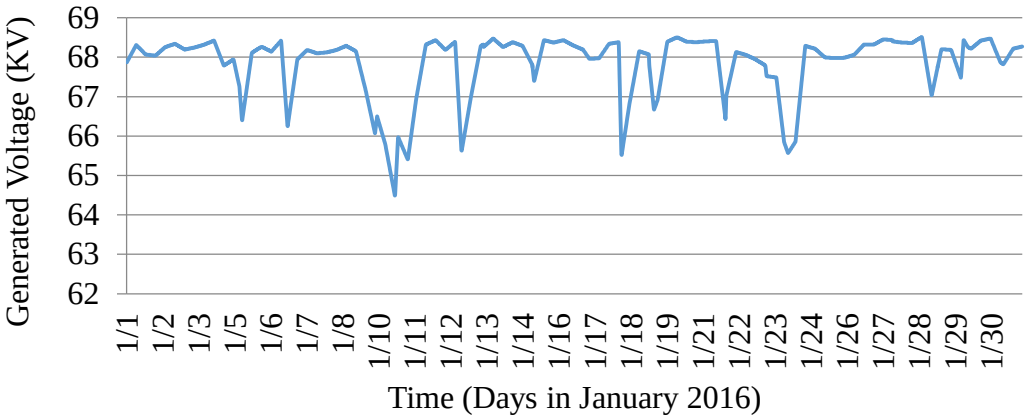

Figure 3. 3: Variations in voltage measured at wind farm 1

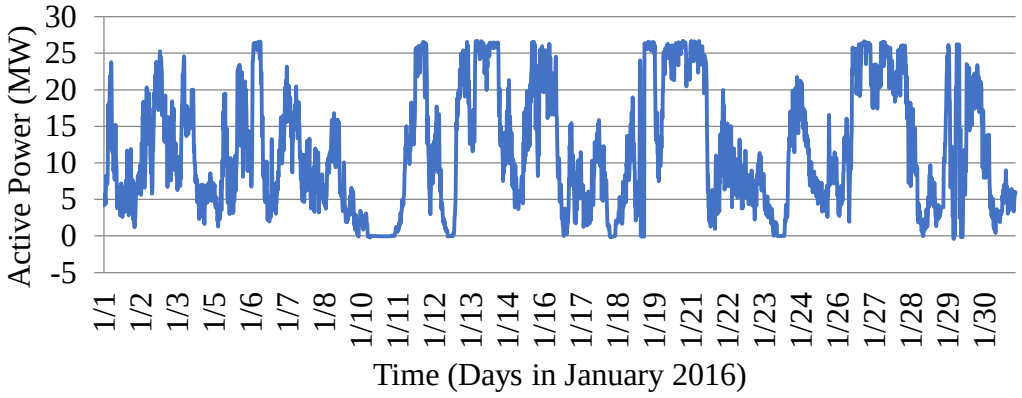

(a)

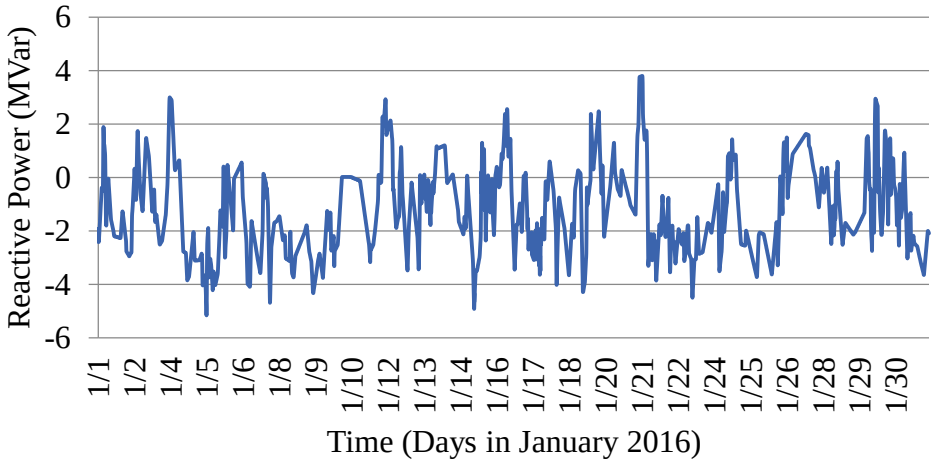

(b)

Figure 3. 4: Power measurements for wind farm 1: (a) active power; (b) reactive power.

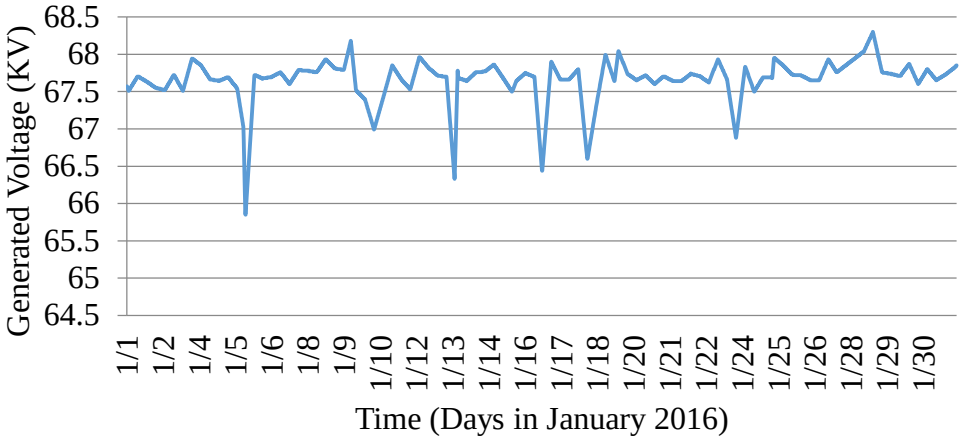

Figure 3. 5: Variations in voltage measured at wind farm 2

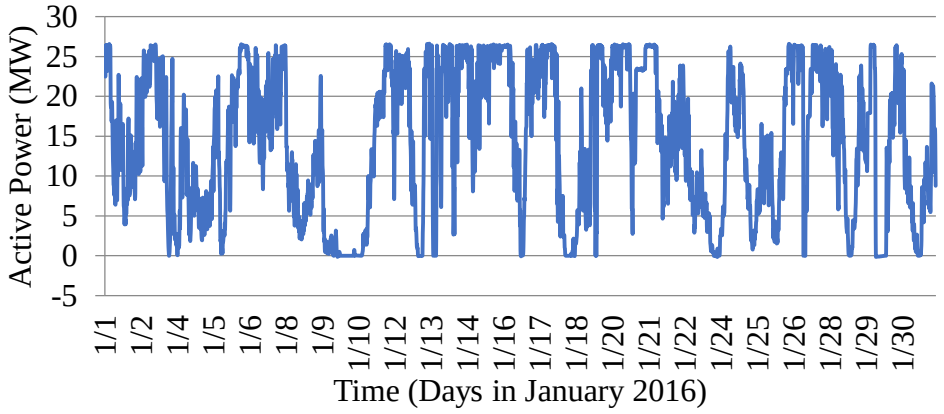

(a)

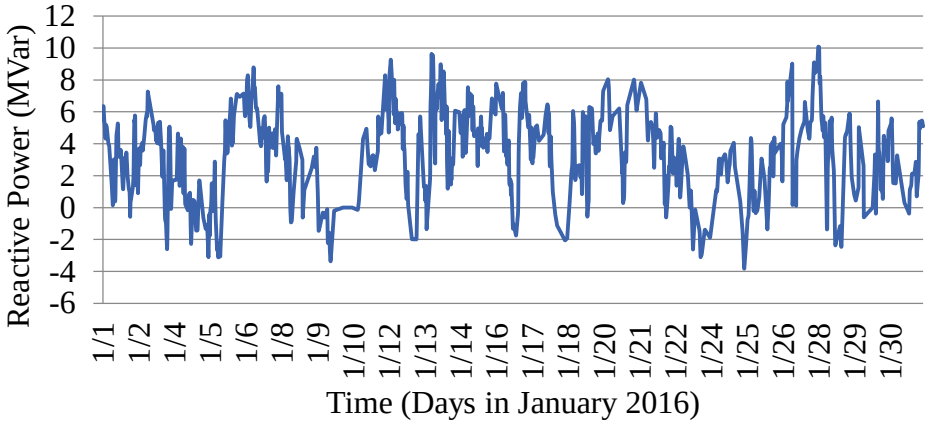

(b)

Figure 3. 6: Power measurements for wind farm 2: (a) active power; (b) reactive power.

The variation in generated active and reactive power measured at wind farms 1 and 2 are shown in Figs. 3.4 and 3.6 respectively. A continuous variation in active and reactive power can be observed due to interaction of wind farms with the grid. It is evident from the graphs that wind farms generate small amount of reactive power when there is no or small active power is generated. However, with the increase of active power generation, wind farms are found to contribute enough reactive power to the grid, which is required by transformers connected to the grid. Thus, wind farms can help to maintain the power factor to unity by providing enough reactive power to the grid. As shown in the measurement data, the levels of reactive power generation of the two wind farms used in the case study are different. Wind farms may also absorb reactive power from the grid to maintain a unity power factor, when there is not enough reactive power generation is available due to the absence of reactive power compensation devices in the system [28, 30].

3.5.1 Case Study 1 - Wind Farm 1

In this section, different curve fitting models discussed in Section 3.3 are evaluated to establish a relationship between reactive power Q and voltage V for wind farm 1. The best fitted model is determined based on different graphical and numerical evaluation metrics using the MATLAB curve fitting toolbox. At first, the residuals, a graphical analysis measure is evaluated for different models to see if the best fit can be determined based on it. The fits and residuals for the Gaussian (Gauss) 2, Rational (Rat) 24 (order 24) and Rational 44 (order 44) models are presented in the Figs. 3.7, 3.8 and 3.9 respectively.

It is found that no regular pattern of the residual values can be observed in Figs 3.7-3.9, residual values are found to be scattered randomly for all the models, which indicates that these models fit data in an appropriate manner. Evaluations with higher degree of Gaussian functions are not presented, as they do not seem to improve the fit significantly and in some cases they overfit the

acquired data. Again, only those Rational models are evaluated which ensure similar performance like Polynomial and Gaussian models. The fits are presented in Fig. 3.10 with an extended X-axis. Fig. 3.10 shows that the models, Polynomial 5 (Poly 5, 5^{th} degree), Rational 35 (order 35) and Rational 54 (order 54), appear to fit data poorly while examined beyond the data range to predict the data outside the defined range. The equations for the fitted curves based on selective curve fitting models and the corresponding coefficients with confidence bounds are provided in Tables 3.1-3.3.

The confidence bounds on coefficients are useful measures to compare the fits. The accuracy of the fitted coefficients mainly depends on confidence bounds. For a linear coefficient, it cannot be certainly determined whether the coefficient value is zero or not when a zero crossing exits within the bounds. A coefficient with a zero value cannot help to improve the accuracy of a fit. From the data presented in Tables 3.2 and 3.3, confidence bounds cross zero on all the coefficients for Raional 35, Rational 54 models and on one coefficient (*b2*) for Gaussian 3 model, which is an indication that these models overfit the measured data [31].

The goodness of fit statistics is then evaluated to determine the best fit. The goodness of fit statistics for selective curve fitting models is presented in the Table 3.4. Although the least SSE and RMSE values are observed for Gaussian 3 model, this model cannot ensure a good fit, as it is found to overfit the measured data as discussed earlier. The SSE and RMSE values for Gaussian 2, Rational 24 and Rational 44 models are found to be reasonably lower among other models. Therefore, these models are considered as good fits based on the SSE and RMSE data.

Additionally, the R-squared values for these models are found to be around 42%, which indicates that the variance of the error will be 42% less than the variance of the dependent variable,

the reactive power *Q*. An even higher value of R-square can be attained by adjusting the level of confidence or by imposing key limits to the data interval [26].

The Gaussian 2 fitting curve of the measured data along with the prediction bounds are shown in the Fig. 3.11. The prediction bounds define an upper and lower boundary and indicate that there is a 95% chance that any future observed data will fall within this boundary.

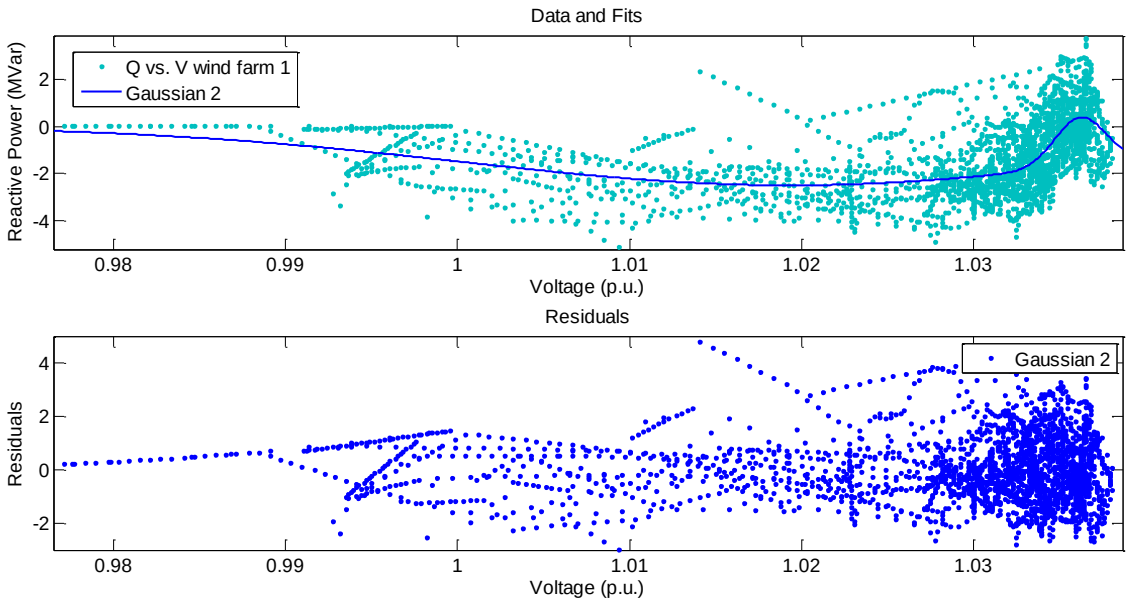

Figure 3. 7: The Q-V curve obtained by Gaussian 2 (degree 2) curve fitting compared to measurements, and the residuals of the Gaussian 2 model for wind farm 1.

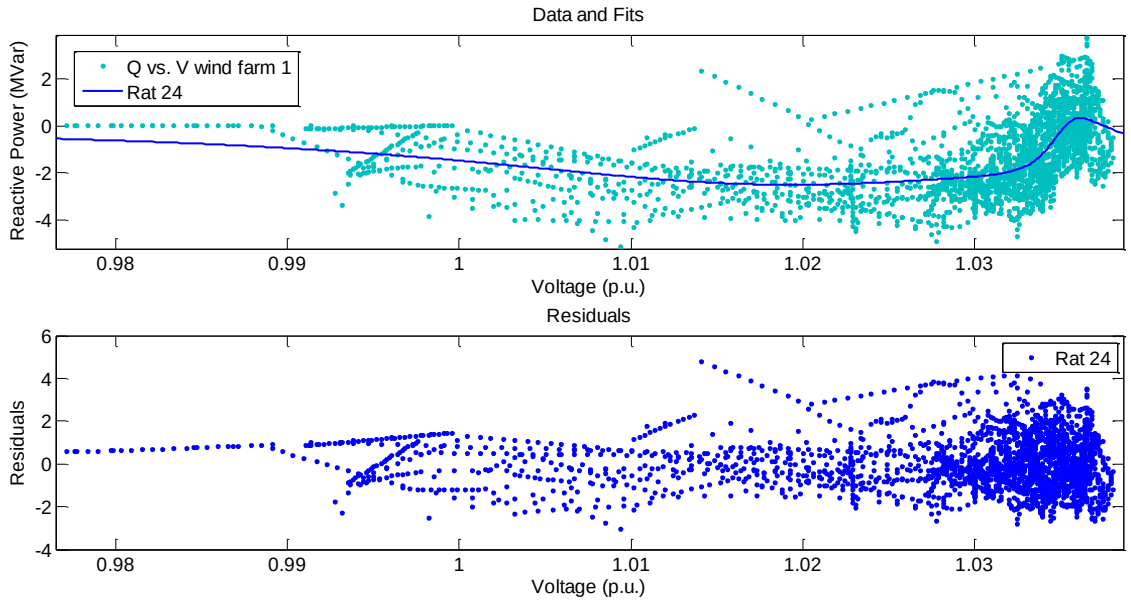

Figure 3. 8: The Q-V curve obtained by Rational 24 (order 24) curve fitting compared to measurements, and the residuals of the Rational 24 model for wind farm 1.

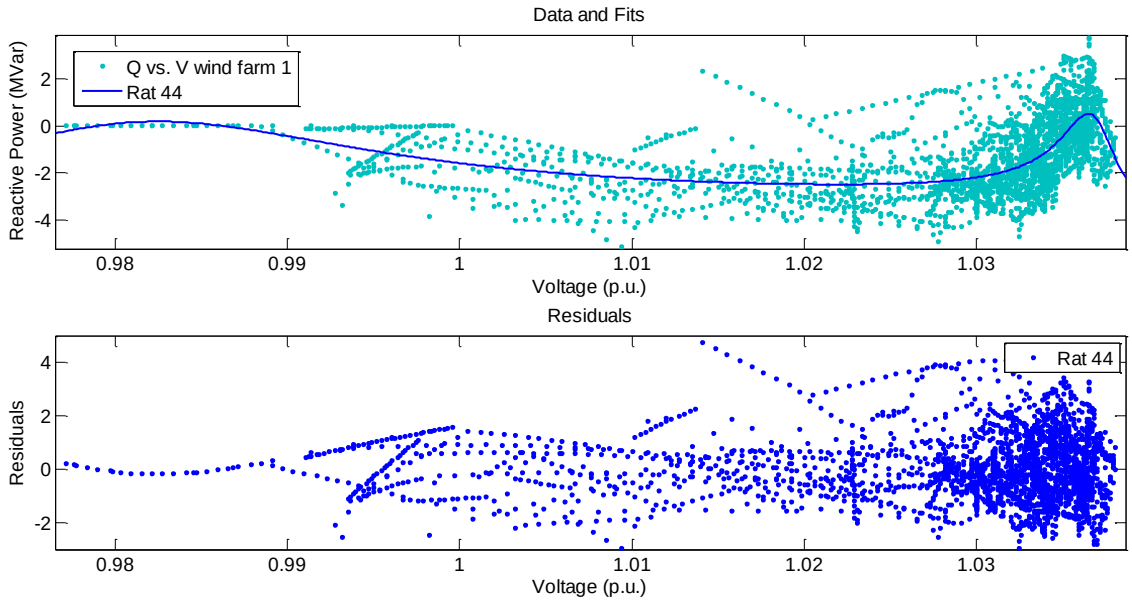

Figure 3. 9: The Q-V curve obtained by Rational 44 (order 44) curve fitting compared to measurements, and the residuals of the Rational 44 model for wind farm 1.

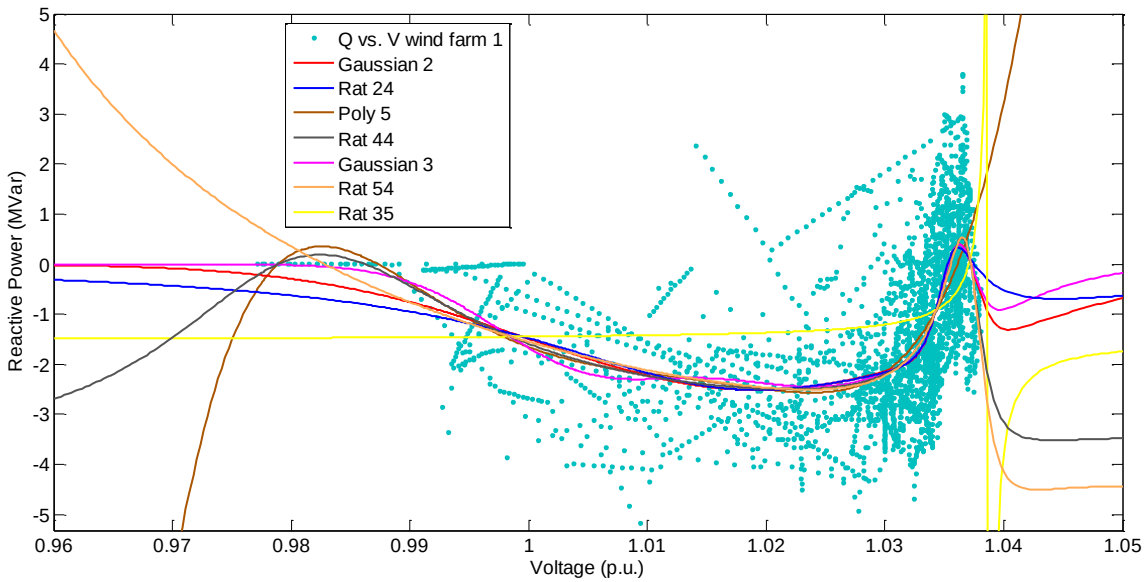

Figure 3. 10: The Q-V characteristic curve using various fitting models for wind farm 1 with an extended X-axis (dots are measurements).

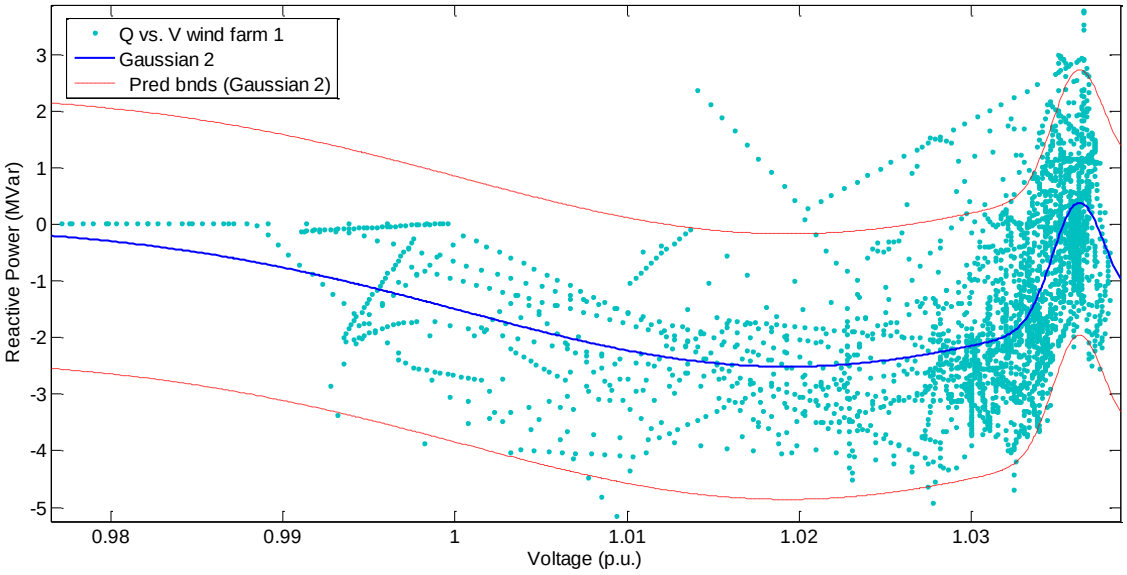

Figure 3. 11: The Q-V characteristic curve obtained using Gaussian 2 with prediction bounds for wind farm 1 (dots are measurements).

Table 3. 1: Equations of fitted curves for different models

Curve fitting model	Equation of fitted curve
Polynomial 5	$f(x) = p_1x^5 + p_2x^4 + p_3x^3 + p_4x^2 + p_5x + p_6$
Gaussian 2	$f(x) = a_1e^{-\left(\frac{x-b_1}{c_1}\right)^2} + a_2e^{-\left(\frac{x-b_2}{c_2}\right)^2}$
Gaussian 3	$f(x) = a_1e^{-\left(\frac{x-b_1}{c_1}\right)^2} + a_2e^{-\left(\frac{x-b_2}{c_2}\right)^2} + a_3e^{-\left(\frac{x-b_3}{c_3}\right)^2}$
Rational 24	$f(x) = (p_1x^2 + p_2x + p_3)/(x^4 + q_1x^3 + q_2x^2 + q_3x + q_4)$
Rational 35	$f(x) = (p_1x^3 + p_2x^2 + p_3x + p_4)/\ (x^5 + q_1x^4 + q_2x^3 + q_3x^2 + q_4x + q_5)$
Rational 44	$f(x) = (p_1x^4 + p_2x^3 + p_3x^2 + p_4x + p_5)/(x^4 + q_1x^3 + q_2x^2 + q_3x + q_4)$
Rational 54	$f(x) = (p_1x^5 + p_2x^4 + p_3x^3 + p_4x^2 + p_5x + p_6)/(x^4 + q_1x^3 + q_2x^2 + q_3x + q_4)$

Table 3. 2: Coefficients with 95% confidence bounds for Rational models (wind farm 1)

Model	Rational 24	Rational 35	Rational 44	Rational 54
Coefficients with 95% Confidence bounds	p_1 = -9.109 (-12.39, -5.824) p_2 = 13.17 (8.6, 17.74) p_3 = -4.672 (-6.266, -3.078) q_1=0.5818 (0.08888, 1.075) q_2 = 3.018 (1.565, 4.471) q_3 = -5.335	p_1 = 230.1 ($-9.822*10^6$, $9.823*10^6$) p_2 = -1.573e+004 ($-1.432*10^{13}$, $1.432*10^{13}$) p_3 = -466 ($-1.331*10^{15}$, $1.331*10^{15}$) p_4 = -9.532 ($-1.182*10^{17}$, $1.182*10^{17}$) q_1 = -136.7	p_1 = -3.61 (-5.587, -1.633) p_2 = -23.87 (-36.62, -11.11) p_3 = -18.06 (-28.74, -7.374) p_4=69.02 (31.46, 106.6) p_5 = -30	p_1 = 0.04504 ($-1.092*10^4$, $1.092*10^4$) p_2 = -5.967 ($-4.032*10^9$, $4.032*10^9$) p_3 =197.5 ($-7.84*10^{11}$, $7.84*10^{11}$) p_4 = -9.067 ($-1.329*10^{14}$, $1.329*10^{14}$) p_5 = -0.3755

	(-7.121, -3.548) q_4 = 2.069 (1.401, 2.737)	(-6.224*10^{10}, 6.224*10^{10}) q_2 = 4678 (-6.837*10^{12}, 6.837*10^{12}) q_3 = -223.9 (-8.692*10^{14}, 8.692*10^{14}) q_4 = -13.02 (-3.515*10^{16}, 3.515*10^{16}) q_5 = 0.1976 (-2.727*10^{15}, 2.727*10^{15})	(-46.38, -13.63) q_1 = 6.89 (4.35, 9.431) q_2 = 7.156 (2.253, 12.06) q_3 = -25.6 (-38.88, -12.33) q_4 = 12.77 (6.05, 19.49)	(-4.825*10^{15}, 4.825*10^{15}) p_6 = 0.02044 (-4.023*10^{14}, 4.023*10^{14}) q_1 = -137.9 (-8.951*10^{10}, 8.951*10^{10}) q_2 = 4752 (-1.723*10^{13}, 1.723*10^{13}) q_3 = 178.2 (-3.06*10^{15}, 3.06*10^{15}) q_4 = 5.659 (-1.161*10^{17}, 1.161*10^{17})

Table 3. 3: Coefficients with 95% confidence bounds for Polynomial and Gaussian models (wind farm 1)

Curve fitting model	Polynomial5	Gaussian 2	Gaussian 3
Coefficients with 95% Confidence bounds	p_1 = 0.04624 (0.03199, 0.06048) p_2 = 0.4386 (0.3288, 0.5483) p_3 = 1.433 (1.194, 1.672) p_4 = 2.116 (1.96, 2.273) p_5 = 1.083 (0.8955, 1.271) p_6 = -2.388 (-2.466, -2.309)	a_1 = 2.076 (1.909, 2.243) b_1 = 0.7053 (0.6921, 0.7185) c_1 = 0.1867 (0.1643, 0.209) a_2 = -2.511 (-2.629, -2.393) b_2 = -0.7844 (-0.8928, -0.676) c_2 = 2.363 (2.107, 2.619)	a_1 = 1.83 (1.406, 2.254) b_1 = 0.6992 (0.6826, 0.7158) c_1 = 0.1734 (0.1384, 0.2084) a_2 = -2.367 (-2.719, -2.015) b_2 = -0.252 (-0.761, 0.2569) c_2 = 1.355 (0.4483, 2.263) a_3 = -1.781 (-3.105, -0.4578) b_3 = -2.085 (-2.621, -1.548) c_3 = 1.006 (0.5584, 1.454)

Table 3. 4: Goodness of fit statistics for different fits (wind farm 1)

Model name	SSE	R-Square	Adj R-sq	RMSE
Gauss2	4252.0696	0.4194	0.4184	1.1967
Gauss3	4232.7422	0.4220	0.4205	1.1946
Poly5	4497.7569	0.3858	0.3848	1.2308
Rat24	4281.4067	0.4154	0.4142	1.2010
Rat35	4515.8402	0.3834	0.3817	1.2339
Rat44	4235.0144	0.4217	0.4202	1.1949
Rat54	4524.5132	0.3822	0.3803	1.2353

3.5.2 Case Study 2- Wind Farm 2

Similar to wind farm 1, in this section, different curve fitting models are evaluated to establish a relationship between reactive power and voltage at the POI for wind farm 2. The best fitted model is determined based on different graphical and numerical evaluation metrics using MATLAB curve fitting toolbox.

At first, the residuals is evaluated for selective models. The fits and residuals for Gaussian 2, Rational 44 and Polynomial 5 models are presented in Figs. 3.12, 3.13 and 3.14 respectively. No regular pattern of the residual values can be observed in these figures. For all the models, residual values are found to be scattered randomly, which indicates that these models fit data in an appropriate manner. If simply based on graphical evaluation, the best fit cannot be determined. Again the evaluations with higher degree of Gaussian functions are not presented, as they do not seem to improve the fit significantly and in some cases they overfit the acquired data. Only those

Rational models are evaluated which ensure similar performance like Polynomial and Gaussian models.

The fits are presented in Fig. 3.15 with an extended X-axis. From Fig. 3.15, it is evident that the models, Polynomial 5, Rational 24, Rational 35, and Rational 54, appear to fit data poorly while examined beyond the data range to predict the data outside the defined range.

The equations for the fitted curves based on the selective curve fitting models listed in Table 3.1 are used. The corresponding coefficients with confidence bounds for wind farm 2 are presented in Tables 3.5 and 3.6. The two tables indicate that the confidence bounds cross zero on all the coefficients for Rational 24, Rational 35, Rational 54 models, on five coefficients for Rational 44 model, on two coefficients for Gaussian 3 model, and on one coefficient for Polynomial 5 model. This is an indication that these models overfit the measured data [31]. Based on the confidence bounds, it appears that the Gaussian 2 model is the only model that fits the data in an appropriate manner among all evaluated models. To validate this estimation, the performance of this model is further measured based on other evaluation metrics. The goodness of fit statistics is then evaluated to determine the best fit. The goodness of fit statistics for the selective curve fitting models for wind farm 2 is presented in Table 3.7.

Although the least SSE and RMSE values are observed for Rational 44 model, this model cannot ensure a good fit because it is found to overfit the measured data as discussed earlier. The SSE and RMSE values for Gaussian 2 model are found to be reasonably lower among the other models. Therefore, this model can be considered to ensure a good fit based on the SSE and RMSE data. Additionally, the R-squared value for this model is found to be around 20%, which indicates that the variance of the error will be 20% less than the variance of the dependent variable, the reactive power *Q*. Moreover, the R-Square values for Rational 24 and Rational 35 models are found to be

negative, which indicates that, the fits based on these models are worse than just fitting a horizontal line [26].

The Gaussian 2 fitting curve of the measured data along with prediction bounds are shown in Fig. 3.16. The prediction bounds define an upper and lower boundary and indicate that, there is a 95% chance that any future observed data will fall within this boundary.

The prediction bounds (also known as prediction interval) can be a useful measure to quantify the level of uncertainty in the future predicted data. The level of uncertainty in the predicted data for wind farms may vary due to several reasons including change in operating conditions, and seasonal variation of weather, it also depends on the sample size. The width of the prediction bounds provides the decision makers valuable information about data accuracy. The wider prediction bounds indicate higher level of uncertainty in the predicted data. Therefore, more caution should be exercised for decision making based on the predicted data with wider prediction bounds [32, 33].

Based on both graphical and numerical evaluation results presented for the two wind farms, it is concluded that the relation between the generated reactive power Q and the voltage V for both wind farms can be represented most accurately based on the Gaussian 2 (degree 2) curve fitting model.

Once a Q-V curve is obtained at the POI of a wind farm, it can be used for designing voltage control schemes for power quality improvement or conducting voltage stability evaluation.

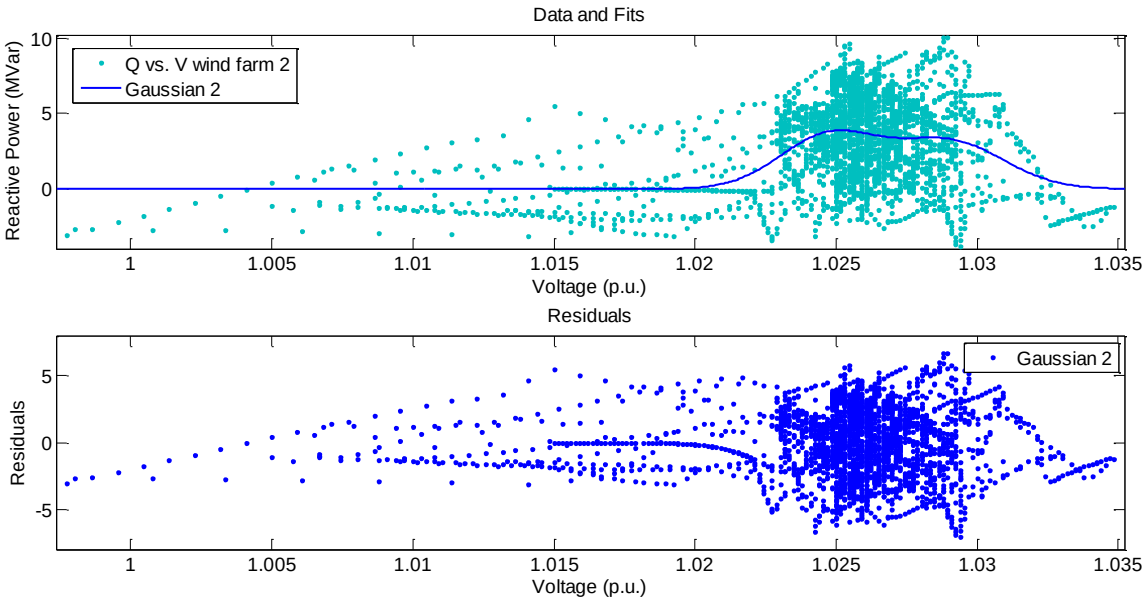

Figure 3. 12: The Q-V curve obtained by Gaussian 2 (degree 2) curve fitting compared to measurements, and the residuals of the Gaussian 2 model for wind farm 2.

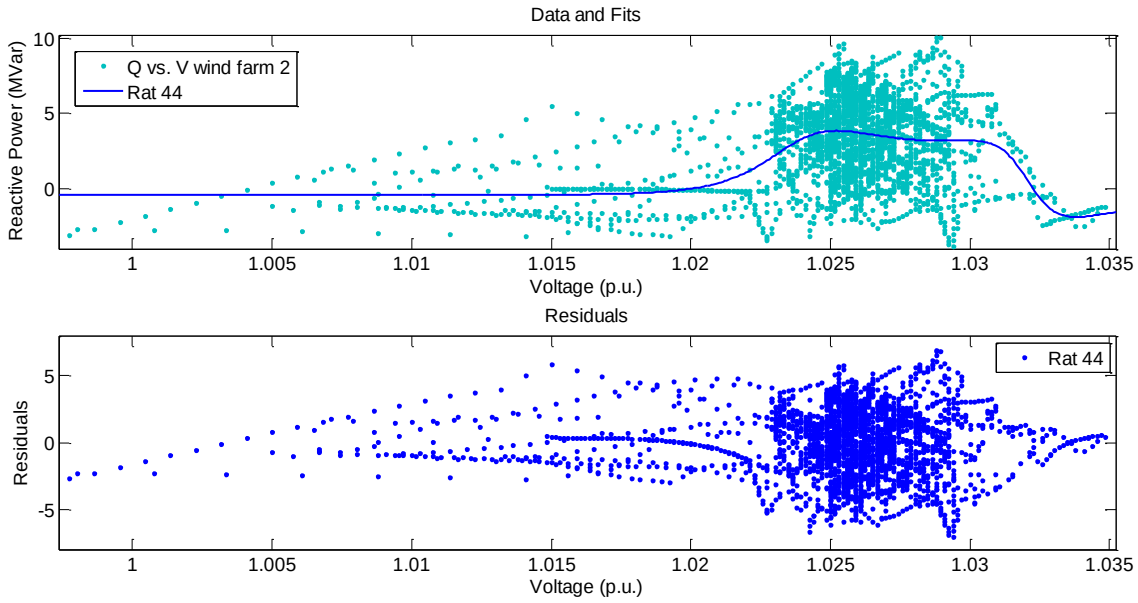

Figure 3. 13: The Q-V curve obtained by Rational 44 (order 44) curve fitting compared to measurements, and the residuals of the Rational 44 model for wind farm 2.

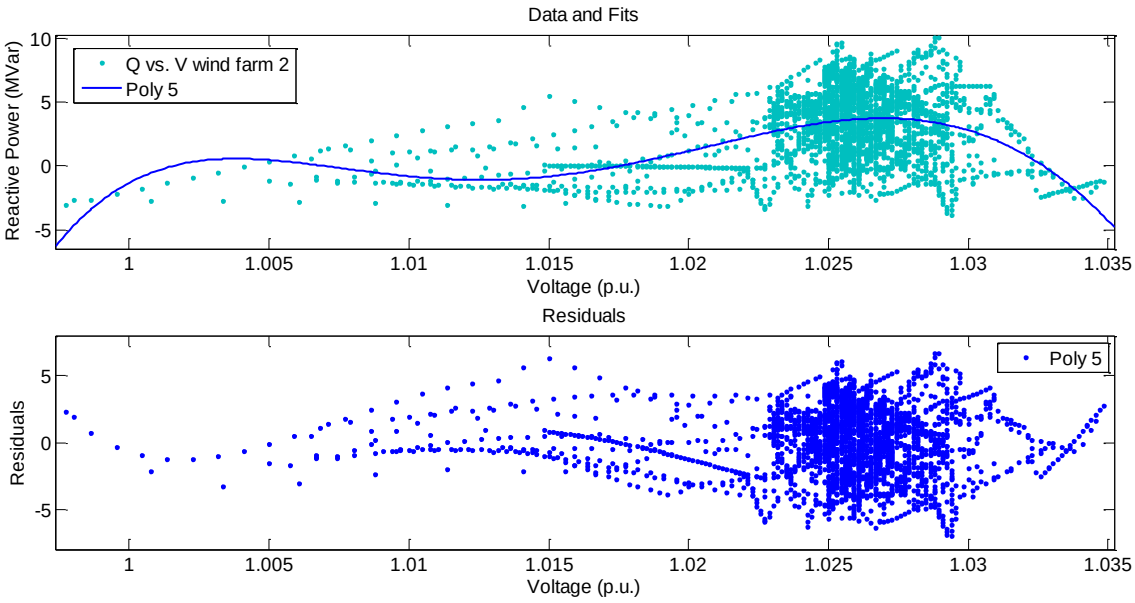

Figure 3. 14: The Q-V curve obtained by Polynomial 5 curve fitting compared to measurements, and the residuals of the Polynomial 5 model for wind farm 2.

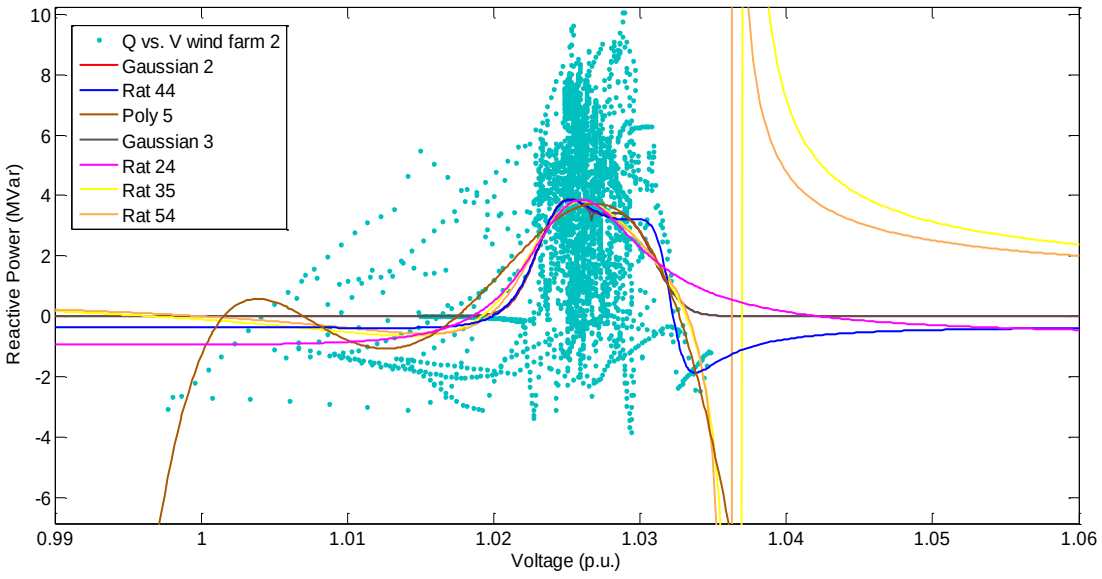

Figure 3. 15: The Q-V characteristic curve using various fitting models for wind farm 2 with an extended X-axis (dots are measurements).

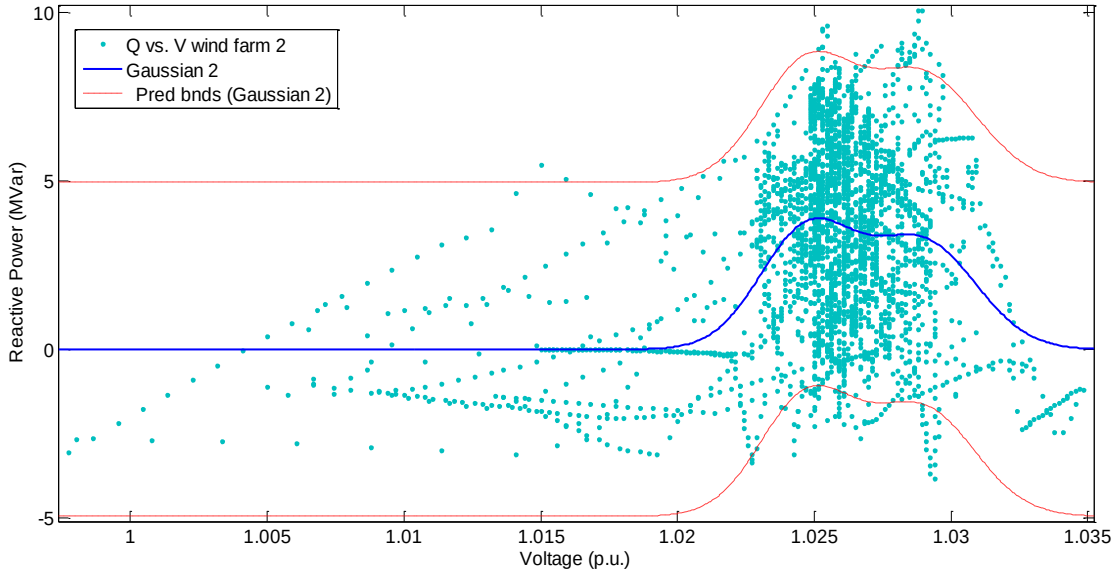

Figure 3. 16: The Q-V characteristic curve obtained using Gaussian 2 with prediction bounds for wind farm 2 (dots are measurements).

Table 3. 5: Coefficients with 95% confidence bounds for Polynomial and Gaussian models (wind farm 2)

Curve fitting model	Polynomial 5	Gaussian 2	Gaussian 3
Coefficients with 95% Confidence bounds	p_1=0.0031 (0.0002, 0.0059) p_2 = -0.006 (-0.0331, 0.0211) p_3 = -0.3237 (-0.3879, -0.2595) p_4 = -0.9916 (-1.128, -0.8547) p_5 = 1.044 (0.8241, 1.264) p_6 = 3.489 (3.375, 3.603)	a_1 = 3.15 (2.608, 3.692) b_1 = 67.91 (67.85, 67.98) c_1 = 0.181 (0.0993, 0.2627) a_2 = 3.538 (2.653, 4.423) b_2 = 67.63 (67.58, 67.68) c_2 = 0.1634 (0.1142, 0.2126)	a_1 = 3.099 (2.455, 3.742) b_1 = 67.92 (67.85, 67.99) c_1 = 0.1816 (0.0951, 0.2681) a_2 = 3.534 (2.572, 4.495) b_2 = 67.64 (67.58, 67.69) c_2 = 0.1677 (0.1139, 0.2214) a_3 = -0.3689 (-0.959, 0.2213) b_3 = 67.76 (67.74, 67.78) c_3 = 0.0077 (-0.0078, 0.02332)

Table 3. 6: Coefficients with 95% confidence bounds for Rational models (wind farm 2)

Model	Rational 24	Rational 35	Rational 44	Rational 54
Coefficients with 95% Confidence bounds	p_1 = 90.21 ($-1.758*10^8$, $1.758*10^8$) p_2 = 1.803 ($-1.059*10^{15}$, $1.059*10^{15}$) p_3 = 0.8197 ($-1.492*10^{17}$, $1.492*10^{17}$) q_1 = -65.69 ($-1.174*10^{13}$, $1.174*10^{13}$) q_2 = -0.4901 ($-1.498*10^{15}$, $1.498*10^{15}$) q_3 = 0.9032 ($-1.087*10^{17}$, $1.087*10^{17}$) q_4 = 0.792 ($-1.541*10^{15}$, $1.541*10^{15}$)	p_1 = 106.5 ($-4.361*10^9$, $4.361*10^9$) p_2 = 1.952 ($-3.091*10^{15}$, $3.091*10^{15}$) p_3 = 0.6785 ($-7.675*10^{16}$, $7.675*10^{16}$) p_4 = 0.1715 ($-9.439*10^{18}$, $9.439*10^{18}$) q_1 = -65.68 ($-2.902*10^{13}$, $2.902*10^{13}$) q_2 = -0.545 ($-1.385*10^{15}$, $1.385*10^{15}$) q_3 = 0.2745 ($-5.58*10^{16}$, $5.58*10^{16}$) q_4 = 0.04623 ($-5.822*10^{18}$, $5.822*10^{18}$) q_5 = 0.09713 ($-8.41*10^{16}$, $8.41*10^{16}$)	p_1 = -0.3408 (-1.091, 0.4093) p_2 = 0.8261 (-0.583, 2.235) p_3 = -2.666 (-6.459, 1.126) p_4 = -0.1478 (-3.752, 3.456) p_5=7.113 (3.293, 10.93) q_1 = -2.754 (-3.129, -2.379) q_2 = 1.462 (0.36, 2.563) q_3 = -0.05837 (-1.239, 1.123) q_4=1.842 (0.8174, 2.867)	p_1 = 0.1877 ($-1.056*10^7$, $1.056*10^7$) p_2 = -12.52 ($-3.666*10^{13}$, $3.666*10^{13}$) p_3 = -0.3248 ($-4.468*10^{14}$, $4.468*10^{14}$) p_4 = 0.6207 ($-1.055*10^{17}$, $1.055*10^{17}$) p_5 = 0.7087 ($-3.402*10^{18}$, $3.402*10^{18}$) p_6 = 0.7547 ($-1.517*10^{16}$, $1.517*10^{16}$) q_1 = -63.77 ($-1.954*10^{14}$, $1.954*10^{14}$) q_2 = -1.345 ($-2.261*10^{15}$, $2.261*10^{15}$) q_3 = 0.6096 ($-5.256*10^{17}$, $5.256*10^{17}$) q_4 = 0.1617 ($-1.733*10^{19}$, $1.733*10^{19}$)

Table 3. 7: Goodness of fit statistics for different fits (wind farm 2)

Model name	SSE	R-Square	Adj R-sq	RMSE
Poly5	19293.0279	0.1908	0.1895	2.5491
Gauss2	18994.4392	0.2033	0.2020	2.5293
Gauss3	18984.7285	0.2038	0.2016	2.5299
Rat44	18834.8250	0.2100	0.2079	2.5199
Rat24	41528.7471	-0.7416	-0.7451	3.7406
Rat35	40117.9892	-0.6824	-0.6870	3.6777
Rat54	21693.3064	0.0902	0.0874	2.7048

6. Conclusions

In this paper, a data driven analytics approach based on the curve fitting procedure is proposed to determine the Q-V characteristic curve at the POI of large wind farms. The developed Q-V curve and associated functions can be readily used for voltage controller design in order to reduce voltage fluctuations or for voltage stability evaluation at the POI of a grid-connected wind farm.

The proposed method employs the data driven analytics approach by using measurement data recorded at the POI. The knowledge of the system configuration and parameters of wind farms are not required. Several curve fitting techniques are evaluated and compared in a case study with two grid-connected wind farms currently in operation in Newfoundland and Labrador, Canada. It is found that the best fitting model is Gaussian 2 (degree 2) curve fitting model for the two wind farms under study.

References

[1] S. Yuanzhang, W. Jun and L. Guojie, “Influence research of wind power generation on power systems,” *Power System Technology*, vol. 31, no. 20, pp. 55-62, Oct. 2007.

[2] W. Hu, Z. Chen, Y. Wang, and Z. Wang, "Flicker mitigation by active power control of variable-speed wind turbines with full-scale back-to-back power converters," *IEEE Trans. Energy Conversion*, vol. 24, no. 3,pp. 640-649,Sep. 2009 .

[3] C. J. Melhorn and M. F. McGranaghan, "Interpretation and analysis of power quality measurements," *IEEE Trans. Industry Applications*, vol. 31, no. 6, pp. 1363-1370, Nov/Dec 1995.

[4] B. Ge, W. Wang, D. Bi, C. B. Rogers, F. Z. Peng, A. T. Almeida and H. Abu-Rub, "Energy storage system-based power control for grid-connected wind power farm," *Electrical Power and Energy Systems (Elsevier)*, vol. 44, no. 1, pp. 115-122, Jan. 2013.

[5] X. Liang, "Emerging power quality challenges due to integration of renewable energy sources," *IEEE Trans. Industry Applications*, vol. 53, no. 2, pp. 855-866, Nov. 2016.

[6] F. A. Viawan and D. Karlsson, “Voltage and reactive power control in systems with synchronous machine-based distribution generation,” *IEEE Trans. Power Delivery*, vol. 23, no. 2, pp. 1079-1087, Apr. 2008.

[7] K. Turitsyn, P. Sulc, S. Backhaus, and M. Chertkov, "Options for control of reactive power by distributed photovoltaic generators," *Proceedings of the IEEE*, vol. 99, no. 6, pp. 1063-1073, Jun. 2011.

[8] D. Mascarella, P. Venne, D. Guérette, and G. Joos, "Flicker mitigation via dynamic volt/var control of power-electronic interfaced WTGs," *IEEE Trans. Power Delivery*, vol. 30, no. 6, pp. 2451-2459, Dec. 2015.

[9] S. Yin, X. Li, H. Gao, and O. Kaynak, "Data-based techniques focused on modern industry: an overview," *IEEE Trans. Industrial Electronics*, vol. 62, no. 1, pp. 657-667, Jan. 2015.

[10] S. A. Chen, A. Vishwanath, S. Sathe, S. Kalynaraman, and S. Lu, "Understanding the performance of solar PV systems using data-driven analytics," in *Proc. IEEE Innovative Smart Grid Technologies - Asia (ISGT ASIA)*, pp. 1-6, 2015.

[11] P. C. Sekhar, S. Mishra, and R. Sharma, "Data analytics based neuro-fuzzy controller for diesel-photovoltaic hybrid AC microgrid," *IET Generation, Transmission & Distribution*, vol. 9, no. 2, pp. 193-207, Jan. 2015.

[12] H. Zhang, H. Jiang, Y. Luo, and G. Xiao, "Data-driven optimal consensus control for discrete-time multi-agent systems with unknown dynamics using reinforcement learning method," *IEEE Trans. Industrial Electronics*, vol. 64, no. 5, pp. 4091-4100, Mar. 2016.

[13] J. Kim, J. Seok, E. Muljadi, and Y. C. Kang, "Adaptive Q–V scheme for the voltage control of a DFIG-based wind power plant," *IEEE Trans. Power Electronics*, vol. 31, no. 5, pp. 3586-3599, May 2016.

[14] J. Martínez, P. C. Kjær, P. Rodriguez, and R. Teodorescu, "Design and analysis of a slope voltage control for a DFIG wind power plant," *IEEE Trans. Energy Conversion*, vol. 27, no. 1, pp. 11-20, Mar. 2012.

[15] Z. Huang, L. Bao, and W. Xu, "A method to measure QV curves and its applications in power systems," *Electrical Power and Energy Systems (Elsevier)*, vol. 29, pp. 147–154, 2007.

[16] R. S. Moura, A. C. Z. de Souza, B. I. L. Lopes, and F. W. Mohn, "Effects of QV curves in the dynamic behavior of power systems," *IET Generation, Transmission & Distribution*, vol. 10, no. 12, pp. 2861–2870, 2016.

[17] J. Dragosavac, Z. Janda, and J. V. Milanovic, "Coordinated reactive power-voltage controller for multimachine power plant," *IEEE Trans. Power Systems*, vol. 27, no. 3, pp. 1540-1549, 2012.

[18] Y. K. Gounder, D. Nanjundappan, and V. Boominathan, "Enhancement of transient stability of distribution system with SCIG and DFIG based wind farms using STATCOM," *IET Renewable Power Generation*, vol. 10, no. 8, pp. 1171-1180, 2016.

[19] S. Hashemi and J. Østergaard, "Methods and strategies for overvoltage prevention in low voltage distribution systems with PV," *IET Renewable Power Generation*, vol. 11, no. 2, pp. 205-214, 2016.

[20] L. Fang and D.C. Gosard, "Multidimensional curve fitting to unorganized data points by nonlinear minimization," *Computer Aided Design (Elsevier)*, vol. 27 no. 1, pp.48-58, 1995.

[21] S. A. Hosseini and H. Ghassemian, "A novel approach to hyperspectral data feature extraction using rational function curve fitting," in *Proc. IEEE International Conf. Signal and Image Processing Applications (ICSIPA)*, pp. 494-499, 2015.

[22] http://www.mathstat.dal.ca/cluster/manuals/matlab/toolbox/curvefit/ch_fitt6.html#63727. 2016.

[23] F. Kong, C. Dong, X. Liu, and H. Zeng, "Quantity versus quality: optimal harvesting wind power for the smart grid," *Proceedings of the IEEE*, vol. 102, no. 11, pp. 1762-1776, Nov. 2014.

[24] L. Fahrmeir, T. Kneib, S. Lang, and B. Marx, "Regression: models, methods and applications," *Springer Science & Business Media*, May 2013.

[25] http://www.mathstat.dal.ca/cluster/manuals/matlab/toolbox/curvefit/ch_fitt9.html. 2016.

[26] G. Oprea and H. Andrei, "Measurement data analysis of power quality for industrial loads," in *Proc. Ninth International Symp. Advanced Topics in Electrical Engineering (ATEE)*, pp. 893-898, 2015.

[27] "Electricity", http://www.nr.gov.nl.ca/nr/energy/electricity/, visited at 12:00 pm on August 28, 2016.

[28] A. Elsherif, T. Fetouh, and H. Shaaban, "Power quality investigation of distribution networks embedded wind turbines," *Journal of Wind Energy*, vol. 2016, pp. 1-17, Mar. 2016.

[29] P. Sorensen, N. A. Cutululis, T. Lund, A. D. Hansen, T. Sorensen, J. Hjerrild, M. H. Donovan, L. Christensen, and H. K. Nielsen, "Power quality issues on wind power installations in Denmark," in *Proc. IEEE Power Engineering Society General Meeting*, pp. 1-6, 2007.

[30] Y. K. Wu, G. W. Chang, and L. Wang, "Power quality measurements and analysis for Zhong-Tun Wind Farm in Penghu," in *Proc. CACS International Automatic Control Conf.*, pp. 433-438, 2013.

[31] "Polynomial Curve Fitting", http://www.mathworks.com/help/curvefit/examples/polynomial-curve-fitting.html, visited at 8:00 am on August 20, 2016.

[32] A. Khosravi, S. Nahavandi, and D. Creighton. "Prediction intervals for short-term wind farm power generation forecasts," *IEEE Trans. Sustainable Energy*, vol. 4, no. 3, pp. 602-610, Jul. 2013.

[33] C. Andalib-Bin-Karim, X. Liang, N. Khan, and H. Zhang, "Determine Q-V Characteristics of Grid Connected Wind Farms for Voltage Control Using Data Driven Analytics Approach", Proceedings of 2017 IEEE Industrial and Commercial Power Systems (I&CPS) Conference, pp. 1-14, May 7th - 11th, Niagara Falls, ON, Canada, 2017.

Chapter 4

Fuzzy Secondary Controller Based Virtual Synchronous Generator Control Scheme for Microgrids

[1]Chowdhury Andalib-Bin-Karim, *Student Member, IEEE*, [1]Xiaodong Liang, *Senior Member, IEEE*, [2]Huaguang Zhang, *Fellow, IEEE*

[1]Faculty of Engineering and Applied Science, Memorial University of Newfoundland, St. John's, Newfoundland, Canada.

[2]College of Information Science and Engineering, Northeastern University, Shenyang, Liaoning, China.

An initial version of this work has been published in the proceeding of *IEEE Industry Application Society Annual Meeting, 2017, Cincinnati, OH, USA*. A version of this chapter has been published in the *IEEE Transactions on Industry Applications, March/April 2018*. The author of this manuscript Chowdhury Andalib-Bin-Karim developed this work under the supervision of Dr. Xiaodong Liang. Mr. Karim's contribution to this paper is as follows:

- Performed all literature searches required for background information.
- Developed dynamic models in MATLAB/Simulink and performed simulation.
- Analyzed the results.
- Wrote the paper.

Dr. Xiaodong Liang provided continuous technical guidance, checked the results, reviewed the manuscript, provided important suggestions to accomplish the work, and modified the final version

of the manuscript. Dr. H. Zhang reviewed the manuscript and provided expert opinion to improve the work. In this chapter, the manuscript is presented with altered figure numbers, table numbers and reference formats in order to match the thesis formatting guidelines set out by Memorial University of Newfoundland.

Abstract- In a microgrid with distributed generation (DG) units, proper control of the grid interfacing inverter is critical to facilitate safe and stable operation of the system. The droop control mechanism is a widely accepted control method in a microgrid operation. However, a droop controller is unable to provide inertia support in such systems, and thus, cannot contribute in primary frequency control during disturbances. The virtual synchronous generator (VSG) method was introduced in 2007 for the grid interfacing inverter control, this approach can provide virtual inertia support along with emulation of steady-state droop characteristics of synchronous generators. In this paper, a fuzzy secondary controller (FSC) based VSG control scheme is proposed for voltage and frequency regulation in microgrids. The proposed control scheme shows significantly improved dynamic performance when compared with conventional droop and conventional VSG control through several case studies. Its effectiveness and robustness is further evaluated through sensitivity studies.

Keywords- Droop control, frequency control, fuzzy secondary controller, microgrids, virtual synchronous generator (VSG), voltage control.

4.1 Introduction

Renewable energy sources such as solar photovoltaic (PV) panels and wind turbines are getting popularity due to their economic and environmental advantages over fossil fuel based conventional power generation. A microgrid is a low voltage small-scale power system that is mainly driven by power electronic inverter interfaced renewable energy sources, it can be either designed as a stand-alone or a grid-connected power system. A grid-connected microgrid should also be able to operate in a stand-alone mode (or known as an islanded mode) when there is power interruption from the utility grid [1]. Distributed generation (DG) units are usually connected through a voltage source inverter (VSI) in a microgrid. VSIs as a grid interface are advantageous over current source inverters due to their ability to keep the voltage stable during autonomous operation mode and to allow DG units to be connected in parallel, thus providing the opportunity to expand generation capacity when desired [2]. However, integration of large number of DG units poses a great challenge for safe and stable operation of microgrids [3].

In the grid-connected mode, a microgrid supplies or absorbs power to or from the grid according to active and reactive power set points of the control system. When a disturbance in the grid side occurs, the microgrid may be required to operate in an autonomous mode supplying power to critical local loads only. In this mode, voltage and frequency of each DG unit need to be controlled independently by local controllers based on the information available in the DG unit itself. Appropriate power sharing among DG units needs to be ensured as well. Therefore, it is important to design control mechanism accurately so that operating requirements of microgrids in both grid-connected and islanded modes can be satisfied. The droop control mechanism is a widely accepted control strategy for VSIs in microgrids. This method is particularly given preference over the centralized control method because it allows parallel connected inverters to operate without any

external communication among them, thus eliminating economic and technical barriers associated with communication links [4]. The configuration of a droop controller is also simple and easy to implement. However, inverter interfaced DG units will result in less inertia, a droop controller cannot provide inertia support in such systems, and thus, cannot contribute in primary frequency control during disturbances.

The virtual synchronous generator (VSG) control strategy was first introduced in 2007 by Beck and Hesse [5] to overcome this limitation. VSG control enables the VSI to emulate steady-state droop characteristics as well as dynamic characteristics of a synchronous generator by providing virtual inertia support during disturbances. As an emerging new control method, VSG control can achieve voltage and frequency control, and oscillation damping [6]-[14]. VSG control has the ability of providing grid support by automatically changing its active and reactive power according to the frequency and amplitude of grid voltage, respectively [7]. In [8], an experimental study has been carried out to analyze the effect of virtual rotating mass and virtual damper of VSG control in counteracting grid frequency drop and reducing grid oscillations. In [9], an autonomous power system is considered and the performance of VSG control to regulate network frequency is evaluated. In [10], an energy storage device is included in VSG control to inject or absorb power according to grid requirement considering a PV-hydro based microgrid, energy storage requirements for different PV penetration levels are determined. VSG is also capable to reduce rate of change of frequency during solar irradiance or load variations, as reported in this work. In [11], a VSG control mechanism with variable optimal inertia is developed for an energy storage system operating in a mini grid. An improved frequency control is achieved comparing to conventional fixed inertia based method. In addition to frequency control, a modification in VSG control strategy is proposed in [12] to reduce harmonic content in the output current of the inverter.

The modified strategy eliminates the use of current control loop in fundamental frequency, rather incorporates a resonant controller to provide additional control action. In [13], [14], a VSG control scheme with cascaded voltage and current control loops is presented and a small signal model of the control system is developed to facilitate application of linear analysis techniques for stability assessment and tuning of controller parameters.

In recent studies, the secondary control mechanism has been examined in droop controlled microgrids to improve the voltage and frequency regulation performance under load variation by modifying droop controller's operating points under disturbances [15], [16]. The fuzzy logic technique has been widely accepted for its ability to manage multiple variables and translate complex algorithms through simple fuzzy rules, this technique combined with droop control has been proven to be successful in managing microgrids based on local measurements, reducing dependency of the hierarchical control structure on communication links [17], [18]. Although there are a few applications reported in droop control, no publication has been found using the fuzzy secondary control mechanism combined with VSG control. To fill in this gap, a fuzzy secondary controller (FSC) based VSG control scheme is investigated in this paper.

As two major control methods, conventional droop and conventional VSG control have been compared in [19]-[22] in terms of stability in microgrid. It is proved that the small-signal response of inertia emulation characteristics of VSG control is equivalent to conventional droop control. Thus, droop gain and filter time constant of the power feedback in a droop controller can be directly associated with damping factor and inertia constant of a VSG controller [21]. However, comparative studies for droop and VSG control on power quality aspects have not been conducted. In this paper, conventional droop and conventional VSG control are compared from power quality

aspects, which will facilitate better understanding of the two important control methods. Their performance is then further compared with the proposed FSC based VSG control scheme.

In this paper, a FSC based VSG control mechanism is proposed for the grid-interfacing inverter control in microgrids. Outputs of the FSC are switched to appropriate references of the VSG controller when the microgrid is subjected to the operating mode change, which cancels out the requirement of switching on an additional tertiary control layer during grid-connected operation. Several case studies are carried out using MATLAB/SIMULINK simulation to evaluate the effectiveness and robustness of the proposed method by comparing with conventional droop and conventional VSG control methods.

The paper is arranged as follows: in Section 4.2, the principle of the proposed FSC based VSG control scheme is presented; a description of test system under study is provided in Sections 4.3; case and sensitivity studies are conducted in Sections 4.4 and 4.5, respectively to evaluate the performance of the proposed control system; conclusions are drawn in Section 4.6.

4.2 The Proposed FSC Based VSG Control Scheme

In this section, the principle of the proposed FSC based VSG control scheme is demonstrated. The whole control scheme consists of a primary controller using VSG control, and a secondary controller using fuzzy control. The references of the primary controller are modified using the outputs of the secondary controller.

4.2.1 Primary Controller Using VSG Control

Renewable energy sources are integrated to power grid through power electronic inverters. These inverters are static without rotational energy, which results in negligible inertia. Extensive usage

of such inverters can considerably reduce the equivalent rotational inertia of power grid. Low moment of inertia degrades frequency stability because power system frequency is inversely proportional to the system's inertia, and could cause large frequency oscillations during disturbances. The main idea of VSG control is to emulate characteristics of a real synchronous machine: inertial characteristics and damping of electromechanical oscillation [5], [22]-[24]. To achieve this, VSG control contains a mathematical model of a real synchronous machine including governor model and excitation system model such that, the grid-tied inverter reflects dynamic characteristics of a synchronous generator. Moreover, some additional control blocks, such as active power regulator and reactive power regulator, can also be adopted to ensure an autonomous operation of the grid interfacing inverter. Since there is no existence of magnetic poles and mechanical shafts for VSG controllers, they are realized virtually with the help of a mathematical model in the control system.

Corresponding parameters of the mathematical model can be chosen independently to control the virtual torque and excitation voltage, thus achieving the desired behavior. For example, if there is any frequency change in the grid, active power is required to be supplied by the inverter, which can be realized by influencing the virtual torque value of the VSG, while the direct voltage side of the inverter provides the required energy. Similarly, voltage support to the grid can also be provided by controlling the virtual excitation voltage and supplying the required reactive power. In this case, the capacitor in the intermediate circuit of VSG supplies the required reactive current [5], [24].

The procedure of the VSG control implementation is summarized as follows: (1) Step 1 - the real time measurement of grid voltage is acquired and sent to the process computer, which contains the VSG control algorithm; (2) Step 2 - the process computer utilizes the synchronous machine

model to compute the stator current of the VSG in real time situation; (3) Step 3 - based on the calculated reference current, a current controller sends appropriate gating signal to the inverter. In this approach, parameters of the VSG model can be chosen independently in order to operate the inverter in a desired manner. These parameters directly affect the generation of reference current and thus have influence on operating behavior of the inverter [8].

The swing equation of synchronous generator is adequate to represent inertia and damping properties of a synchronous generator. Utilizing the well-known swing equation, virtual inertia control of the inverter can be realized, thus making the inverter to emulate the characteristics of the rotor. The swing equation can be expressed by [22], [25],

$$J\frac{d\omega}{dt} = T_m - T_e - D(\omega - \omega_g) \tag{4.1}$$

$$\delta = \int \omega \, dt \tag{4.2}$$

where, J is the rotor inertia, ω is the angular speed of the generator and ω_g is the angular frequency of the utility grid. T_m and T_e are the mechanical and electrical torque, respectively. D is a damping coefficient which characterizes the torque developed in the damper winding during a transient condition. The damping coefficient D usually varies depending on the operating condition. Here, δ represents the virtual rotor angular position and gives the phase angle of the voltage generated by the VSG model [22]. T_m and T_e can also be expressed conveniently in terms of the input active power (P_{in}) and output active power (P_{out}) of the inverter using the following expressions: $T_m = P_{in} / \omega$ and $T_e = P_{out} / \omega$.

The electrical part of the VSG controller mainly utilizes the stator model of synchronous generator to compute the reference currents for the current controller. The mathematical model is

usually kept very simple only incorporating essential features of a synchronous generator. The electrical part is later connected to the mechanical part of the controller through a power balance considering both electrical and mechanical power. The equivalent circuit of a stator can be expressed by [6], [26],

$$\vec{e} - \vec{u}_{grid} = \vec{\imath}_{ref}.R_s + L_s.\frac{d\vec{\imath}_{ref}}{dt} \tag{4.3}$$

where, $\vec{e} = [e_1\ e_2\ e_3]^T$ is the induced electromotive force (EMF) in the stator winding and $\vec{u}_{grid} = [u_1\ u_2\ u_3]^T$ represents the utility grid voltage at the point of common coupling (PCC). R_s and L_s represent the stator resistance and inductance respectively. The induced EMF $\vec{e}$ can be expressed in terms of amplitude E_p derived from a reactive power regulation block and phase angle δ calculated using Equation (4.2) as follows [6]:

$$\vec{e} = \begin{bmatrix} e_1 \\ e_2 \\ e_3 \end{bmatrix} = E_p.\begin{bmatrix} \sin(\delta) \\ \sin(\delta - \frac{2}{3}\pi) \\ \sin(\delta + \frac{2}{3}\pi) \end{bmatrix} \tag{4.4}$$

The reference current ($\vec{\imath}_{ref}$) computed using Equations (4.3) and (4.4) are then compared with the measured inverter output current in the current controller, and appropriate gating signal for the inverter is generated. The block diagram of synchronous machine model including both mechanical and electrical parts is presented in Fig. 4.1.

Mechanical power input of a synchronous generator is adjusted by the governor system based on the grid frequency deviation, which is called the active power-frequency (*P-f*) static feature of synchronous generator. A *P-f* droop controller can be introduced in the VSG control structure to facilitate emulation of this feature by the inverter. This type of auxiliary control mechanism is

particularly essential for providing frequency support and maintaining stability in a weak grid [27]. The *P-f* droop control mechanism can be expressed by

$$P_{ref} = P_{in} + k_f(f_0 - f_g) \tag{4.5}$$

where, P_{ref} and P_{in} are the reference and initial active power input of the inverter, respectively; f_0 and f_g are the nominal and actual value of the grid frequency; k_f is the droop constant which facilitates the frequency regulation [28].

The reactive power supply of a synchronous generator is regulated by the exciter system depending on the terminal voltage of the generator. Similar reactive power regulation by the inverter can be realized by the inclusion of a reactive power-voltage (*Q*-*V*) droop controller in the VSG control structure, which can be expressed by [14], [25],

$$E_p = E_0 + k_q(Q_{ref} - Q) + k_v(U_0 - U) \tag{4.6}$$

where, E_0 and E_p are the amplitude of nominal and reference voltage of VSG, respectively. *Q* and Q_{ref} represent actual and reference reactive power output of the VSG. *U* and U_0 are actual and nominal values of the grid voltage. *kv* and *kq* are the proportional gains for terminal voltage and reactive power regulation. Additionally, a first order delay controller can be incorporated in the droop control structure, which makes the process of active power reaching a new value slow, thus reducing its adverse effect on the system in certain operating conditions. Moreover, a PI controller can be included to maintain a stable value of output voltage [27]. The overall control structure of a VSG control is depicted in Fig. 4.2, where it is utilized to control an inverter connecting a distributed energy resource to the utility grid.

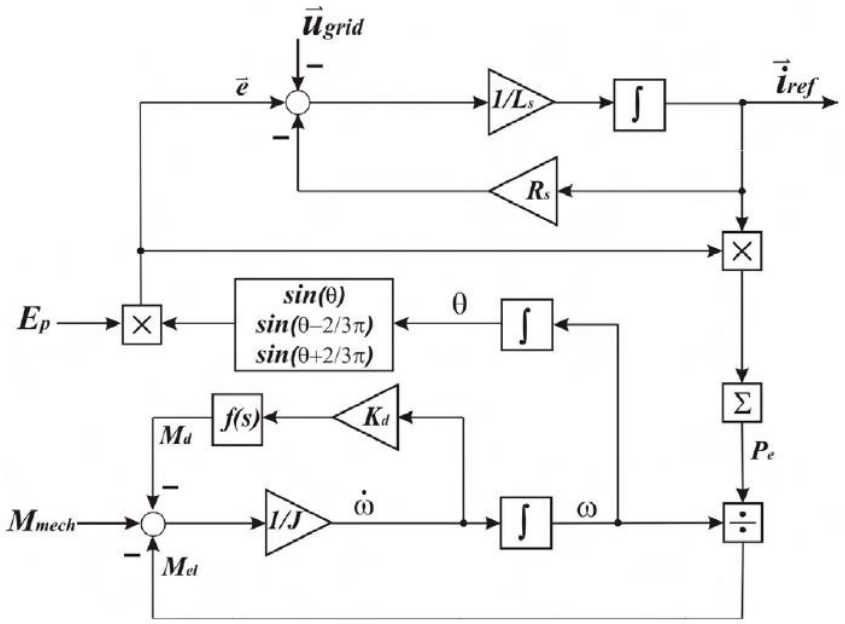

Figure 4. 1: Synchronous machine model for VSG control implementation [6]

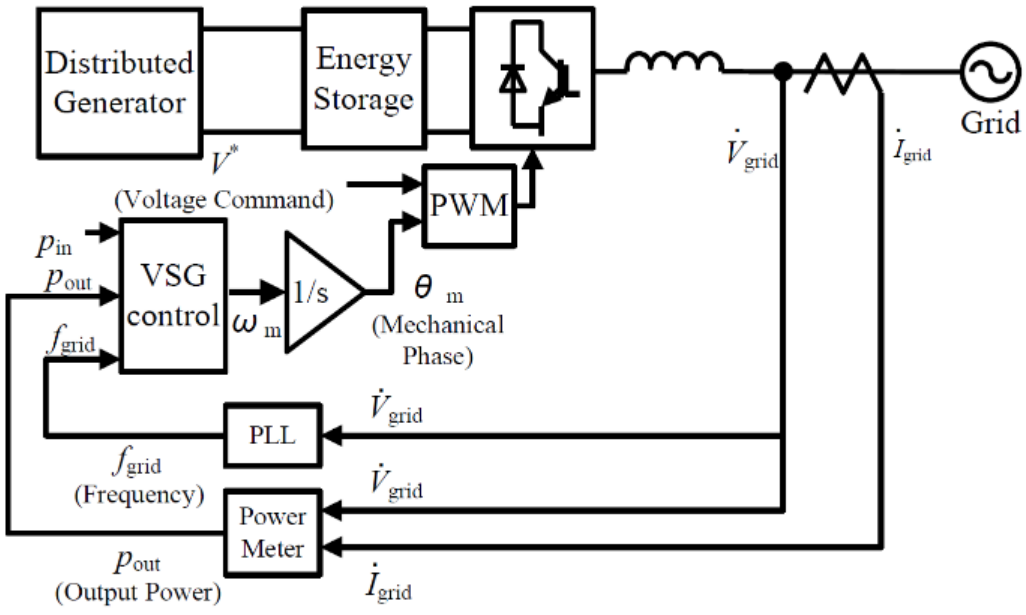

Figure 4. 2: Overall control structure of VSG control [29]

4.2.2 Secondary Controller Using Fuzzy Control

The secondary controller is realized through fuzzy control to reduce voltage and frequency deviations during disturbances. There are total six inputs for the proposed FSC, which can be obtained based on local measurements of DG units only. The inputs include active and reactive power errors (e_P and e_Q), voltage and frequency deviations (e_E and e_ω), and voltage and frequency gradients (dE and $d\omega$).

Voltage and frequency deviation inputs of FSC (e_E and e_ω) can be defined by

$$e_E = (E_0 - E)K_{eE} \tag{4.7}$$

$$e_\omega = (\omega_0 - \omega)K_{e\omega} \tag{4.8}$$

where, E_0 and ω_0 are the microgrid reference values of voltage and frequency respectively, E and ω are the voltage and frequency signals measured at the PCC, respectively; K_{eE} and $K_{e\omega}$ are the gains that normalize crisp values into the range values of e_E and e_ω, respectively. In the proposed FSC, the e_E and e_ω inputs are defined using three triangle membership functions as shown in Fig. 4.3(a). The input ranges are normalized between [−1; 1] with the crossing points being located at −0.5 and 0.5. The crossing points are meant to allow a preset steady state error while supplied power values are slightly different from their reference values [15, 16].

Active and reactive power error inputs of FSC (e_P and e_Q) can be defined as,

$$e_P = \left(P_{ref} - P\right)K_{eP} \tag{4.9}$$

$$e_Q = \left(Q_{ref} - Q\right)K_{eQ} \tag{4.10}$$

where, P_{ref} and Q_{ref} are the reference values of active and reactive power to be supplied to the grid, P and Q are the active and reactive power signals measured at the PCC, K_{eP} and K_{eQ} are the gains that normalize crisp values into the range values of e_P and e_Q, respectively. In the proposed FSC, the e_P and e_Q inputs are defined using one triangle and two trapezoid membership functions as shown in Fig. 4.3(b). The input ranges are normalized between [−1; 1] with the crossing points being located at −0.05 and 0.05, resulting in a narrow 'zero' range. The width of 'zero' range mainly determines the amplitude of oscillatory steady state error [15, 16].

Voltage and frequency gradient inputs (dE and $d\omega$) are used to prevent the FSC from operating during voltage and frequency transient conditions. In the proposed FSC, the dE and $d\omega$ inputs are defined using a triangle and a trapezoid membership functions as shown in Fig. 4.3(c). The input ranges are normalized between [0; 1] with the crossing points being located at 0.05 [15, 16].

The outputs of the proposed FSC are computed by combination of input quantities based on a defined set of fuzzy logic rules. Outputs of the FSC are different in the two operation modes. In an islanded mode, the outputs are frequency and voltage incremental offsets ($\Delta\omega$ and ΔE), which are utilized to adjust frequency and voltage references of the VSG controller; in a grid-connected mode, the outputs are active and reactive power incremental offsets (ΔP and ΔQ), which are utilized to adjust active and reactive power references of the VSG controller. Therefore, output gains of the FSC only need to be adjusted accordingly when the operation mode changes, while its inputs remain the same in both operation modes. There is no communication required among DG units. The two output gains (K_{of} and K_{ov}) of the FSC are hand tuned based on microgrid's dynamic response characteristics.

In the proposed FSC, the outputs are defined using five singleton membership functions as shown in Fig. 4.3(d), which allows the utilization of whole output range. The output ranges are normalized between [−1; 1] with the singletons being located at −1, −0.5, 0, 0.5 and 1.

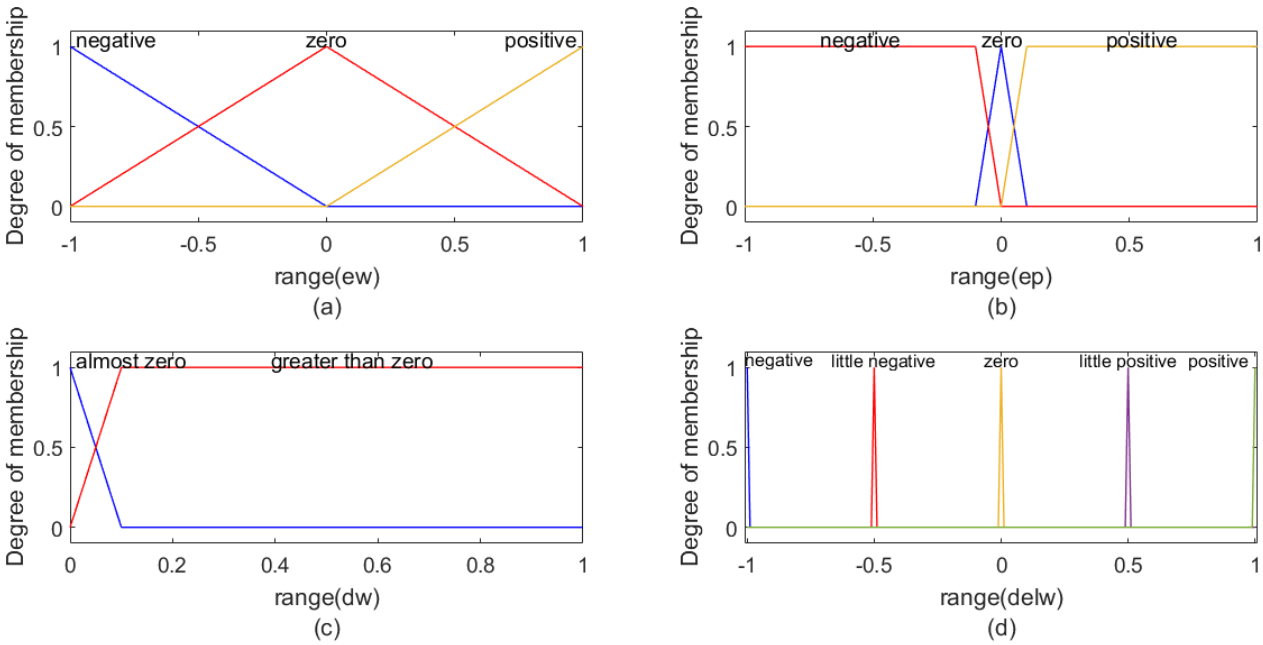

Figure 4. 3: Membership functions of the FSC: (a) e_ω and e_E inputs, (b) e_P and e_Q inputs, (c) $d\omega$ and dE inputs, and (d) $\Delta\omega$ and ΔE outputs.

For voltage and frequency deviation inputs: the limit values are defined according to the rated values of voltage and frequency. It is considered that the voltage and frequency value can drop to any value between 1 p.u. to 0 p.u. or rise to any value between 1 p.u. to 2 p.u. Triangular membership functions are used instead of trapezoidal functions to allow a bigger steady state error. Triangular membership functions are symmetric in nature and fuzzy logic controller boundary values are conventionally defined as 0 to 1 or -1 to 1; which is adopted in this study. Similar approach has been followed to define limit values, membership functions etc. for other inputs.

The proposed FSC operates using 20 fuzzy logic rules. 10 rules are allocated for each output, which generate appropriate output quantities based on the combined input quantities. An islanding

detection scheme needs to be integrated in the control system in order to detect if the microgrid is operating in an islanded mode. In an islanded mode, there are two outputs $\Delta\omega$ and ΔE for the FSC. When the input $d\omega$ is 'almost zero', the output $\Delta\omega$ can be either greater or less than zero, depending on the status of the inputs e_ω and e_P . e_ω mainly determines the sign of $\Delta\omega$. When e_ω is 'positive', $\Delta\omega$ is greater than zero. The magnitude of $\Delta\omega$ is determined by e_P, where 'negative' and 'positive' status of e_P result in 'little positive' and 'positive' values of $\Delta\omega$, respectively. Again, when e_ω is 'negative', $\Delta\omega$ is less than zero, the magnitude of $\Delta\omega$ is also determined by e_P, where 'positive' and 'negative' status of e_P result in 'little negative' and 'negative' values of $\Delta\omega$, respectively. The output is 'zero' when $d\omega$ is 'greater than zero', thus ensuring the FSC not to operate during transient conditions. Similar rules are applied for the output ΔE, which is determined based on the status of the inputs dE, e_E and e_Q. The Fuzzy logic rules for the outputs, $\Delta\omega$ and ΔE, are presented graphically in Figs. 4.4 and 4.5.

In a grid-connected mode, there are two outputs ΔP and ΔQ for the FSC. The Fuzzy logic rules for ΔP and ΔQ are very similar to the outputs $\Delta\omega$ and ΔE in an islanded mode except that $\Delta\omega$ is replaced by ΔP, ΔE is replaced by ΔQ.

The FSC operation for the microgrid overload condition is not considered in this study, so the number of fuzzy rules required for the FSC to operate can be significantly reduced, and thus, computational burden of the FSC is reduced, this also makes the FSC's structure simpler and improves the response time of the controller.

The main advantage of the proposed FSC over the conventional secondary controller is that it is not required to switch on an additional tertiary control layer in a grid-connected mode, and outputs of the FSC are switched to appropriate references of the VSG controller when the operation mode of a microgrid is changed.

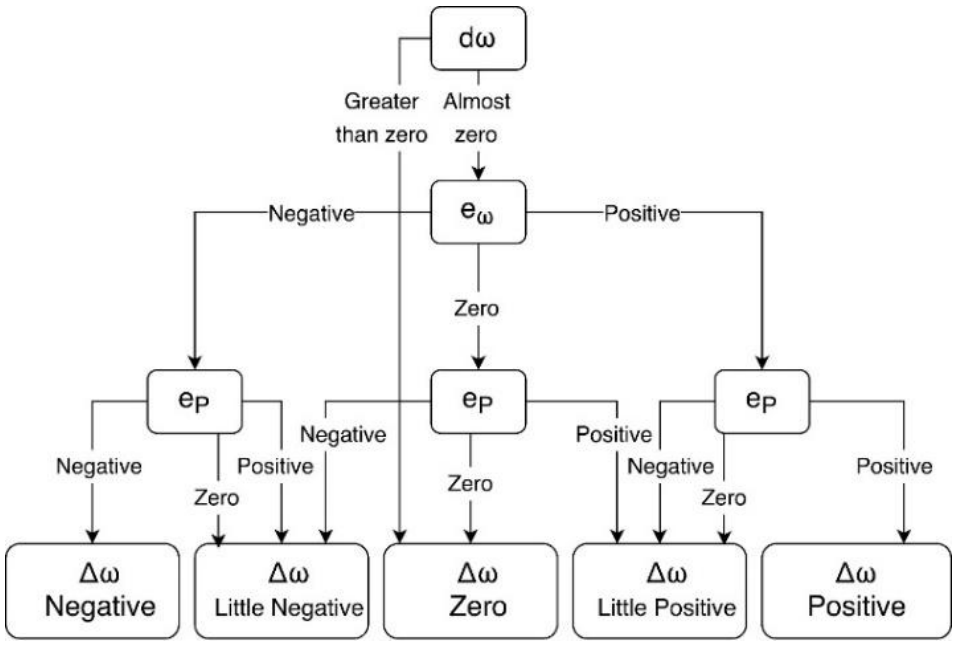

Figure 4. 4: Fuzzy logic rules for $\Delta\omega$ output of the FSC in an islanded mode

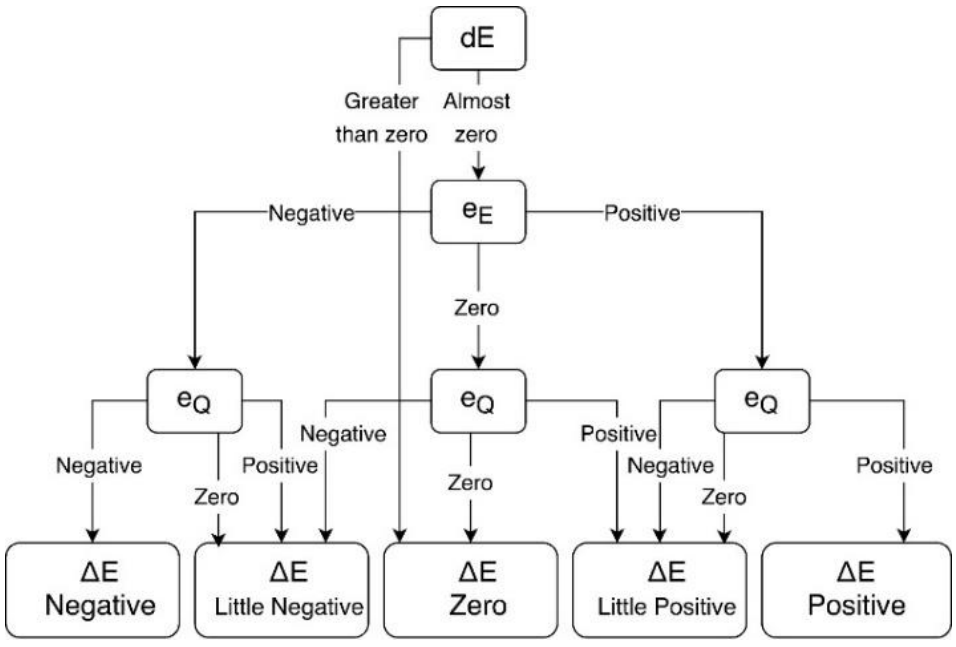

Figure 4. 5: Fuzzy logic rules for ΔE output of the FSC in an islanded mode

4.3 Test System Description

A microgrid comprising two DG units serves as a test system in this paper to evaluate the effectiveness of the proposed FSC based VSG control scheme. An overall system configuration of the microgrid is provided in Fig. 4.6.

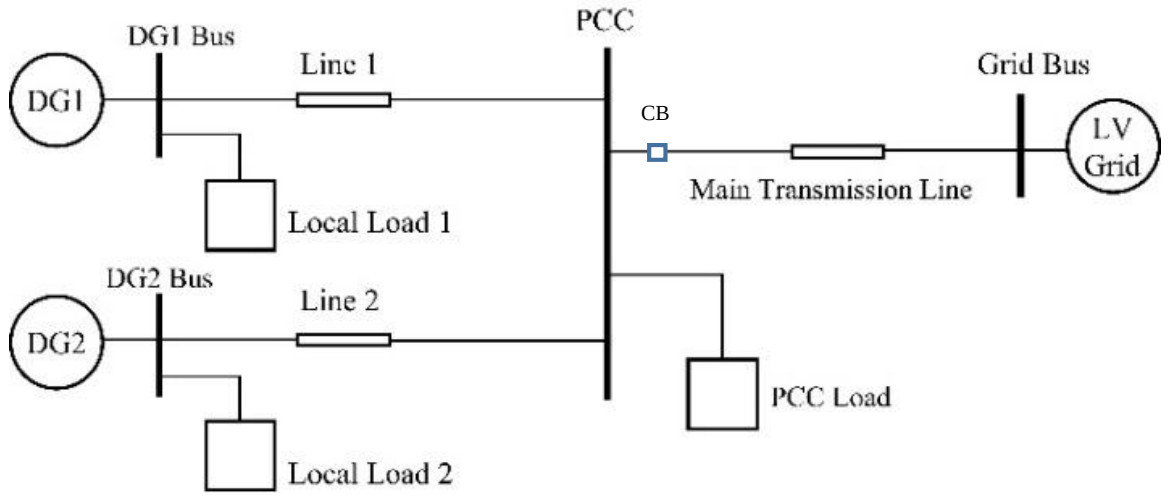

Figure 4. 6: The system configuration of the test microgrid

The two DG units are connected in parallel, where each DG unit contains a distributed generation source, a pulse width modulation (PWM) controlled VSI, and a LC filter for harmonic mitigation. The distributed generation source can be any type of renewable energy sources, such as PV panels, wind turbines, or energy storage system. Initially, renewable energy sources such as PV panels are modeled as constant DC sources inside DG units. The purpose is to allow better understanding of the proposed controller's performance when the microgrid is subjected to grid-side disturbances. A 5 kW, 1 kVar local load is connected to the output of a LC filter at each DG unit.

The microgrid is connected to a 380 V_{RMS} rated low voltage power grid through a circuit breaker (CB) and a main transmission line. The circuit breaker may operate during disturbances allowing

the microgrid to continue its operation in an islanded mode. A 8 kW load is connected to the PCC. Inverters in DG units are controlled by the proposed control scheme. The parameters of the test system are provided in Table 4.1. The simulation model of the proposed control scheme is developed using Matlab/Simulink as shown in Fig. 4.7.

Table 4. 1: Test system parameters

Parameters		Values
Nominal DC bus voltage		700V
Nominal AC bus RMS line voltage		380V
Inverter filter	Resistance, R_f	0.2Ω
	Inductance, L_f	3×10^{-3} H
	Capacitance, C_f	15×10^{-6} F
Line impedance	R_L	0.641 Ω/km
	X_L	0.101 Ω/km
Droop coefficients	*1/m*	1×10^{-5}
	1/n	0.3×10^{-5}
Voltage controller	Proportional gain	0.2
	Integral gain	280.8
Current controller	Proportional gain	0.24

Droop coefficients, gains of the current controllers for the primary VSG controller are shown in Table 4.1. They are common parameters used in all three control mechanisms (the proposed FSC based VSG control, conventional droop control, and conventional VSG control) evaluated in this paper. The main difference between conventional droop and conventional VSG control is the

addition of a mechanical part in VSG control along with the *P-f* droop controller, which incorporates a swing equation for an improved active power regulation performance. Two important parameters of the swing equation are virtual inertia (*J*) and virtual damping factor (*kd*), which are chosen as 0.5 kg.m^2 and 10, respectively, in this study. The stator resistance (R_s) and inductance (*Ls*) values for VSG are chosen as 0.01 Ω and 3.56 mH, respectively. Gains of the FSC are presented in later section of the paper.

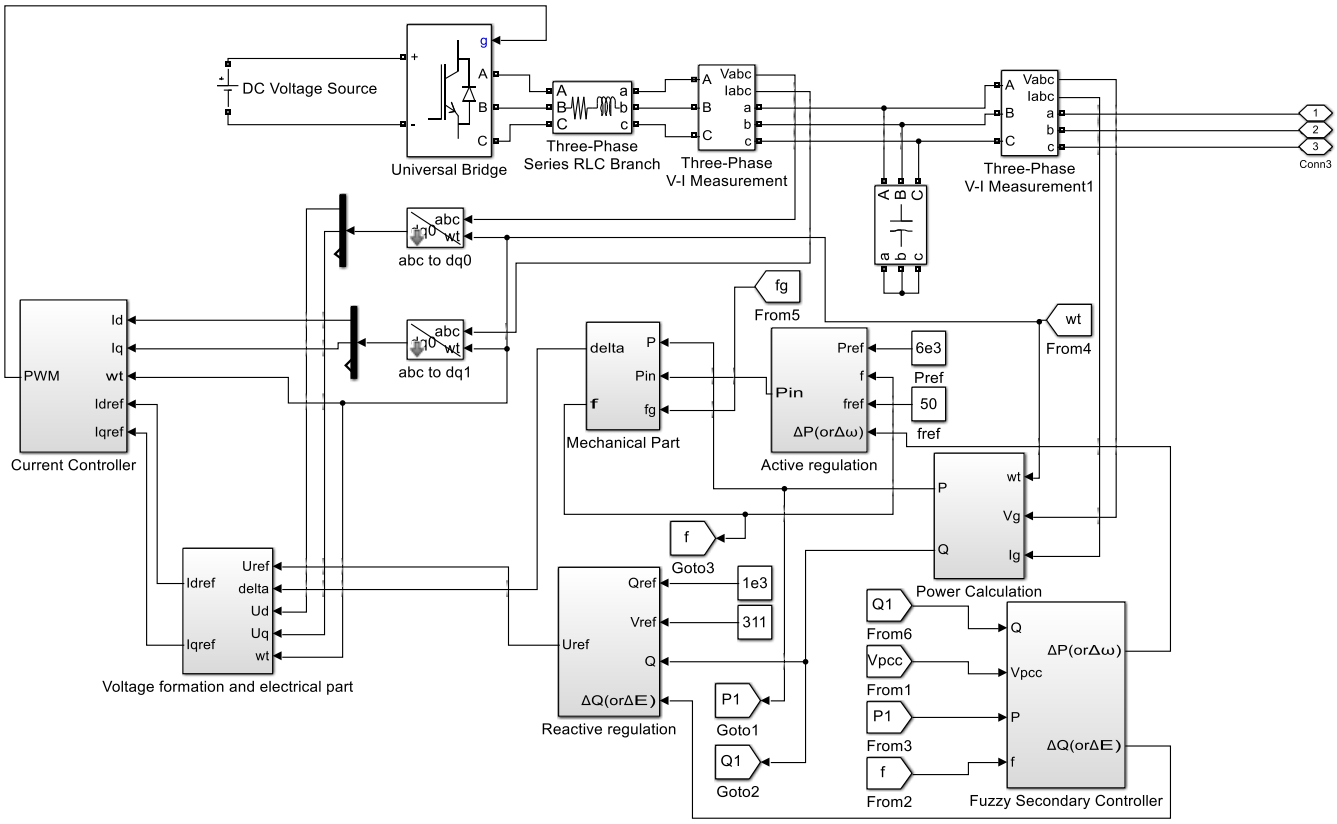

Figure 4. 7: The model developed in Matlab/Simulink for the proposed FSC based VSG control scheme.

4.4 Case Studies

To validate the effectiveness of the proposed FSC based VSG control scheme, several case studies are conducted in this section. Through the case studies, the proposed control scheme has significantly improved dynamic characteristics of the microgrid compared to conventional droop and conventional VSG control methods.

4.4.1 Case 1: Grid Side Voltage Disturbances in Grid-Connected Mode

In the proposed control scheme, active and reactive power references for the VSG controller are set as 6 kW and 1 kVar, respectively, for each DG unit in a grid-connected mode. The two output quantities (ΔP and ΔQ) derived from the FSC is added to power references of the VSG controller, thus controlling active and reactive power supply of DG inverters based on the FSC's frequency and voltage deviation inputs.

In this case study, a 50% grid-side voltage sag occurs at the grid bus from 1 s to 1.2 s. The grid frequency remains at the nominal frequency.

Active and reactive power supplied by DG units during the event are shown in Fig. 4.8. It is found that when the microgrid is controlled using the proposed control scheme, power deviation is very small and it takes least time for power to return to their nominal values after the disturbance dies out. However, for the same event, conventional droop and conventional VSG control methods lead to a much higher power deviation and a much longer time to return to their nominal values.

Dynamic response of voltage and frequency at the PCC and the grid bus during the event are presented in Fig. 4.9. It is found that conventional droop control has the worst frequency response

with the largest frequency deviation. The proposed method is comparable and during most of the time is better than the conventional VSG control.

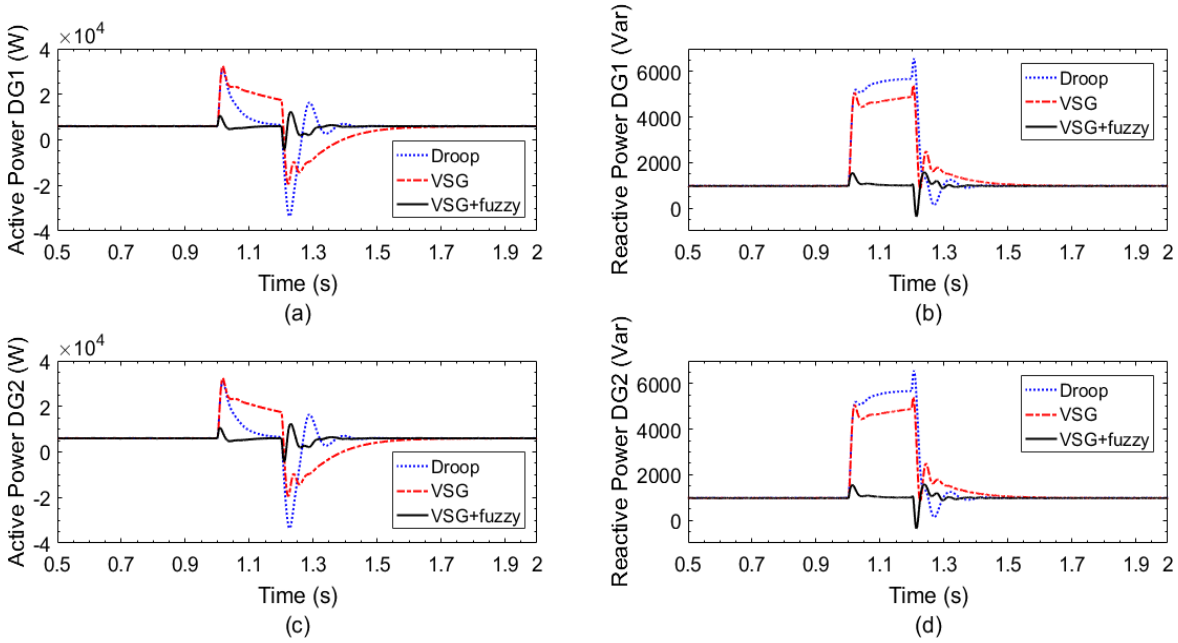

Figure 4. 8: (a) Active and (b) reactive power supplied by DG unit 1, (c) active and (d) reactive power supplied by DG unit 2 (Case 1)

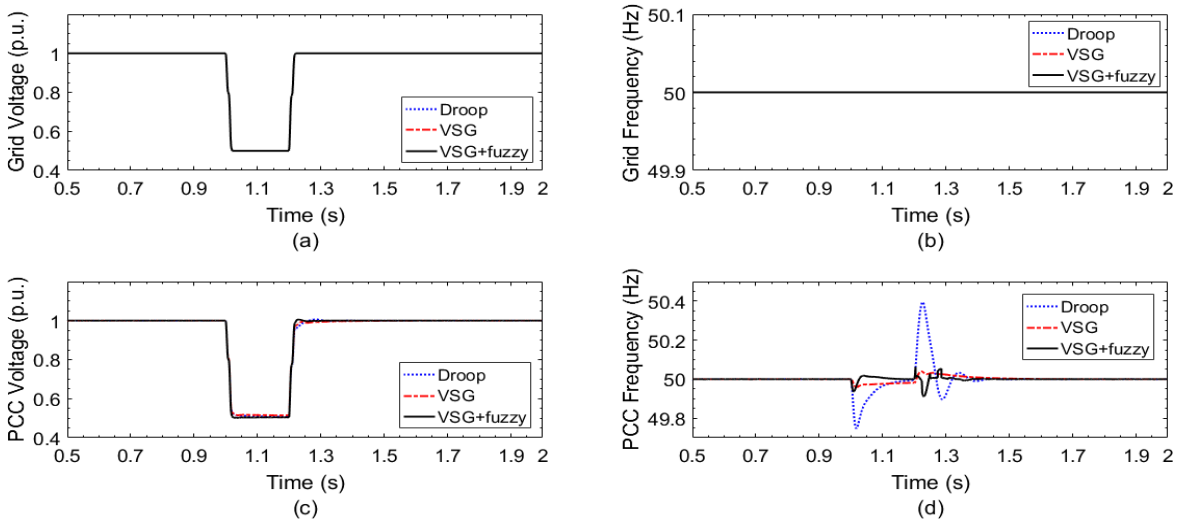

Figure 4. 9: (a) Voltage and (b) frequency at the grid bus, (c) voltage and (d) frequency at the PCC (Case 1)

4.4.2 Case 2: Grid Side Frequency Disturbance in Grid-Connected Mode

In this case study, a 0.05 Hz grid side frequency drop occurs at the grid bus from 1 s to 1.1 s. Active and reactive power supplied by DG units for the event are shown in Fig. 4.10. It is found that the conventional VSG control shows the largest deviation of active and reactive power from their nominal values during disturbance. The proposed method, on the other hand, shows much less power deviations, and it takes least time for power to return to their nominal values after disturbance. The conventional droop control offers similar performance for active and reactive power dynamic response compared to the proposed method.

Dynamic response of voltage and frequency at the PCC and the grid bus can be found in Fig. 4.11 for this event. The voltage at the PCC shows deviation during the event, and the largest voltage deviation occurs when the microgrid is controlled by the conventional VSG method, while the conventional droop control and the proposed method offer similar performance for the PCC voltage with much reduced deviation.

Because the PCC is connected to the grid bus through a short transmission line, it experiences large frequency variations as well. The conventional VSG control shows better performance this time, the proposed method and the droop control show comparable performance.

From this case study, it is found that the output gain of the FSC, K_{of}, directly influences the magnitude of the power deviation during disturbance. A higher value of K_{of} can offer significant reduction in power deviation as compared to conventional VSG, but at a cost of deterioration of frequency profile i.e, a larger oscillation of the PCC frequency during disturbance. Therefore, an optimum value of K_{of} needs to be chosen, which can offer a good reduction in power deviation, as well can maintain the PCC frequency to remain within acceptable range.

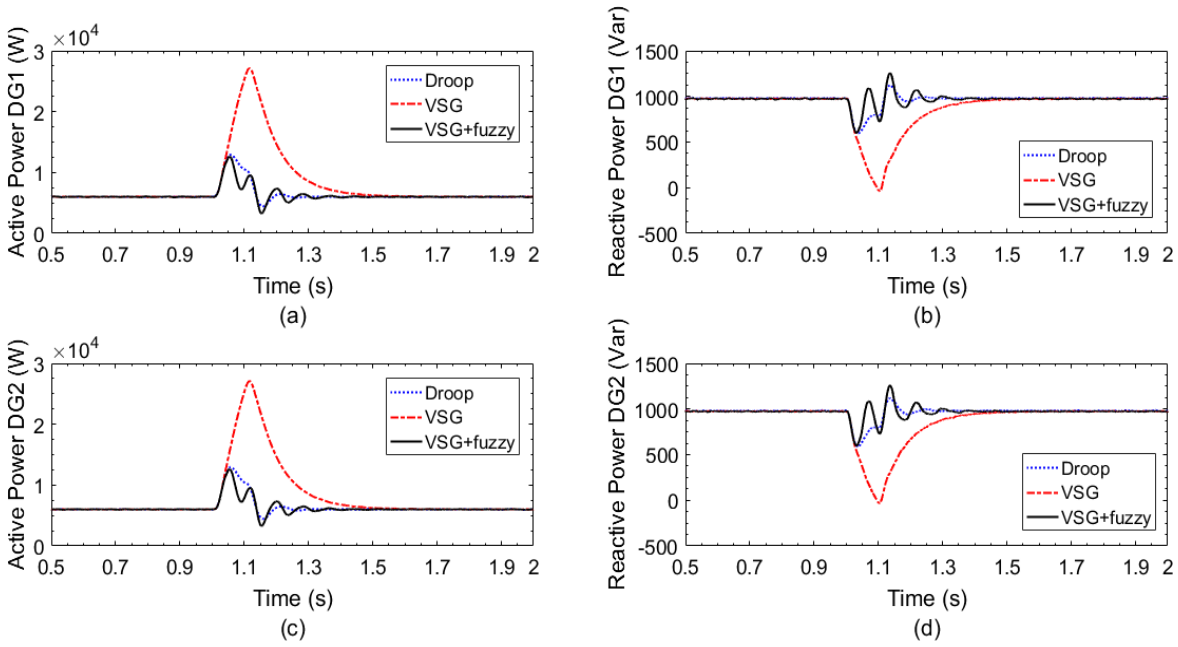

Figure 4. 10: (a) Active and (b) reactive power supplied by DG unit 1, (c) active and (d) reactive power supplied by DG unit 2 (Case 2)

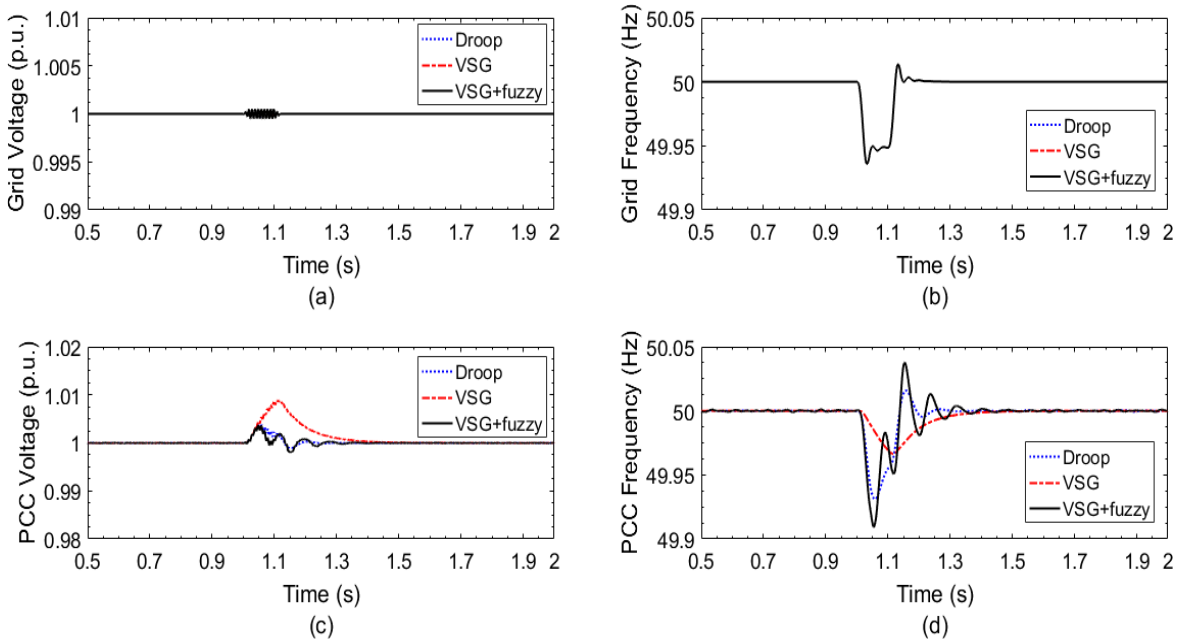

Figure 4. 11: (a) Voltage and (b) frequency at the grid bus, (c) voltage and (d) frequency at the PCC (Case 2)

4.4.3 Case 3: Sudden Load Variation in Islanded Mode

The microgrid is required to continue its operation in an islanded mode when disturbances sustain longer than the permitted fault clearance time. In this mode, the microgrid is disconnected from the utility grid, and DG units solely maintain uninterrupted power supply to the loads. Unlike in a grid-connected mode, where the voltage and frequency of the mircrogrid are governed by the utility grid, in an islanded mode, the voltage and frequency of the microgrid are controlled by DG units.

In this case study, sudden load variation occurs in the islanded microgrid. Before the load variation, both DG units are operating close to their capacity (rated at 10 kVA for each DG) supplying power to two local loads (rated at 5 kW, 1 kVar each) and one PCC load (rated at 8 kW). The load variation applied to the microgrid is described as follows:

1) At 0.5 s, 4 kW PCC load is disconnected;

2) At 1 s, the remaining 4 kW PCC load is disconnected (at this point, only the two local loads are connected to the mircogrid);

3) At 1.5 s, 4 kW PCC load is added, and

4) At 2 s, another 4 kW PCC load is added.

Active and reactive power supplied by DG units during this event are shown in Fig. 4.12. It is found that DG units share active and reactive power appropriately according to their pre-set droop coefficients with the varying load demand. The three control methods show comparable performance for real and reactive power at each DG unit.

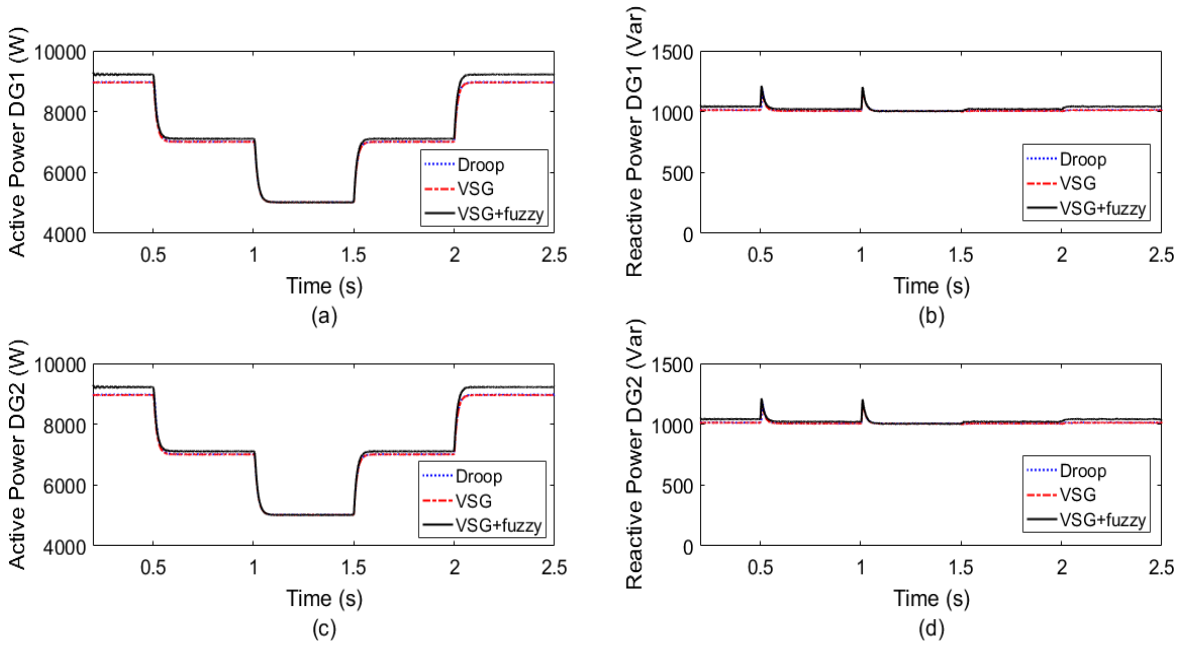

Figure 4. 12: (a) Active and (b) reactive power supplied by DG unit 1, (c) active and (d) reactive power supplied by DG unit 2 (Case 3)

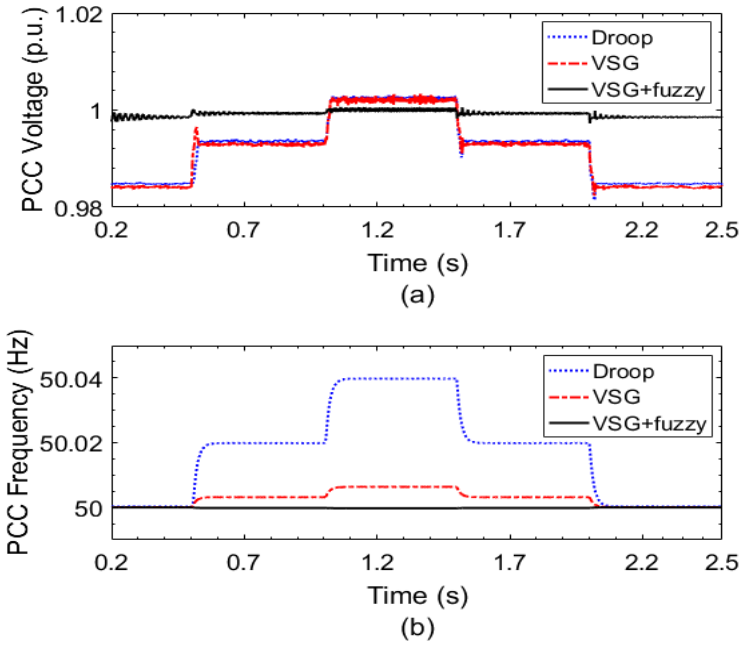

Figure 4. 13: (a) Voltage and (b) frequency at the PCC (Case 3)

Dynamic response of voltage and frequency at the PCC are provided in Fig. 4.13 for the event. The proposed method shows superior performance during this event with both voltage and

frequency very close to nominal values, while conventional droop and conventional VSG control methods lead to large variations for voltage and frequency at the PCC. The conventional VSG does show better frequency control than the conventional droop control.

4.4.4 Case 4: Sudden Irradiance Variation in Islanded Mode

In this case study, a sudden irradiance variation is applied to PV panels to evaluate the effect of renewable generation side disturbance. For this purpose, the DC source in the simulation model in Fig. 4.7 is replaced by a real PV generation system, which consists of a PV array and a DC-DC boost converter. The duty cycle of boost converter is designed such that 700 V dc link voltage is maintained during normal operating condition to match the voltage of DC source previously considered. The PV array consists of the total 14 strings connected in parallel with 5 series connected modules in each string, generating 6 kW of PV power under 1000 W/m^2 of irradiance.

In this case study, the irradiance value is reduced from 1000 W/m^2 to 300 W/m^2 at 0.5 s, and then increased back to 1000 W/m^2 at 0.7 s.

The simulation indicates that irradiance variation does not affect power significantly at each DG as long as there is enough generation available for the load. The dynamic response of active and reactive power for this event is not shown here because they remain almost constant. In the case when the generation cannot satisfy the load demand, shedding of non-critical loads needs to be considered if the battery backup is not available.

Dynamic response of voltage and frequency at the PCC for the event can be found in Fig. 4.14 along with the irradiance variation and the dc link voltage. It is found that the dc link voltage is dropped with irradiance variation. A slight frequency deviation at the PCC from its nominal value can be observed when conventional droop control is employed, however, there is almost no

frequency deviation if the proposed method or conventional VSG method is employed. The voltage response is very similar among three methods.

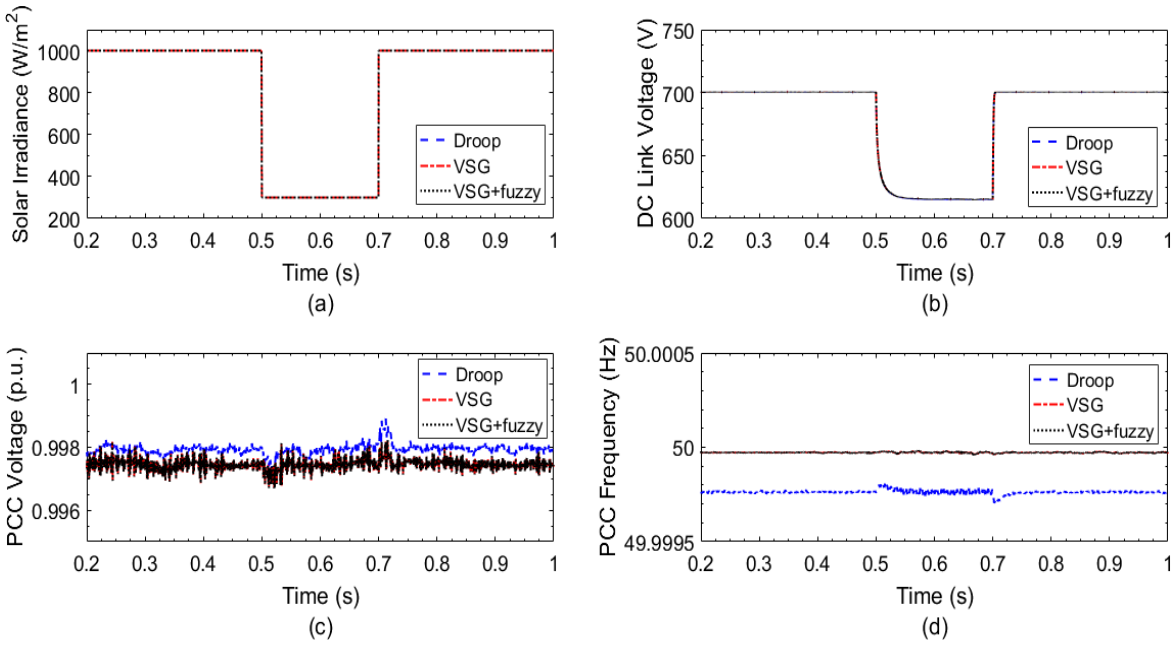

Figure 4. 14: (a) Solar irradiance, (b) DC link voltage, (c) voltage and (d) frequency at the PCC (Case 4)

4.5 Sensitivity Studies

In this section, sensitivity studies are conducted to evaluate the influence of several factors on dynamic performance of the proposed FSC based VSG control scheme: 1) length and R/X ratio of the main transmission line, and 2) output gains of the FSC. The same microgrid used in the case studies (Fig. 4.6) is adopted in the sensitivity studies.

4.5.1 Sensitivity Study 1: Length and R/X Ratio of Transmission Lines

In a grid-connected microgrid, DG units are connected to the utility grid through transmission lines. The droop and VSG control are based on the assumption of weak P–V and Q–δ couplings,

one of the requirements is that *R/X* ratios of all lines are low in order to maintain such weak couplings. However, the *R/X* ratio of a transmission line in a microgrid can be potentially high since it is a low-voltage network [1]. In this sensitivity study, the influence of length and *R/X* ratios of a transmission line is evaluated on dynamic performance of the proposed scheme.

Firstly, the influence of the length of the transmission line is investigated. The system configurations with three different lengths of the main transmission line between the PCC and the grid bus are considered: 100 m, 1 km and 5 km. The line resistance R is 0.35 Ω/km, and the line reactance is 0.23 Ω/km. A grid-side 50% voltage sag is applied at the grid bus from 1 s to 1.2 s while the grid frequency remains constant.

The active and reactive power supplied by DG units during this event are shown in Fig. 4.15 for the three configurations. Fig. 4.15 indicates that the length of the transmission line certainly has effect on dynamic characteristics of the microgrid using the proposed control scheme. The tendency of active and reactive power fluctuation at DG units is similar with different lengths of a transmission line, but the magnitude of the fluctuation is much larger for a longer transmission line. It also takes a longer time for power values to return to their nominal values during disturbance if a longer line is used. The 5 km line configuration shows more dynamics than the 1 km line configuration although their highest peaks of the power deviation are similar.

The dynamic response of voltage and frequency at the PCC and the grid bus during the disturbance are shown in Fig. 4.16. The voltage sag at the PCC are similar for the three configurations. The frequency at the PCC shows fluctuations, a longer line results in a larger frequency deviation and a longer time to return back to the nominal frequency. The 5 km line configuration shows more dynamics than the 1 km line configuration although their highest peaks of the frequency deviation at the PCC are similar.

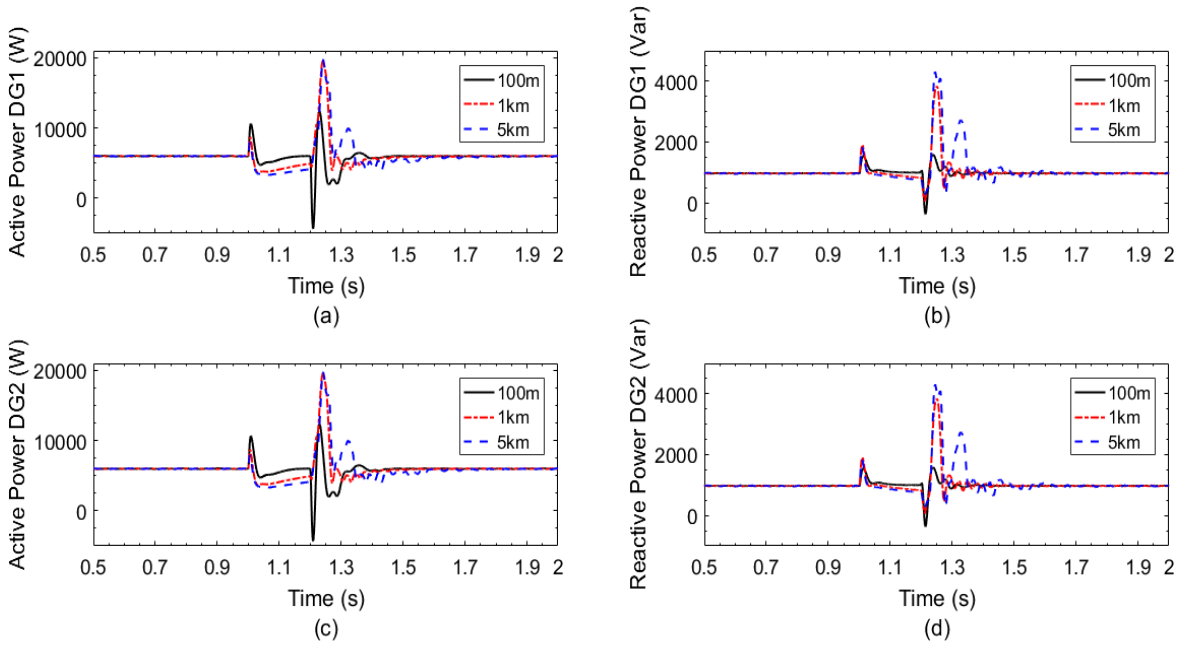

Figure 4. 15: (a) Active and (b) reactive power supplied by DG unit 1, (c) active and (d) reactive power supplied by DG unit 2 (Sensitivity study 1 - Length)

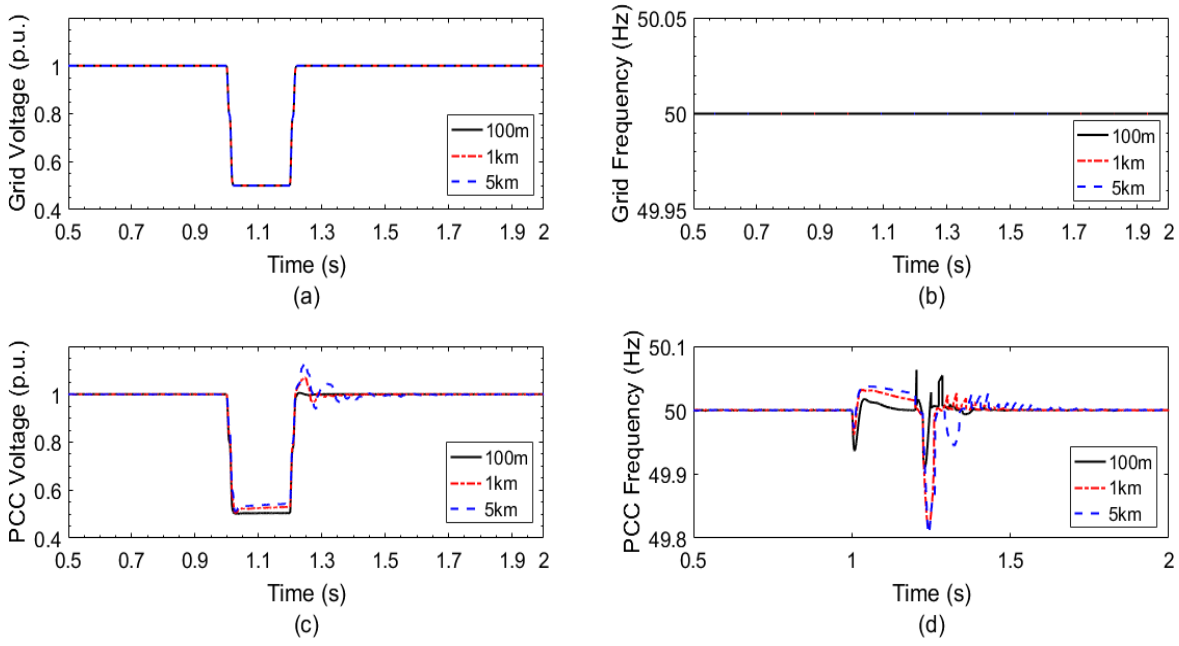

Figure 4. 16: (a) Voltage and (b) frequency at the grid bus, (c) voltage and (d) frequency at the PCC (Sensitivity study 1 - Length)

Secondly, the influence of *R/X* ratio of the transmission line is evaluated. Three different *R/X* ratios of the main transmission line is considered, keeping the transmission line length fixed at 1 km. The line parameters considered are listed in Table 4.2. A grid-side 50% voltage sag is applied at the grid bus from 1 s to 1.2 s while the grid frequency remains constant.

The active and reactive power supplied by DG units, and dynamic response of voltage and frequency at the PCC and the grid bus during this event are shown in Figs. 4.17 and 4.18, respectively, for three *R/X* ratio cases. The two figures indicate that the *R/X* ratio of the transmission line does have significant effect on both power and frequency fluctuation. For the system with larger *R/X* ratio lines, caution should be exercised during the controller design, more advanced algorithms such as the power transformation technique [1] can be used to improve the system overall performance.

Table 4. 2: Resistance and reactance of the main transmission line

Case no.	Resistance, *R* (Ω/km)	Reactance, *X* (Ω/km)	*R/X* ratio
1	0.175	0.23	0.76
2	0.35	0.23	1.52
3	0.525	0.23	2.28

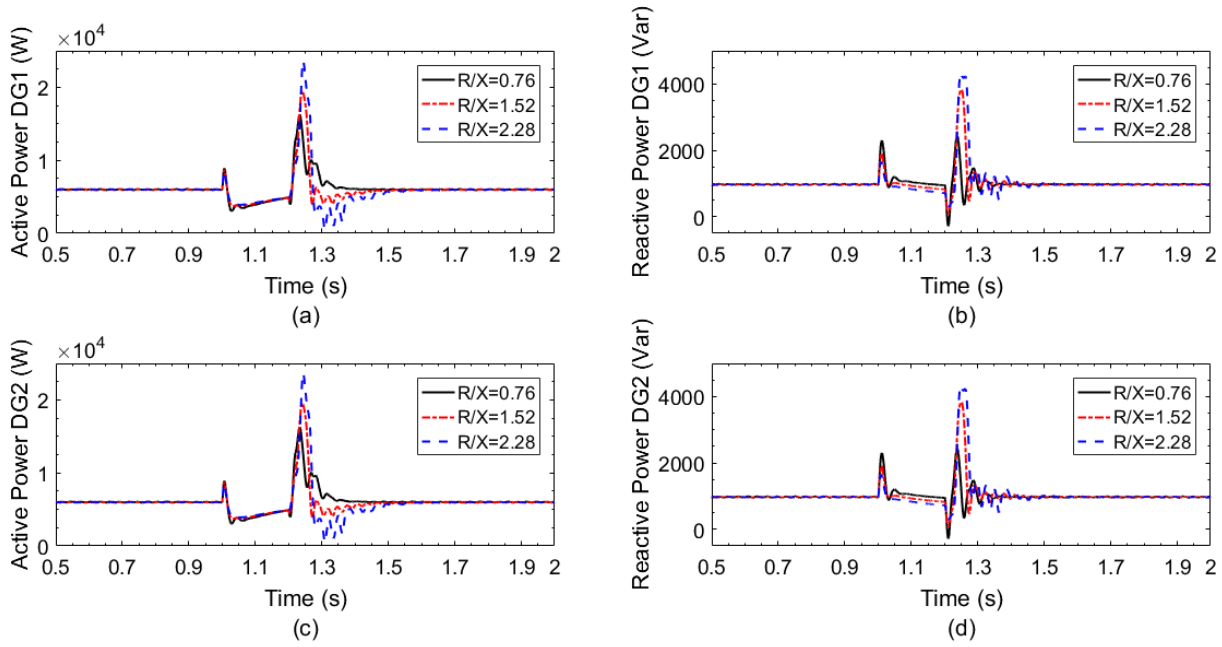

Figure 4. 17: (a) Active and (b) reactive power supplied by DG unit 1, (c) active and (d) reactive power supplied by DG unit 2 (Sensitivity study 1 –*R/X* ratio)

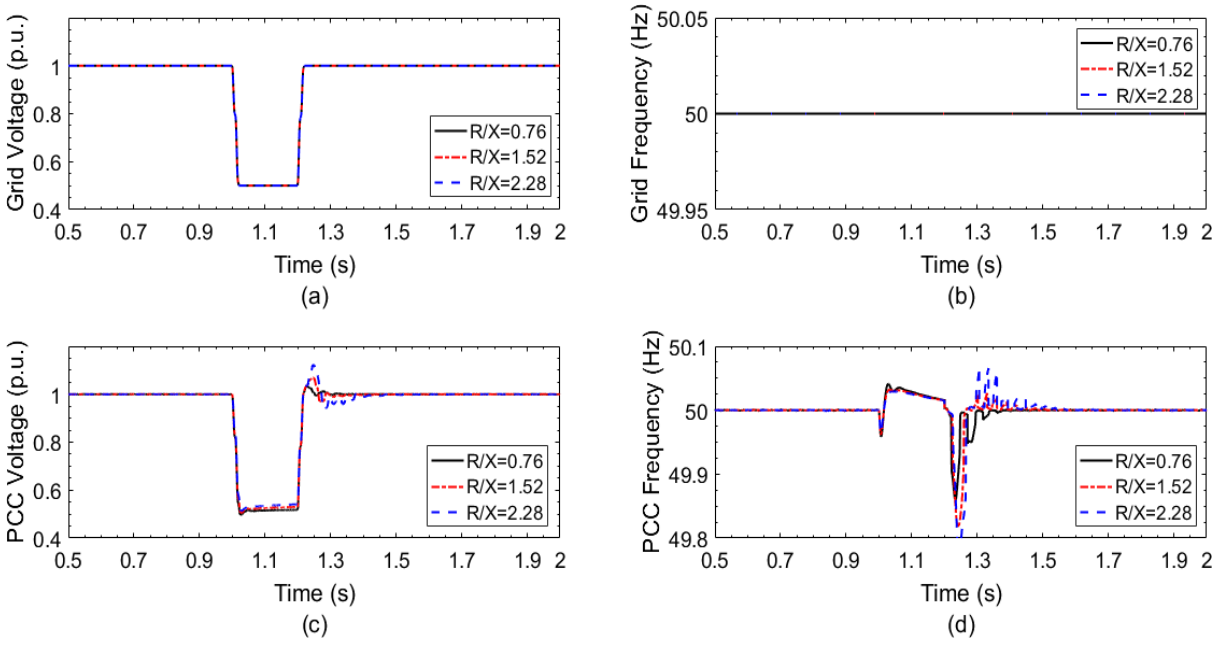

Figure 4. 18: (a) Voltage and (b) frequency at the grid bus, (c) voltage and (d) frequency at the PCC (Sensitivity study 1 – *R/X* ratio)

4.5.2 Sensitivity Study 2: Output Gains of FSC

There are two output gains for a FSC in a grid-connected mode: a ΔQ output gain (K_{ov}) and a ΔP output gain (K_{of}). These gains are important parameters that can potentially affect dynamic characteristics of the proposed control scheme. The design values of the two output gains of the FSC for this test microgrid are listed as follows: K_{ov} = 9500, and K_{of} = 10*10^5. The gains of the FSC used in the simulation are listed in Table 4.3.

Four gains $K_{e\omega,}$ $K_{ep,}$ $K_{eQ,}$ and K_{eE} in Table 4.3 are used for normalizing input variables of the FSC according to input ranges presented in Fig. 4.3. Each of these gains can be assigned a single value for a specific input range defined by membership functions of the FSC. Therefore, these gains are kept constant at a specific value for sensitivity studies. Note: some other values can also be assigned to the gains if input variables are allowed to vary within a range that is different from the range considered in this study.

Table 4. 3: Gains of the FSC used in the simulation

Gain	Value
$K_{e\omega}$	0.02
K_{of}	10*10^5
$K_{ep,}$ K_{eQ}	0.0001
K_{eE}	1
K_{ov}	9500

Three different ΔQ output gains for the FSC are considered while keeping the ΔP output gain constant at 10*10^5: K_{ov1}= 9000, K_{ov2} = 9500 and K_{ov3} = 10,000. The influence of the three gains is investigated by applying a grid-side 50% voltage sag to the grid bus from 1 s to 1.2 s.

During the event, active and reactive power supplied by each DG unit are shown in Fig. 4.19. A fluctuation in active and reactive power values can be observed when the disturbance occurs, and the reactive power deviation during the disturbance is more severe than the active power deviation. The least deviation in the reactive power is observed when the ΔQ output gain K_{ov2} is chosen. The active power deviation is found to be similar for all three gains as the ΔP output gain of the FSC is kept constant.

The corresponding dynamic response of the voltage and frequency is shown in Fig. 4.20. It is found that only frequency fluctuation is experienced at the PCC, and they are very similar for the three ΔQ output gains.

Similarly, three different ΔP output gains of the FSC are considered while keeping the ΔQ output gain K_{ov} constant at 9500: K_{of1}= 10*10^5, K_{of2} = 5*10^5 and K_{of3} = 3*10^5. In this case, a grid side 0.05 Hz frequency disturbance is applied to the grid bus from 1s to 1.1s.

During this event, active and reactive power supplied by the DG units are presented in Fig. 4.21. The least deviation in active power is observed when the output gain K_{of1} is chosen. The corresponding dynamic response of the voltage and frequency is shown in Fig. 4.22. It is found that both voltage and frequency at the PCC experience fluctuations. Based on the sensitivity study results, output gains of the FSC can be properly chosen for the best system performance.

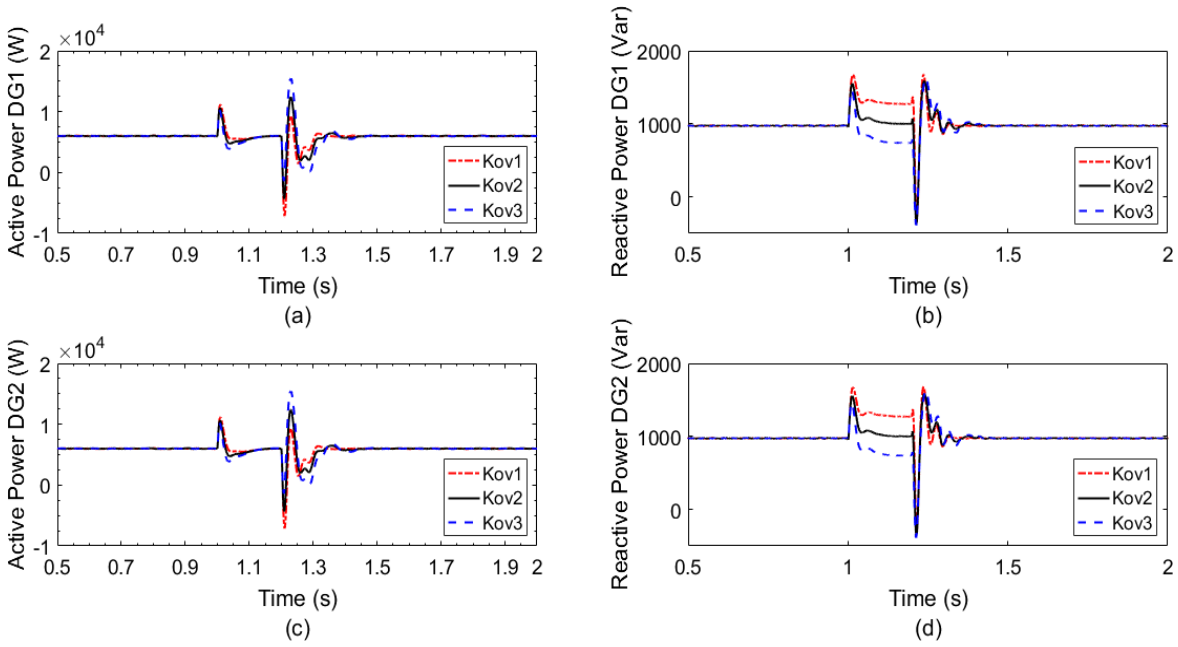

Figure 4. 19: (a) Active and (b) reactive power supplied by DG unit 1, (c) active and (d) reactive power supplied by DG unit 2 (Sensitivity study 2 - *Kov*)

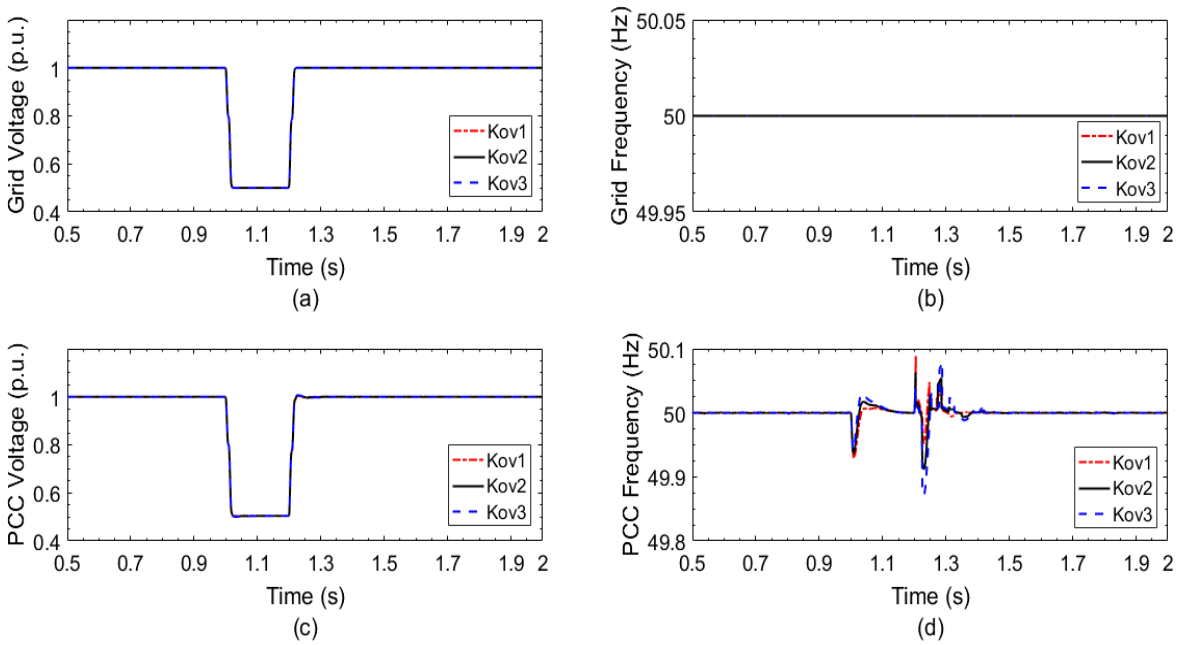

Figure 4. 20: (a) Voltage and (b) frequency at the grid bus, (c) voltage and (d) frequency at the PCC (Sensitivity study 2 - *Kov*)

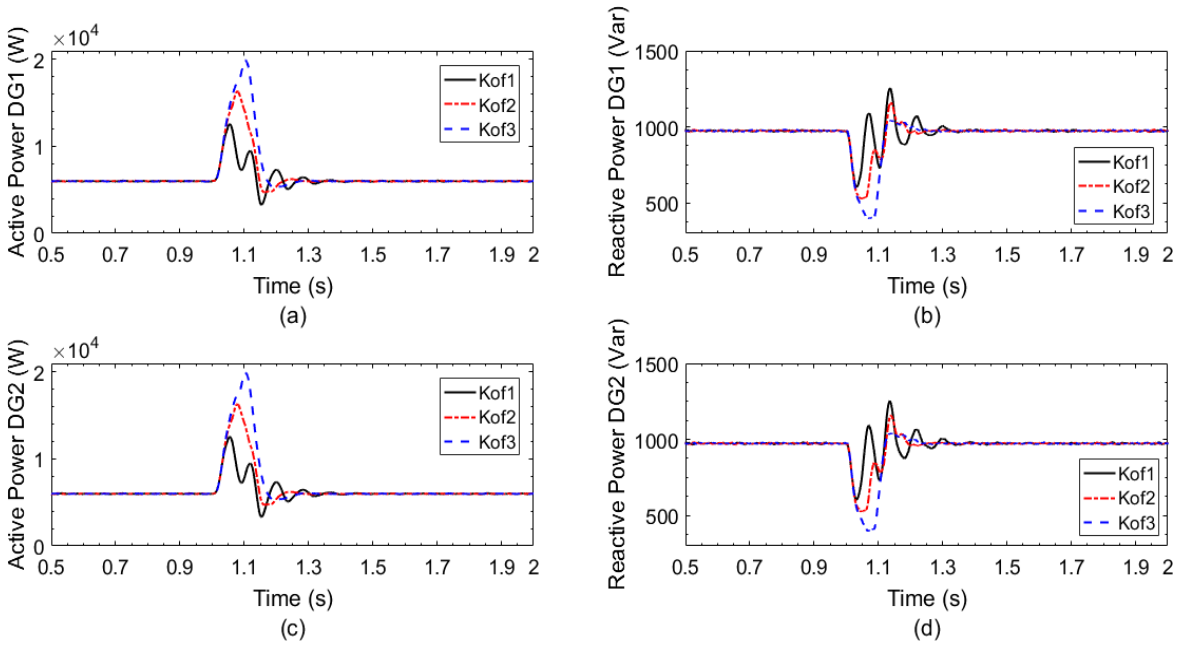

Figure 4. 21: (a) Active and (b) reactive power supplied by DG unit 1, (c) active and (d) reactive power supplied by DG unit 2 (Sensitivity study 2- *Kof*)

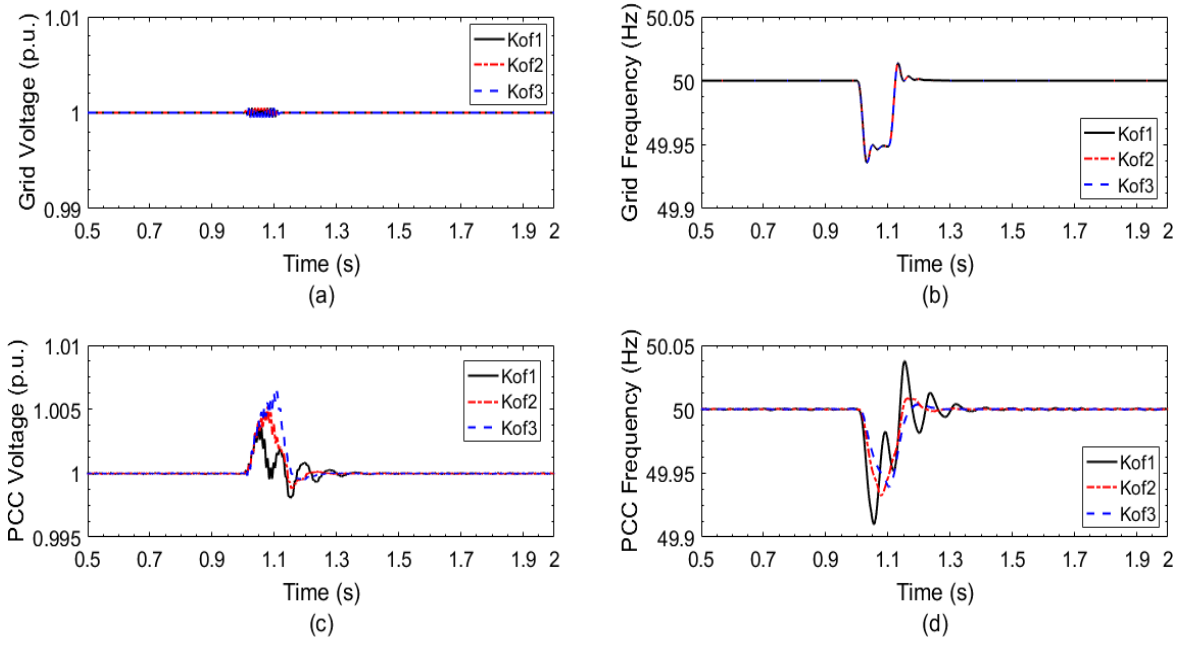

Figure 4. 22: (a) Voltage and (b) frequency at the grid bus, (c) voltage and (d) frequency at the PCC (Sensitivity study 2- *Kof*)

4.6 Conclusion

In this paper, a fuzzy secondary controller based virtual synchronous generator control scheme is proposed to improve voltage and frequency regulation and dynamic performance of a microgrid. Several case and sensitivity studies are carried out to verify the effectiveness of the proposed control scheme, its performance is also compared with that of conventional droop control and conventional VSG control.

It is found that the proposed control scheme can effectively regulate the voltage and frequency, and significantly improve dynamic characteristics of the microgrid. To be specific, In grid connected mode, 95% and 99.2% reduction in PCC frequency deviation has been achieved by the proposed scheme compared to the conventional VSG and droop control scheme, respectively (case 1). In islanded mode, 96% and 99.4% reduction in PCC frequency deviation has been achieved by the proposed scheme compared to the conventional VSG and droop control scheme, respectively (case 3).

The output gains of the Fuzzy secondary controller can be chosen based on a sensitivity study, their proper selection is essential for the overall system dynamic performance.

The proposed method can be adopted for microgrids with higher number of DG units connected in parallel.

The paper also provides a comparison between conventional droop control and conventional VSG control on power quality during various disturbances, which can facilitate deeper understanding of the two promising control techniques for renewable energy integration.

References

[1] M. Kallamadi, and V. Sarkar, “Enhanced real-time power balancing of an AC microgrid through transiently coupled droop control”, *IET Gener. Transm. Distrib*., Vol. 11 Iss. 8, pp. 1933-1942, 2017.

[2] C. J. Vasquez, J. M. Guerrero, A. Luna, P. Rodríguez, and R. Teodorescu, "Adaptive droop control applied to voltage-source inverters operating in grid-connected and islanded modes," *IEEE Trans. Industrial Electronics,* vol. 56, no. 10, pp. 4088-4096, Oct 2009.

[3] W. Bai, M. R. Abedi, and K. Y. Lee, "Distributed generation system control strategies with PV and fuel cell in microgrid operation," *Control Engineering Practice,* vol. 53, pp. 184-193, Feb 2016.

[4] Q. C. Zhong and Y. Zeng, "Universal droop control of inverters with different types of output impedance," *IEEE Access*, vol. 4, pp. 702-712, Feb. 2016.

[5] H. P. Beck and R. Hesse, "Virtual synchronous machine," in *Proc. 9th Int. Conf. Electrical Power Quality and Utilisation*, 2007, pp. 1-6.

[6] Y. Chen, R. Hesse, D. Turschner, and H. P. Beck, "Improving the grid power quality using virtual synchronous machines," in *Proc. IEEE Int. Conf. Power engineering, energy and electrical drives*, 2011, pp. 1-6.

[7] H. Wu, X. Ruan, D. Yang, X. Chen, W. Zhao, Z. Lv, and Q.-C. Zhong, “Small-signal modeling and parameters design for virtual synchronous generators”, IEEE Trans. Industrial Electronics, Vol. 63, No. 7, pp. 4292-4303, July 2016.

[8] Y. Chen, R. Hesse, D. Turschner, and H. P. Beck, "Dynamic properties of the virtual synchronous machine (VISMA)," in *Proc. Int. Conf. Renewable Energies and Power Quality*, 2011, pp. 1-6.

[9] M. Torres and L. A. C. Lopes, "Frequency control improvement in an autonomous power system: An application of virtual synchronous machines," in *Proc. IEEE 8th Int. Conf. Power Electronics and ECCE Asia,* 2011, pp. 2188-2195.

[10] U. Tamrakar, D. Galipeau, R. Tonkoski, and I. Tamrakar, "Improving transient stability of photovoltaic-hydro microgrids using virtual synchronous machines," in *Proc. IEEE PowerTech,* 2015, pp. 1-6.

[11] M. Torres and L. A. C. Lopes, "Virtual synchronous generator a control strategy to improve dynamic frequency control in autonomous power systems," *Energy and Power Engineering,* vol. 5, no. 2A, pp. 32-38, Apr 2013.

[12] C. F. Santos, F. B. Grigoletto, and M. Stefanello, "Power quality improvement in a grid connected voltage source inverter using the concept of virtual synchronous machine," in *Proc. IEEE 13th Brazilian Power Electronics Conference and 1st Southern Power Electronics Conference,* 2015, pp. 1-5.

[13] S. D'Arco, J. A. Suul, and O. B. Fosso, "A virtual synchronous machine implementation for distributed control of power converters in smartgrids," *Electric Power Systems Research,* vol. 122, pp. 180-197, May 2015.

[14] S. D'Arco, J. A. Suul, and O. B. Fosso, "Small-signal modeling and parametric sensitivity of a virtual synchronous machine in islanded operation," *Int. Journ. Electrical Power & Energy Systems,* vol. 72, pp. 3-15, Nov 2015.

[15] E. J. Agnoletto, R. V. A. Neves, R. F. Bastos, R. Q. Machado, and V. A. Oliveira, "Fuzzy secondary controller applied to autonomous operated AC microgrid," in *Proc. IEEE European Control Conference,* 2016, pp. 1788-1793.

[16] R. V. A. Neves, R. Q. Machado, V. A. Oliveira, F. Blaabjerg, and X. Wang, "Fuzzy secondary controller for autonomous stand-alone and grid-connected AC microgrid," in *Proc. IEEE Industrial Electronics Society Annual Conference,* 2016, pp. 7028-7033.

[17] S. Ahmadi, S. Shokoohi, and H. Bevrani, "A fuzzy logic-based droop control for simultaneous voltage and frequency regulation in an AC microgrid," *Int. Journ. Electrical Power & Energy Systems,* vol. 64, pp. 148–155, Jan. 2015.

[18] H. Bevrani and S. Shokoohi, "An intelligent droop control for simultaneous voltage and frequency regulation in islanded microgrids," *IEEE Trans. Smart Grid*, vol. 4, no. 3, pp. 1505–1513, Sept 2013.

[19] J. Liu, Y. Miura, and T. Ise, "Comparison of dynamic characteristics between virtual synchronous generator and droop control in inverter-based distributed generators," *IEEE Trans. Power Electronics,* vol. 31, no. 5, pp. 3600-3611, May 2016.

[20] J. Liu, Y. Miura, and T. Ise, "Dynamic characteristics and stability comparisons between virtual synchronous generator and droop control in inverter-based distributed generators," in *Proc. IEEE Int. Power Electronics Conference,* 2014, pp. 1536-1543.

[21] S. D'Arco, and J. A. Suul, "Virtual synchronous machines — classification of implementations and analysis of equivalence to droop controllers for microgrids", *2013 IEEE Grenoble PowerTech (POWERTECH),* 2013, pp. 1-7.

[22] S. D'Arco and J. A. Suul, "Equivalence of virtual synchronous machines and frequency-droops for converter-based microgrids," *IEEE Trans. Smart Grid,* vol. 5, no. 1, pp. 394-395, Jan. 2014.

[23] X. Liang, "Emerging power quality challenges due to integration of renewable energy sources," *IEEE Trans. Industry Applications,* vol. 53, no. 2, pp. 855-866, Mar. 2017.

[24] X. Liang and C. A. B. Karim, "Virtual synchronous machine method in renewable energy integration," in *Proc. IEEE PES Asia-Pacific Power and Energy Engineering Conference, 2016*, pp. 364-368.

[25] H. Zhao, Q. Yang and H. Zeng, "Multi-loop virtual synchronous generator control of inverter-based DGs under microgrid dynamics," *IET Generation, Transmission & Distribution*, vol. 11, no. 3, pp. 795-803, 2017.

[26] Q. C. Zhong and G. Weiss, "Synchronverters: Inverters that mimic synchronous generators," *IEEE Trans. Industrial Electronics*, vol. 58, no. 4, pp. 1259–1267, April 2011.

[27] J. Meng, X. Shi, Y. Wang, and C. Fu, "A virtual synchronous generator control strategy for distributed generation," in *Proc. IEEE China Int. Conf. Electricity Distribution*, 2014, pp. 495-498.

[28] J. Liu, Y. Miura, H. Bevrani, and T. Ise, "Enhanced virtual synchronous generator control for parallel inverters in microgrids," *IEEE Trans. Smart Grid*, 2016.

[29] J. Alipoor, Y. Miura and T. Ise, "Power system stabilization using virtual synchronous generator with alternating moment of inertia," *IEEE Journal of Emerging and Selected Topics in Power Electronics*, vol. 3, no. 2, pp. 451-458, June 2015.

Chapter 5

Reactive Power Sharing Enhancement Using Adaptive Virtual Impedance in Virtual Synchronous Generator Controlled Microgrids

[1]Chowdhury Andalib-Bin-Karim, *Student Member, IEEE,* [1]Xiaodong Liang, *Senior Member, IEEE*, [2] Weixing Li, *Member, IEEE*

[1]Faculty of Engineering and Applied Science, Memorial University of Newfoundland, St. John's, Newfoundland, Canada.

[2]Department of Electrical Engineering, Harbin Institute of Technology, Harbin, Hilongjiang, China.

This chapter is prepared for submission to a Special Issue on Grid-Connected Power Electronics Systems: Stability, Power Quality, and Protection for *IEEE Transactions on Industry Applications*. The author of this manuscript Chowdhury Andalib-Bin-Karim developed this work under the supervision of Dr. Xiaodong Liang. Mr. Karim's contribution to this paper is as follows:

- Performed all literature searches required for background information.
- Developed dynamic models in MATLAB/Simulink and performed simulation.
- Analyzed the results.
- Wrote the paper.

Dr. Xiaodong Liang provided continuous technical guidance, checked the results, reviewed the manuscript, provided important suggestions to accomplish the work, and modified final version of

the manuscript. Dr. W. Li reviewed the manuscript and provided expert opinion to improve the work. In this chapter, the manuscript is presented with altered figure numbers, table numbers and reference formats in order to match the thesis formatting guidelines set out by Memorial University of Newfoundland.

Abstract- Droop control is widely used in microgrids with parallel connected inverters to realize proper power sharing among distributed generation (DG) units. Virtual Synchronous Generator (VSG) control scheme was first introduced in 2007 for inverter control for renewable energy integration, it is a modified droop control with improved frequency control feature. As a new emerging approach, VSG control has attracted significant research interest recently. However, one issue associated with VSG control is that it cannot ensure accurate proportional reactive power sharing when DG units have unequal line impedances, although active power sharing remains unaffected under such circumstances. A virtual impedance can be incorporated in VSG control scheme to alleviate output impedance difference between inverters, and improve the accuracy of reactive power sharing. In this paper, a new implementation approach of adaptive virtual impedance method for microgrid is proposed to maintain accurate supply of reactive power by DG units under variation of microgrid operating points. The simulation is conducted in MATLAB/Simulink environment to verify the effectiveness of the proposed approach in eliminating reactive power sharing errors induced by line impedance difference among inverters.

Keywords- Adaptive virtual impedance, microgrids, reactive power sharing, virtual synchronous generator (VSG) control.

5.1 Introduction

With increasing concerns on environmental effect caused by conventional fossil fuel based power generation, more distributed generation (DG) units utilizing renewable energy resources are being integrated to power grid in recent years [1], [2]. The microgrid concept has gained popularity as an effective way of integrating various renewable energy sources such as solar photovoltaic (PV), wind turbine, energy storage etc., as it provides increased efficiency in utilization of resources and offers better flexibility in control through power electronic interfaces in order to meet the power quality requirements [3], [4]. The droop control is often adopted to control each DG inverter independently in a microgrid, this method is advantageous because it does not require any communication and coordination among DG units [5], [6]. The virtual synchronous generator (VSG) control strategy has been emerged since 2007, this method is a modified droop control approach and can provide better frequency support by enabling the inverter to emulate rotor inertia and droop characteristics of a synchronous generator [1].

In a practical system, due to feeder impedance mismatch, the droop control exhibits inaccuracy in reactive power sharing among DG units [2], [7]. Moreover, according to the principle of droop control mechanism, the output impedance of DG inverters need to be inductive in nature to realize proper reactive power control, which cannot always be guaranteed in a real system because the inverter output impedance is dependent on the control strategy and controller parameters [8],[9]. The VSG control strategy employs a reactive power (Q)-voltage (V) control loop based on the Q-V droop characteristics, which is similar to the droop control strategy, therefore the VSG control also suffers from same problem.

On the other hand, although reactive power sharing is inaccurate due to difference in line voltage drop, the angular frequency for all nodes in an inductive microgrid remains the same under steady state, which allows frequency droop control to realize accurate active power sharing according to the real power (*P*) –frequency (*f*) droop characteristics [10], [11]. The operational frequency of all the DG units remain the same in steady state [12], which enables *P-f* droop coefficients (m_i) of multiple DGs to satisfy the relationship: $m_1 P_1^* = m_2 P_2^* = \cdots = m_N P_N^*$ [13], where *Pi* is the active power supplied by *ith* DG unit, thus the accurate active power sharing according to DG rated capacity can be ensured [14].

The virtual impedance method has been identified as an effective way to achieve proper reactive power sharing in many recent literatures. The concept of virtual impedance was introduced in [15] to improve reactive power sharing performance by eliminating mismatch between DG output impedances. The virtual impedance is implemented by including an additional control loop in the inverter control scheme. The main idea is to realize a drop in the voltage reference generated by the original control scheme (droop, VSG etc.), which simulates the same effect as an addition of a physical impedance at the output of the inverter [10]. By choosing an appropriate value of virtual impedance, the desired voltage drop can be realized, and thus, the DG output impedance can be adjusted to a desired value. In [16], a resistive virtual impedance method is evaluated to enhance power sharing performance in a low voltage microgrid with DG inverters having resistive output impedance. In [17], the feeder impedance mismatch has been taken into consideration and a virtual impedance control based on the estimation of line impedance has been proposed.

Employing a large virtual impedance, the effect of the line impedance on reactive power sharing accuracy can be reduced, but at a cost of deterioration of the voltage control precision for high capacity inverters, as discussed in [1], [18]. In [19], an adaptive virtual impedance method has

been developed where each DG unit can tune its virtual impedance value by estimating voltage drop due to line impedance mismatch. A systematic approach to determine a feasible range of virtual impedance values to satisfy different performance criteria in a droop controlled DG system has been presented in [10]. However, the evaluation of adaptive virtual impedance method in a VSG controlled microgrid system has not been reported in any literature, which is the main concentration of this research work.

In this paper, a new adaptive virtual impedance method for reactive power sharing improvement in a fuzzy secondary controller based VSG controlled microgrid is proposed, where an adaptive virtual impedance loop is incorporated in the inverter control scheme, and the virtual resistance value is adaptively tuned based on the status of different system quantity measurements, such as load currents, DG output currents etc. The fuzzy secondary controller based VSG control scheme is previously developed by the authors in [20]. The proposed virtual impedance consists of a virtual resistor and a virtual inductor. Appropriate values of the virtual resistance are designed for a test microgrid system in different operating points while the value of the virtual inductance remains the same. The proposed approach does not require any communication among DG units, and functions well based on local measurements. Several case and sensitivity studies are carried out using MATLAB/Simulink simulation to evaluate the effectiveness and robustness of the proposed method.

The paper is arranged as follows: in Section 5.2, the principle of the proposed adaptive virtual impedance method is presented; a description of test system under study is provided in Sections 5.3; case and sensitivity studies are conducted in Sections 5.4 and 5.5, respectively to evaluate the performance of the proposed control system; conclusions are drawn in Section 5.6.

5.2 The Proposed Adaptive Virtual Impedance Method

In this section, the principle of the proposed adaptive virtual impedance utilized in a fuzzy secondary controller based VSG control scheme is demonstrated. To implement this approach, an adaptive virtual impedance loop needs to be incorporated in the VSG control scheme.

Due to extensive usage of power electronic inverters in renewable energy sources interfacing power grids, the equivalent rotational inertia of power grids are considerably reduced because inverters are static without rotational energy, which results in negligible inertia. In order to effectively integrate renewable energy sources, the concept of VSG was introduced in 2007 by Beck and Hesse [21]. The main idea of this approach is to emulate major characteristics of a real synchronous machine: inertial characteristics and damping of electromechanical oscillation [21], [22]-[24].

The authors developed a Fuzzy secondary controller based VSG control scheme in [20], which will be directly used in this paper as the basis for virtual impedance implementation. The fundamental principle of the conventional VSG control method can be found in [21], [25[-[29], the detailed principle of the fuzzy secondary controller based VSG control schemes can be found in [20], and they will not be repeated here.

In a microgrid, DG units are randomly located, therefore, the rated capacity of each DG unit and line impedance is not matched, which can lead to inaccuracy in reactive power sharing [1]. A voltage drop occurs due to the presence of a line impedance between a DG unit and the point of common coupling (PCC). Because the line impedance is usually not matching with the rated capacity of DG unit, the conventional *Q*-*V* droop characteristics inherent in the VSG control mechanism cannot ensure accurate reactive power sharing [1]. In conventional *Q*-*V* droop method,

a linear relationship between the DG reactive power output and the voltage amplitude difference is considered, and a voltage droop slope is established based on that. However, it is demonstrated in [30] that, if the voltage drop due to the line impedance is not taken into consideration while establishing the voltage droop slope, a DG unit may not be able to supply reactive power to its maximum capacity when a maximum demand occurs. Due to the effect of different line impedances, the conventionally assumed relationship between *Q* and *V* is not valid anymore. To solve this problem, the voltage droop slope redefined considering the effect of line impedance is recommended in [30]. In order to realize proper reactive power sharing performance, the overall impedance of a DG unit according to its rated capacity must be adjusted. To be more specific, the line impedance (X_i) must always be inversely proportional to the reactive power rating (Q_i) of the corresponding DG unit, this condition can be expressed by Equation (5.1). However, in real life, this condition cannot always be satisfied due to the variation of lengths and impedances of transmission lines/cables through which DG units are connected to microgrids [2].

$$X_1 Q_1 = X_2 Q_2 = \cdots = X_N Q_N \tag{5.1}$$

Incorporation of a virtual impedance control loop in the inverter control scheme can offer flexibility to adjust the output impedance of a DG unit appropriately, thus facilitating accurate determination of reactive power supply according to the voltage amplitude [3]. When the virtual impedance is incorporated to eliminate reactive power sharing error introduced by unbalanced line impedance, Equation (5.1) can be rewritten as follows:

$$(X_{line1} + X_{V1})Q_1 = (X_{line2} + X_{V2})Q_2 = \cdots = (X_{lineN} + X_{VN})Q_N \tag{5.2}$$

where, *Xline,i* is the line reactance of DG unit ‘i', and *Xv,i* is the virtual reactance to be realized by the controller of DG unit ‘i'. In a real system, *Xline* values differ from one DG unit to another,

therefore, *Xv* value for each DG unit need to be chosen appropriately, so that Equation (5.2) is satisfied. As a result, equal voltage drop occurs from each DG unit to the PCC, thus, circulating currents flow among DG units is almost nullified and accurate proportional reactive power sharing is achieved [2].

The virtual impedance control can be implemented by employing a feedback loop of an injected current which can adjust the voltage reference derived through the VSG method. This type of adjustment of the voltage reference actually simulates a voltage drop across a virtual impedance [3], thus the overall impedance of a DG unit is influenced by the addition of a virtual impedance. The incorporation of a virtual impedance control loop can improve load sharing and overall stability of the system, and also reduces the impact of current circulation among DG units [5]. The approach of implementing a virtual impedance loop can be expressed as follows [5], [8],

$$V_{ref} = V^* - Z_v(s) i_o \tag{5.3}$$

where, *V** is the voltage reference derived by the VSG method, i_0 is the current injected by the inverter, and $Z_v(s)$ is the virtual output impedance. In the *dq0* reference frame, the virtual impedance (Z_v) can be expressed by [3],

$$Z_v = R_v \pm sL_v \frac{\omega_C}{s + \omega_C} \tag{5.4}$$

where, *Rv* is the virtual resistance, *Lv* is the virtual inductance, and ω_C is the cut-off frequency of a low pass filter (LPF). To implement the inductive part of a virtual impedance, the time derivative of inverter output current is obtained and the output voltage reference is drooped proportionally. The time derivative operation can lead to amplification of noises. Therefore, if there are noises present in the current, a LPF can be incorporated in the loop in order to suppress high frequency noises [5]. In [15], another method of calculating the virtual voltage drop is presented which can

avoid the time derivative operation, as a result, a LPF needs not to be included in the loop. This approach approximates *sLv* as jω*Lv,* where direct complex number manipulation is realized in the *dq0* frame. An overall block diagram of virtual impedance implementation is presented in Fig. 5.1. The power controller shown in the figure is considered to be operating according to the VSG control mechanism.

In an established microgrid, where the electrical system configuration and feeder impedances etc. are fixed, reactive power sharing performance is influenced only by load factors. It appears that the reactive power sharing error for a DG unit varies widely with the variation of load combinations [11]. The reactive power sharing error of a DG unit under different load combinations in a microgrid is recorded in [11]. Based on the analysis of recorded data, it is concluded that, for a low-voltage system, the reactive power sharing error is not significantly impacted by reactive power variation of a load, but is mainly influenced by active power variation of a load [11]. Therefore, a fixed virtual impedance can offer good reactive power sharing only when the load demand of a DG unit is constant, i.e., when a microgrid is subjected to load variations, virtual impedance values need to be adjusted accordingly to ensure acceptable reactive power sharing.

Reactive power of a DG unit can be regulated by adjusting either one of the two components of a virtual impedance: 1) virtual resistance (*Rv*), and 2) virtual reactance (*Xv*). Regarding which component should be adjusted, it is recommended in [11] that the virtual reactance *Xv* can be fixed, while the virtual resistance *Rv* can be adjusted for reactive power regulation purpose. It is demonstrated in [11] that, the reactive power regulation can be affected by the value of virtual reactance, *Xv*. For example, for certain values of *Xv*, the reactive power regulation effect is found to be positive, i.e., the DG output reactive power supply is increased by increasing the *Xv* value;

however, for some other values of *Xv*, the reactive power regulation effect is found to be negative, i.e., the DG output reactive power supply is decreased by increasing the *Xv* value. On the other hand, the reactive power regulation trend is found to be consistent for all the values of virtual resistance, *Rv*. Therefore, it is more proper that *Rv* should be chosen as a control variable. In this study, a similar approach is adopted, where the virtual resistance value is adjusted to adapt with the variation of a microgrid's operating points, while the virtual reactance is kept at a fixed value. A new implementation approach for the adaptive virtual impedance loop is proposed in this research work.

To implement the proposed adaptive virtual impedance approach in this paper, three steps are required:

Step 1: Appropriate values of virtual resistance are determined for various operating points, which can ensure almost zero errors of reactive power sharing. Different combinations of local and PCC loads connected to a microgrid can result in different operating points of the microgrid. Therefore, proper values of virtual resistance are determined under different microgrid load combinations.

Step 2: Utilizing the available data from the first step, virtual resistance can be expressed as a function of certain input parameters for an islanded or a grid connected operation mode of a microgrid. For an islanded operation mode, the following two parameters are chosen as input parameters for the function: 1) local load currents, and 2) point of common coupling (PCC) load currents. For a grid connected operation mode, input parameters for the function are chosen to be: 1) DG output currents, and 2) PCC load currents. One advantage of this approach is that only measurements of load and DG output currents are enough, thus the necessity of separately measuring active and reactive power at loads and DG outputs can be eliminated.

Step 3: Based on the established function from the second step, design values of virtual resistance are obtained for a wide range of load and DG output currents, which are then stored in a two-dimensional (2-D) lookup table. In a normal operating condition, the designed 2-D lookup table gives an appropriate value of virtual resistance depending on the status of the corresponding two input parameters.

The proposed 2-D look-up table approach in both operation modes can offer good reactive power sharing performance under numerous operating points of a microgrid given that the adaptive virtual impedance loop is designed properly.

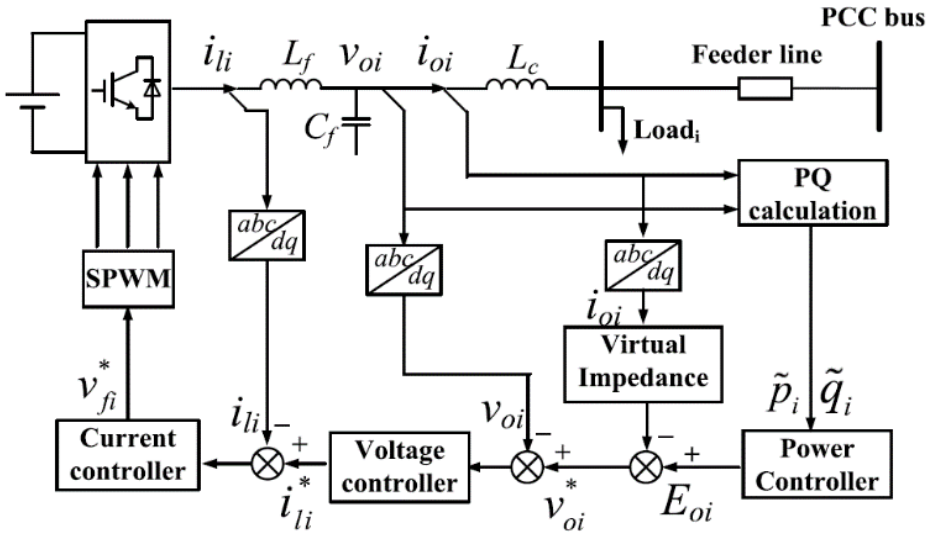

Figure 5. 1: Virtual impedance implementation structure [10]

5.3 Test System Description

A microgrid comprising two DG units serves as a test system in this paper to evaluate the effectiveness of the proposed adaptive virtual impedance method incorporated in the fuzzy

secondary controller based VSG control scheme. An overall system configuration of the microgrid is provided in Fig. 5.2.

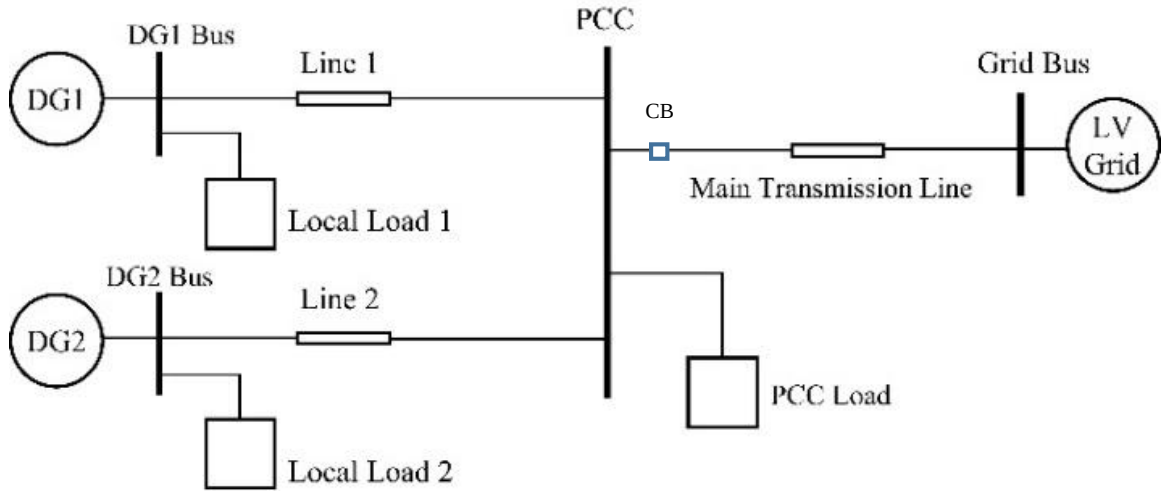

Figure 5. 2: The system configuration of the test microgrid

The two DG units are connected in parallel, where each DG unit contains a renewable energy source, a pulse width modulation (PWM) controlled voltage source inverter (VSI), and a LC filter for harmonic mitigation. The renewable energy source can be solar photovoltaic (PV) panels, wind turbines, or energy storage systems. In this paper, to simply the problem, the renewable energy source such as PV panels is modeled as a constant DC source inside each DG unit. The purpose is to allow better understanding of the proposed controller's performance when the microgrid is subjected to operating point variation in normal operating condition. A variable local load is connected to the output of each DG unit.

The microgrid is connected to a 380 V_{RMS} rated low voltage power grid through a circuit breaker (CB) and a 100 m main transmission line. The circuit breaker may operate during disturbances allowing the microgrid to continue its operation in an islanded mode. A variable load is connected at the PCC. The inverters in DG units are controlled by the proposed control scheme in this paper.

The parameters of the test system are provided in Table 5.1. The simulation model of the proposed control scheme is developed using MATLAB/Simulink as shown in Fig. 5.3.

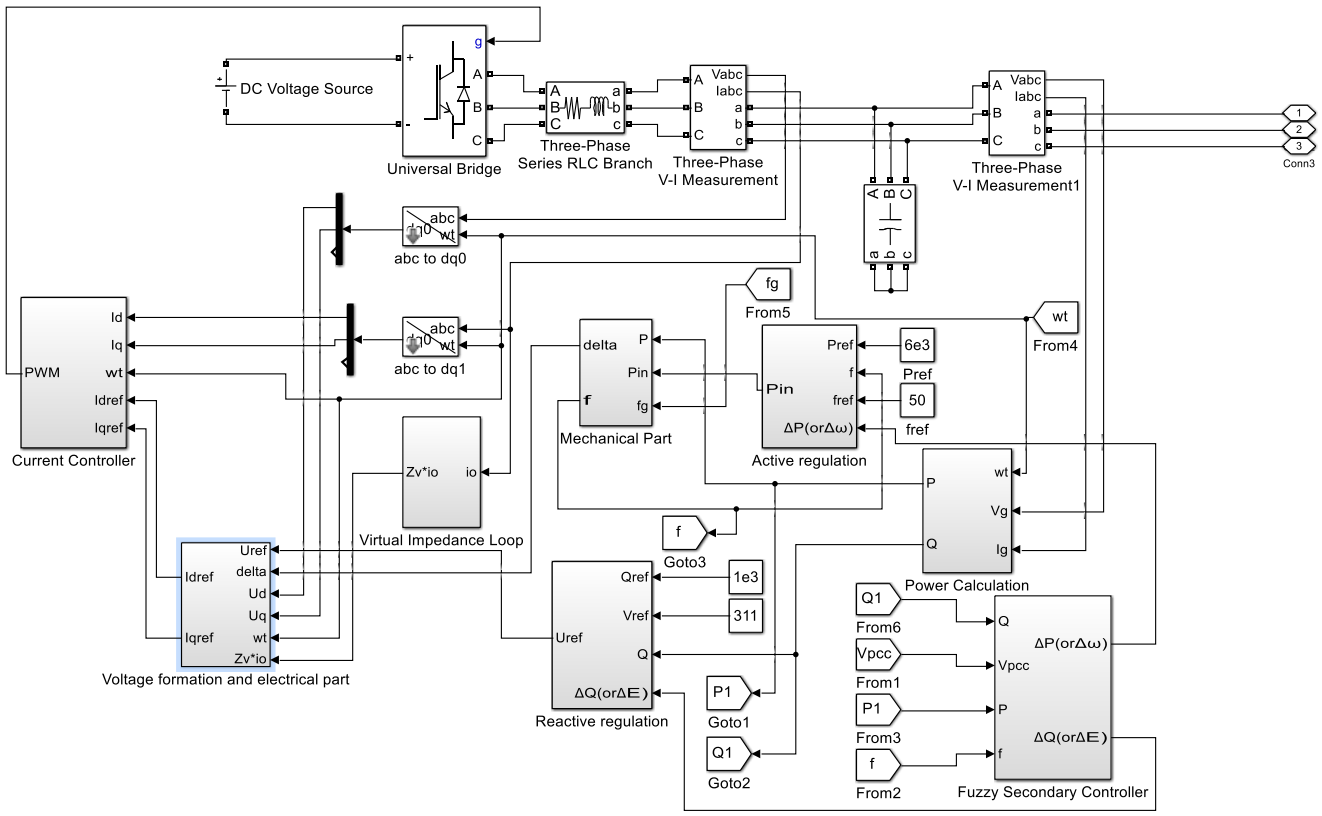

Figure 5. 3: The proposed adaptive virtual impedance based VSG control scheme model developed in Matlab/Simulink

Droop coefficients, the gain of the current controllers for the primary VSG controller are shown in Table I, they are common parameters used in both control mechanisms (VSG control with and without an adaptive virtual impedance loop) evaluated in this paper. The VSG control contains a mechanical part, which incorporates a swing equation for an improved active power regulation performance. Two important parameters of the swing equation are virtual inertia (J) and virtual damping factor (kd), which are chosen as 0.5 kg.m^2 and 10, respectively, in this study. The stator resistance (R_s) and inductance (Ls) values for the VSG are chosen to be 0.01 Ω and 3.56 mH,

respectively. The determined appropriate values of virtual impedances in different operating points of the microgrid are presented in the later section.

Table 5. 1: Test system parameters

Parameters		Values
Nominal DC bus voltage		700V
Nominal AC bus RMS line voltage		380V
Inverter filter	Resistance, R_f	0.2Ω
	Inductance, L_f	3×10^{-3} H
	Capacitance, C_f	15×10^{-6} F
Line impedance	R_L	0.641 Ω/km
	X_L	0.101 Ω/km
Droop coefficients	*1/m*	1×10^{-5}
	1/n	0.3×10^{-5}
Voltage controller	Proportional gain	0.2
	Integral gain	280.8
Current controller	Proportional gain	0.24

5.4 Case Studies

To validate the effectiveness of the proposed approach, several case studies are conducted in this section. It is found that incorporation of an adaptive virtual impedance loop in the VSG control scheme offers significant improvement in reactive power sharing performance.

5.4.1 Case 1: Islanded Operation

The microgrid is required to continue its operation in an islanded mode when grid side disturbances sustain longer than the permitted fault clearance time. In this mode, the microgrid is disconnected from the utility grid, and DG units solely maintain uninterrupted power supply to the loads. Unlike in a grid connected mode, where the voltage and frequency of the mircrogrid are governed by the utility grid, in an islanded mode, the voltage and frequency of the microgrid are controlled by DG units.

In this case study, it is considered that the two DG units are connected to the islanded microgrid system through transmission lines with different line lengths: DG units 1 and 2 have 1 km and 500 m line length, respectively. The controller parameters of both DG units are considered to be the same. The rated capacity of the two DG units are also the same, each is rated at 10 kVA. The difference in line lengths results in the difference in line impedances, which further introduces a difference in output impedances of DG units and affects their reactive power sharing performance. This statement can be explained by Equation (1). According to Equation (1), if the rated capacity of both the DG units is same, i.e. $Q_1 = Q_2$, to ensure accurate reactive power sharing X_1 and X_2 must be equal in magnitude. Therefore, it is required to include a virtual impedance loop in the control system to make output impedances of DG units equal.

The effectiveness of the proposed adaptive virtual impedance based control mechanism using a 2-D lookup table to maintain accurate reactive power sharing among DG units is assessed considering both local and PCC load variations. Before the load variations, each DG unit supplies power to a local load (Fig. 4) rated at 5 kW and 1 kVar. One load rated at 2 kW and 400 Var is connected to the PCC and known as a PCC load.

The load variation event applied to the microgrid is described as follows:

1) At 2 s, a 1 kW and 200 Var local load at DG2 is added, while the local load at DG1 is kept fixed at the previous value;

2) At 3 s, a 1 kW and 200 Var PCC load is added to the PCC bus;

3) At 4 s, another 1 kW and 200 Var local load at DG2 is added, while the local load at DG1 is kept fixed at the previous value; and

4) At 5 s, another 1 kW and 200 Var PCC load is added to the PCC bus.

Without a virtual impedance loop in the fuzzy secondary controller based VSG control scheme, active and reactive power supplied by DG units during this specific event are shown in Fig. 5.4. It can be observed that the reactive power is not shared equally among the DG units during load variations while the active power sharing performance remains unaffected. The reason for the active power to remain unaffected has been discussed briefly in Section 5.1.

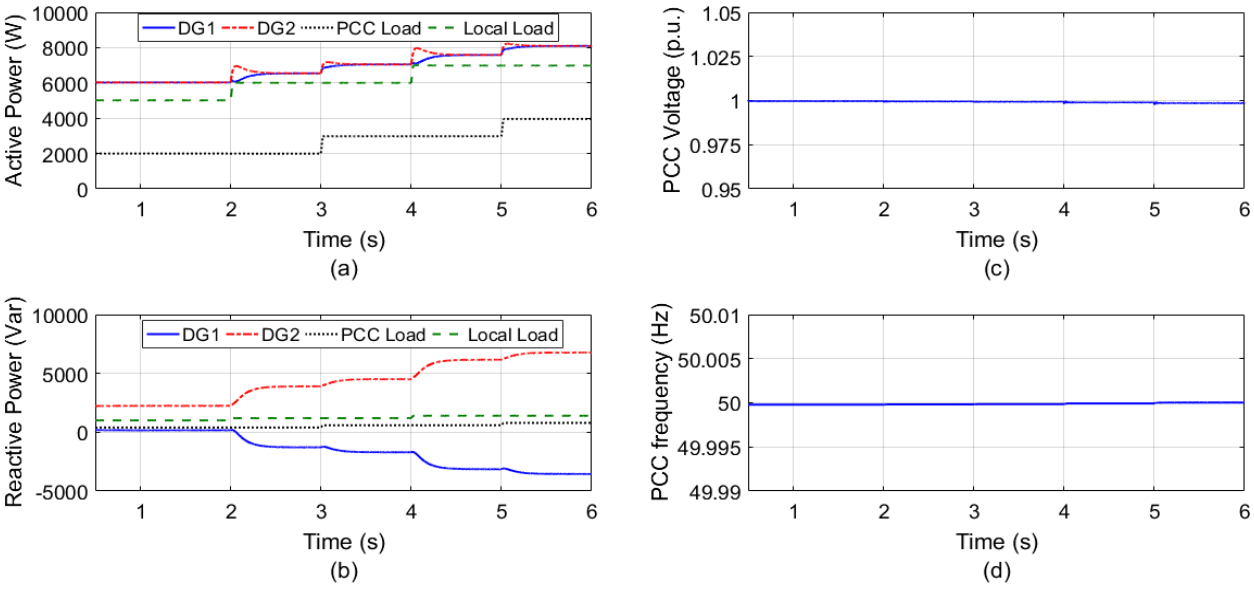

Figure 5. 4: Without a virtual impedance loop: (a) Active and (b) reactive power supplied by DG units, (c) voltage and (d) frequency at PCC (case 1)

In order to improve the reactive power sharing, an adaptive virtual impedance loop is employed where the virtual resistance value is adjusted accordingly with the variation of local load and PCC load currents in an islanded mode. During normal operating condition, when the local load varies, it is reflected by the variation of the local load current; when the PCC load varies, it is reflected by the variation of the PCC load current. In this study, appropriate values of virtual resistances are determined for different combinations of local load and PCC load demand levels, to ensure accurate reactive power sharing. The designed values of virtual resistance are presented in Fig. 5.5, which are determined through simulation of the test microgrid in Fig. 5.2 under various operating points. The maximum allowable reactive power error is considered to be ±0.5% during the design process. Utilizing these data, virtual resistance values can be expressed as a function of both local load and PCC load currents. The adaptive virtual impedance loop can be implemented using this derived function. Such functions are obtained using the surface fitting toolbox in MATLAB, and they are presented in Table 5.2, where x is the local load current, y is the PCC load current. Polynomial 22 model is used to fit the surface to data. If, the adaptive virtual impedance is designed based on only one parameter, it can ensure good power sharing performance either under local load variation or PCC load variation, but not both. To make the control mechanism work effectively under both load variation scenarios, it is required to design the adaptive virtual impedance considering the following two parameters: 1) local load current, and 2) PCC load current.

The adaptive virtual impedance is implemented with the aid of a 2-D lookup table, which has two inputs: 1) local load current, and 2) PCC load current. The designed values are stored in the 2-D lookup table, and the appropriate value of a virtual resistance can be chosen based on the status of the two input parameters.

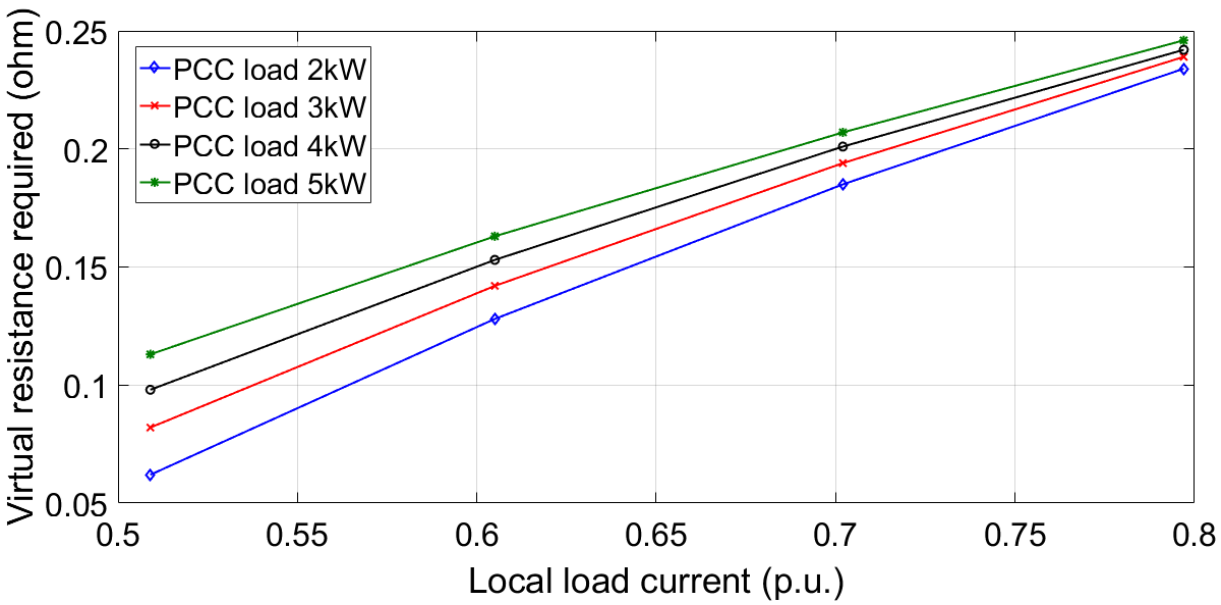

(a)

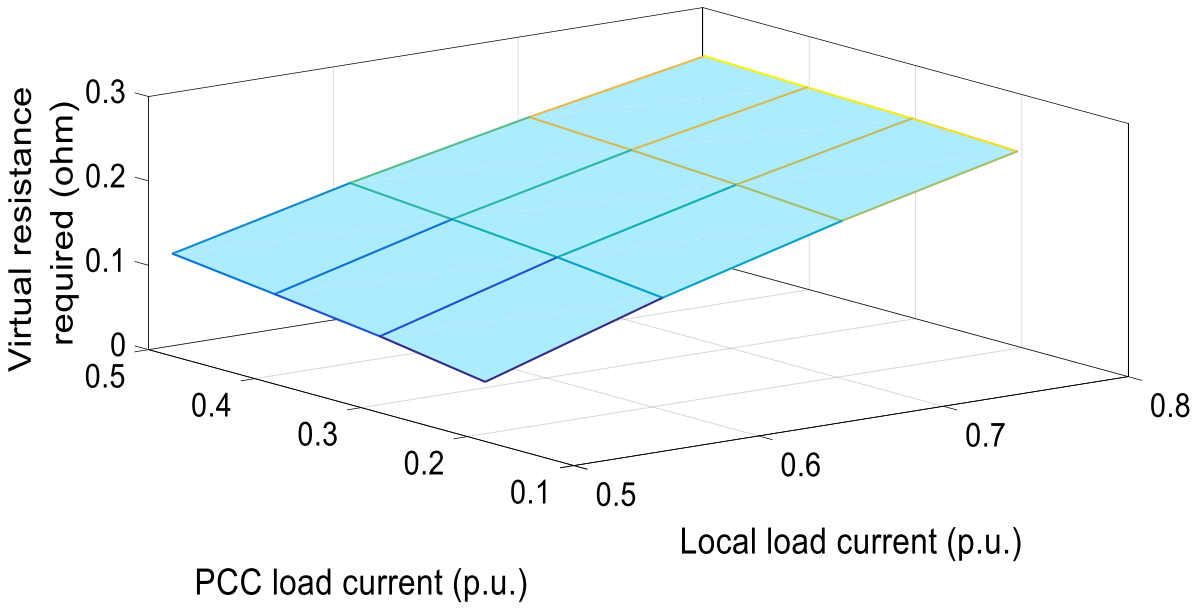

(b)

Figure 5. 5: Required values of virtual resistance in an islanded mode: (a) represented by lines; (b) represented by a surface.

The dynamic response of active and reactive power supplied by DG unit, with the adaptive virtual impedance loop being incorporated in the VSG control scheme are shown in Fig. 5.6. It is

evident that the reactive power is shared equally among DG units under variations of both local and PCC loads, when the adaptive virtual impedance based on the 2-D lookup table is employed. The required values of the virtual resistance during different time spans of the event in this case study are listed in Table 5.3.

The dynamic response of the PCC voltage and frequency shown in Fig. 5.6 is observed to be unaffected and remain close to their nominal values after incorporation of the virtual impedance loop because the fuzzy secondary controller based VSG control mechanism has effectively regulated voltage and frequency.

Therefore, it can be concluded that the proposed adaptive virtual impedance method can facilitate accurate reactive power sharing in an islanded mode of a microgrid under both local and PCC load variations.

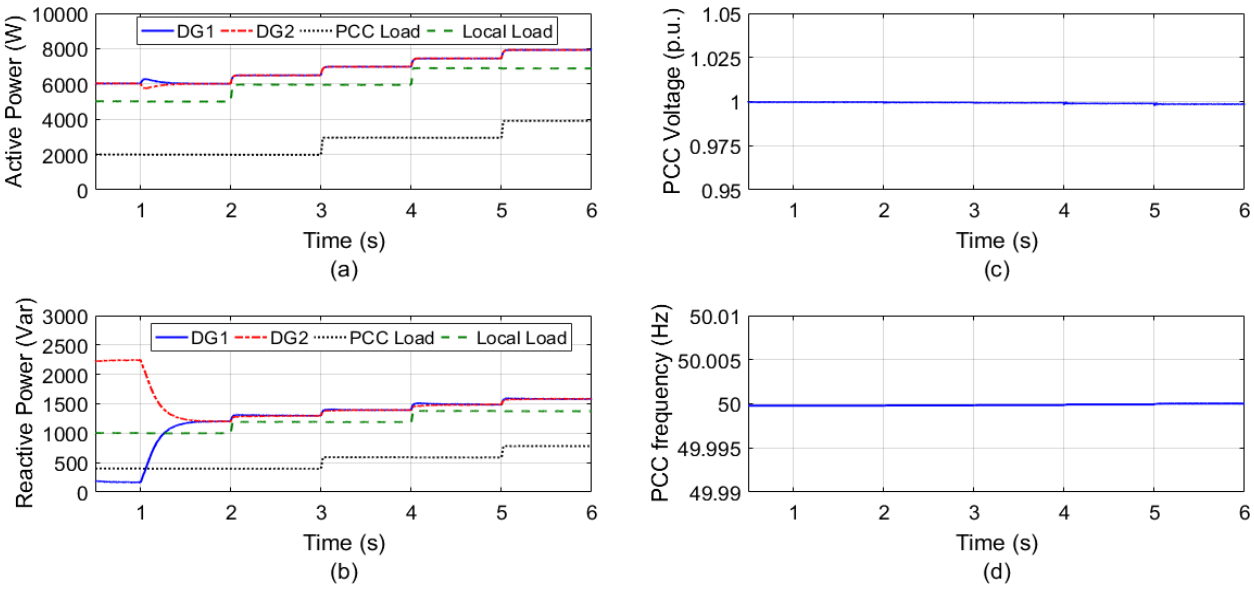

Figure 5. 6: With a virtual impedance loop (a) Active and (b) reactive power supplied by DG units, (c) voltage and (d) frequency at PCC (case 1)

Table 5. 2: Functions used to generate adaptive virtual resistance values

Mode of operation	Islanded	Grid connected	
		DG1	DG2
Equation of fitted surface	$f(x,y) = p_{00} + p_{10}x + p_{01}y + p_{20}x^2 + p_{11}xy + p_{02}y^2$		
Coefficients with 95% Confidence bounds	p_{00} = -0.4775 (-0.5035, -0.4514) p_{10} = 1.172 (1.098, 1.247) p_{01} = 0.4548 (0.408, 0.5017) p_{20} = -0.3734 (-0.4291, -0.3176) p_{11} = -0.4596 (-0.5031, -0.4161) p_{02} = -0.07721 (-0.1307, -0.02371)	p_{00} = 0.6079 (0.5808, 0.635) p_{10} = -1.36 (-1.429, -1.292) p_{01} = 0.112 (0.06941, 0.1545) p_{20} = 0.6188 (0.574, 0.6635) p_{11} = -0.07841 (-0.1149, -0.0419) p_{02} = 0.01118 (-0.03556, 0.05792)	p_{00} = 1.265 (1.033, 1.497) p_{10} = -3.919 (-5.082, -2.755) p_{01} = 0.2518 (-0.1284, 0.6319) p_{20} = 2.883 (1.362, 4.404) p_{11} = -0.3682 (-1.025, 0.2887) p_{02} = 0.009416 (-0.4039, 0.4227)

Table 5. 3: Virtual resistance values for case study 1

Time span	PCC load current (p.u.)	Local load current (p.u.)	R_v (Ω)
0s to 2s	0.203289	0.509868	0.064
2s to 3s	0.203289	0.609211	0.132
3s to 4s	0.303289	0.609211	0.145
4s to 5s	0.303289	0.707237	0.198
5s to 6s	0.403289	0.707237	0.205

5.4.2 Case 2: Grid Connected Operation

In a grid connected mode, the VSG controller is operated in a power control mode, and DG units are required to supply power to the grid according to the power reference set in the controller.

In this case study, the two DG units have different rated capacities although the electrical system configuration remains the same as Fig. 5.2. The rated capacity of DG units 1 and 2 are 10 kVA and 5 kVA, respectively. The effectiveness of the adaptive virtual impedance based control mechanism to maintain accurate reactive power supply to grid is assessed considering both grid side load demand and PCC load variations. Since the two DG units have different rated capacities, they will not supply equal amount of power to the grid rather they are expected to supply power proportionally according to their rated capacity.

Initially, the active and reactive power references in the VSG controller are set to be 6 kW and 1.6 kVar, respectively, for DG1, and 3 kW and 800 Var, respectively, for DG2. Both DG units are supplying power to two local loads (5 kW and 1 kVar each) and one PCC load (2 kW and 400 Var).

In this case study, the grid side load demand and sudden PCC load variations occur in the microgrid, which are described as follows, while the two local loads remain the same:

1) At 4 s, the active power set point in the VSG controller is increased to 7 kW and 3.5 kW respectively, for DG units 1 and 2, in response to the increment in the grid side load demand. The reactive power set points are kept fixed at their previous values for both DG units;

2) At 5 s, a 1 kW and 200 Var PCC load is added at the PCC bus;

3) At 6 s, the active power set point in the VSG controller is increased to 8 kW and 4 kW, respectively, for DG units 1 and 2, in response to the increment in the grid side load demand. The reactive power set points are kept fixed at their previous values for both DG units; and

4) At 7 s, another 1 kW and 200 Var PCC load is added at the PCC bus.

At first, the microgrid is analyzed without employing a virtual impedance loop. The dynamic response of active and reactive power supplied by the two DG units during this event are shown in Fig. 5.7. It can be observed that the microgrid can supply active power appropriately to the grid, but the reactive power supply to the grid is not accurate. The reactive power supply of both DG units are found to vary with the variation of active power, and thus, they are not decoupled.

The dynamic response of the voltage and frequency at the PCC contains observable variations in this case as shown in Fig. 5.7, especially the frequency.

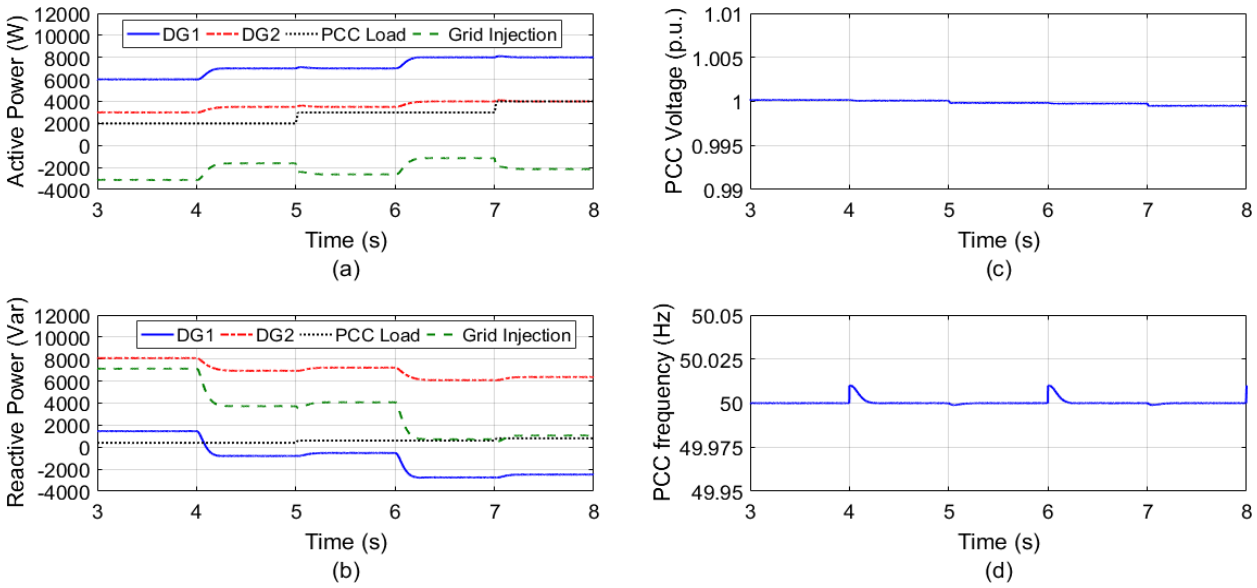

Figure 5. 7: Without a virtual impedance loop: (a) Active and (b) reactive power supplied by DG units, (c) voltage and (d) frequency at PCC (case 2)

To improve reactive power sharing and overall dynamic response of the microgrid, an adaptive virtual impedance loop is now employed, where the virtual resistance values are adjusted accordingly with the variation of DG output current and PCC load current. During a normal operating condition, when the active power supply to the grid varies, it is reflected by the variation of the DG output current; when the PCC load varies, it is reflected by the variation of the PCC load current. The virtual resistance value is adjusted accordingly based on the status of the DG output and PCC load currents.

If the adaptive virtual impedance is designed based on only one parameter, it can ensure good reactive power sharing performance under either the grid side load demand or PCC load variations but not both. To make the control mechanism work effectively under both scenarios, it is required to design the adaptive virtual impedance taking the following two parameters into account: 1) DG output current, and 2) PCC load current.

In the grid connected mode, appropriate values of virtual resistances are determined for different combinations of DG active power supply and PCC load demand levels to ensure accurately share reactive power supply to the grid for the two DG units. The designed values of virtual impedance are presented in Figs. 5.8 and 5.9 for both DG units, which are determined through simulation of the test microgrid under various operating points. The maximum allowable reactive power error is considered to be ±0.5% during the design process. Utilizing these data, the virtual resistance can be expressed as a function of both DG output currents and PCC load currents, and the adaptive virtual impedance loop can be implemented based on this derived function. Similarly, the function is obtained using the surface fitting toolbox in MATLAB for the grid connected mode. Polynomial 22 model is used to fit the surface to data. The functions developed in this case is also provided in Table 5.2, where *x* is the DG output current and *y* is the PCC load current.

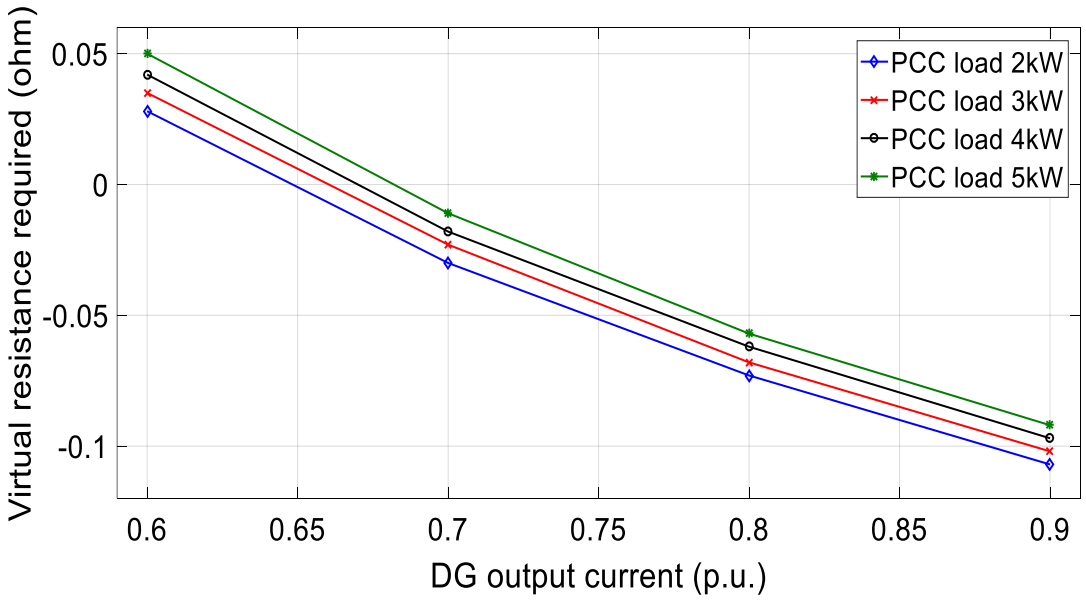

(a)

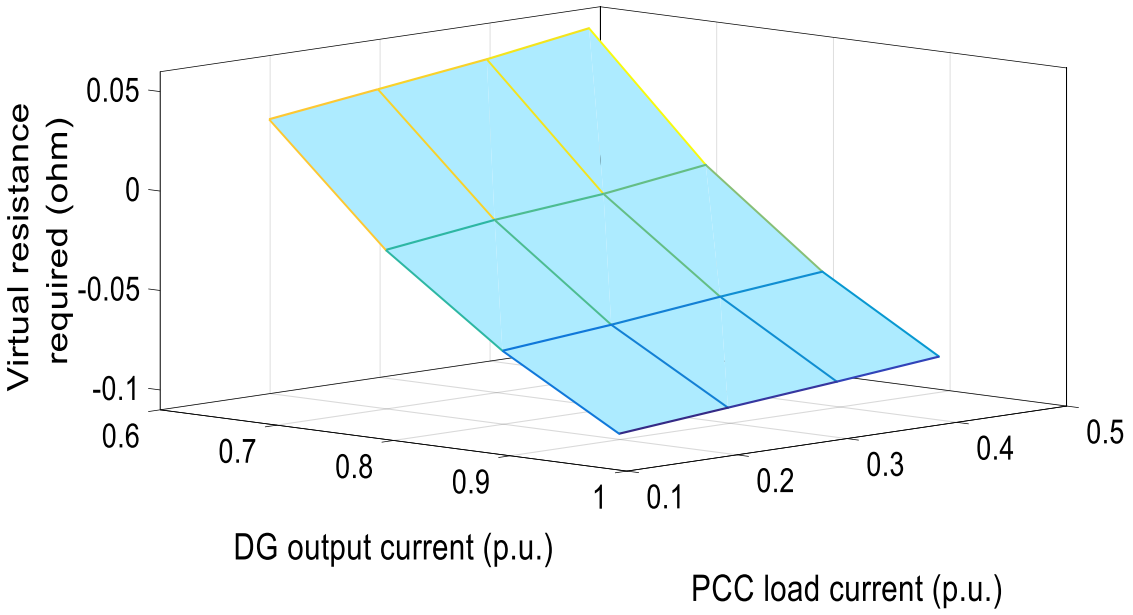

(b)

Figure 5. 8: Required values of virtual resistance for DG1 in a grid connected mode: (a) represented by lines; (b) represented by a surface.

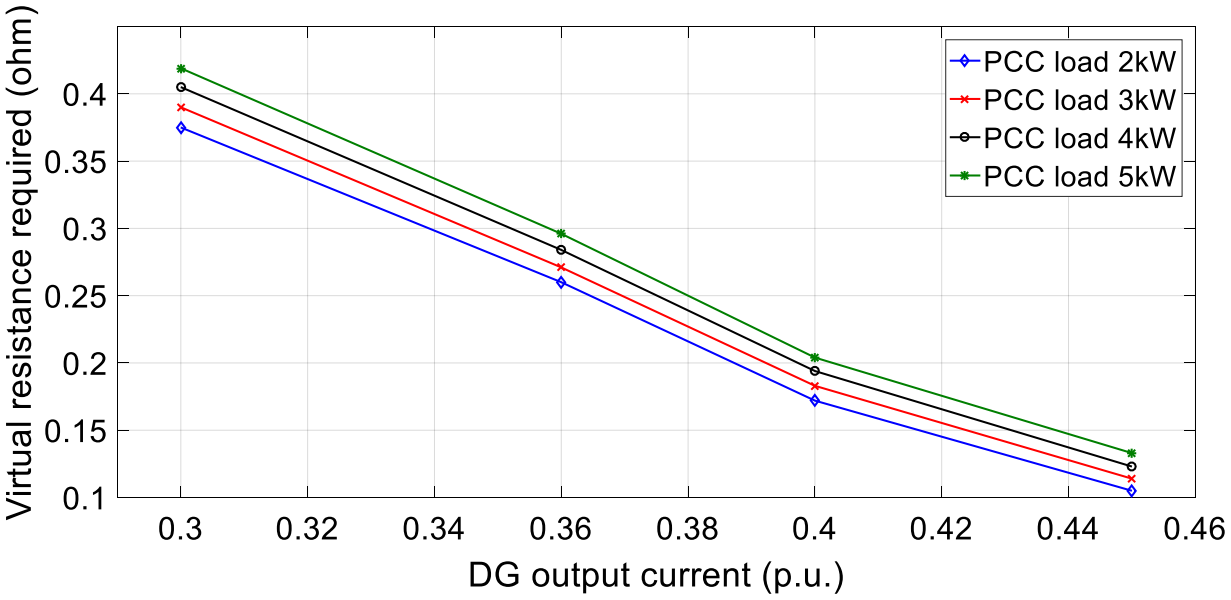

(a)

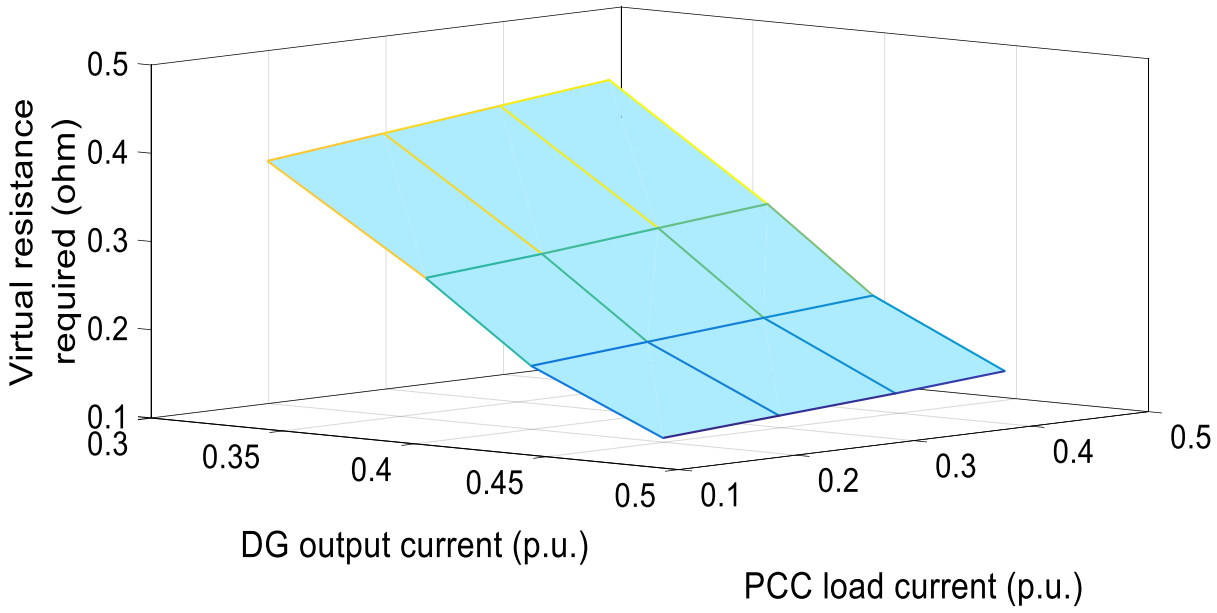

(b)

Figure 5. 9: Required values of virtual resistance for DG2 in a grid connected mode: (a) represented by lines; (b) represented by a surface.

With an adaptive virtual impedance loop being incorporated in the VSG control scheme, the dynamic response of active and reactive power supplied by DG units for the specific event is shown in Fig. 5.10. It is found that the reactive power supply to the grid becomes more accurate when appropriately designed adaptive virtual impedance loop is employed, and both DG units supply constant reactive power to the grid, according to the reactive power set point in the VSG controller under both grid side load demand and PCC load variations.

In a grid connected mode, when there is not enough generation available from DG units, loads connected to a microgrid are powered by the grid; when there is excessive generation available from DG units after meeting load demands in the microgrid, the remaining power is supplied to the grid. The required values of virtual resistance during different time spans for the specific event are listed in Table 5.4.

Table 5. 4: Virtual resistance values for case study 2

Time span	PCC load current (p.u.)	DG output current (p.u.)		Rv (Ω)	
		DG 1	DG 2	DG 1	DG 2
0s to 4s	0.20375	0.608553	0.305263	0.022	0.367
4s to 5s	0.20375	0.705263	0.355263	-0.035	0.253
5s to 6s	0.305592	0.705263	0.355263	-0.028	0.265
6s to 7s	0.305592	0.801316	0.403947	-0.071	0.178
7s to 8s	0.407434	0.801316	0.403947	-0.065	0.19

A slight deviation of the voltage at the PCC is observed when an adaptive virtual impedance loop is incorporated, however, the voltage still remains very close to its nominal value. The frequency at the PCC shows two little spikes corresponding to the two active power set point modifications. However, compared to the case without a virtual impedance loop as shown in Fig. 5.7, the frequency at the PCC returns to its nominal value much more quickly when a virtual impedance loop is incorporated.

Therefore, it can be concluded that proper reactive power sharing can be maintained by incorporating the proposed adaptive virtual impedance loop in the VSG control scheme for a grid connected mode.

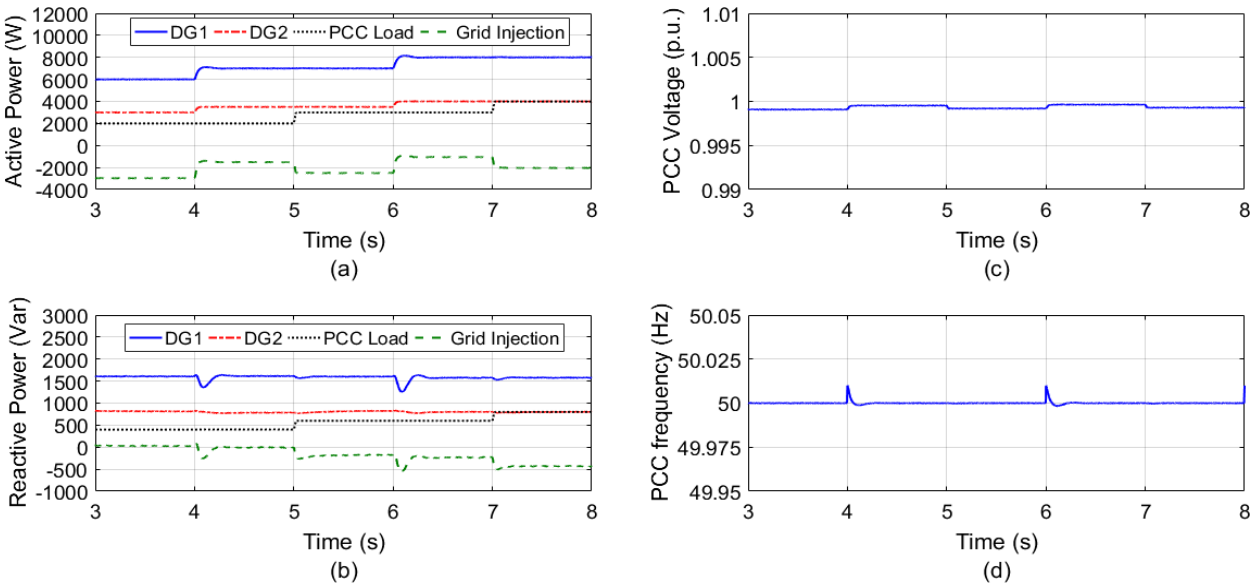

Figure 5. 10: With a virtual impedance loop: (a) Active and (b) reactive power supplied by DG units, (c) voltage and (d) frequency at PCC (case 2)

5.5 Sensitivity Studies

In this section, sensitivity studies are conducted to evaluate the influence of two factors on dynamic performance of the proposed approach: 1) the length of a transmission line, and 2) the value of virtual inductance.

5.5.1 Sensitivity Study 1: Length of Transmission Line

The same microgrid used in Case 2 are adopted in this sensitivity study. Three system configurations with three different lengths of the main transmission line between the PCC and the grid bus are considered: 100 m, 1 km and 5 km. The effect of the transmission line length on dynamic performance of the proposed approach is evaluated under the variation of active power supply by DG units to the grid. Note: this study is only valid for a grid connected mode for the microgrid.

Initially, the active and reactive power references in the VSG controller are set as 6 kW and 1 kVar, respectively, for DG1, and 3 kW and 500 Var, respectively, for DG2. For DG1, the active power set point is increased from 6 kW to 7 kW, 8 kW and 9 kW at 4 s, 6 s and 8 s, respectively, while the reactive power set point is kept fixed at 1 kVar. For DG2, the active power set point is increased from 3 kW to 3.5 kW, 4 kW and 4.5 kW at 4 s, 6 s and 8 s, respectively, while the reactive power set point is kept fixed at 0.5 kVar. In the real life, the active power set point should be adjusted in response to the variation in the grid side load demand. The microgrid is expected to supply power to the grid according to the power references set in the VSG controller.

The simulation results indicate that the length of the transmission line certainly has significant effect on dynamic characteristics of the microgrid using the proposed approach. The active and reactive power supplied by DG units with an adaptive virtual impedance loop are shown in Fig. 5.11.

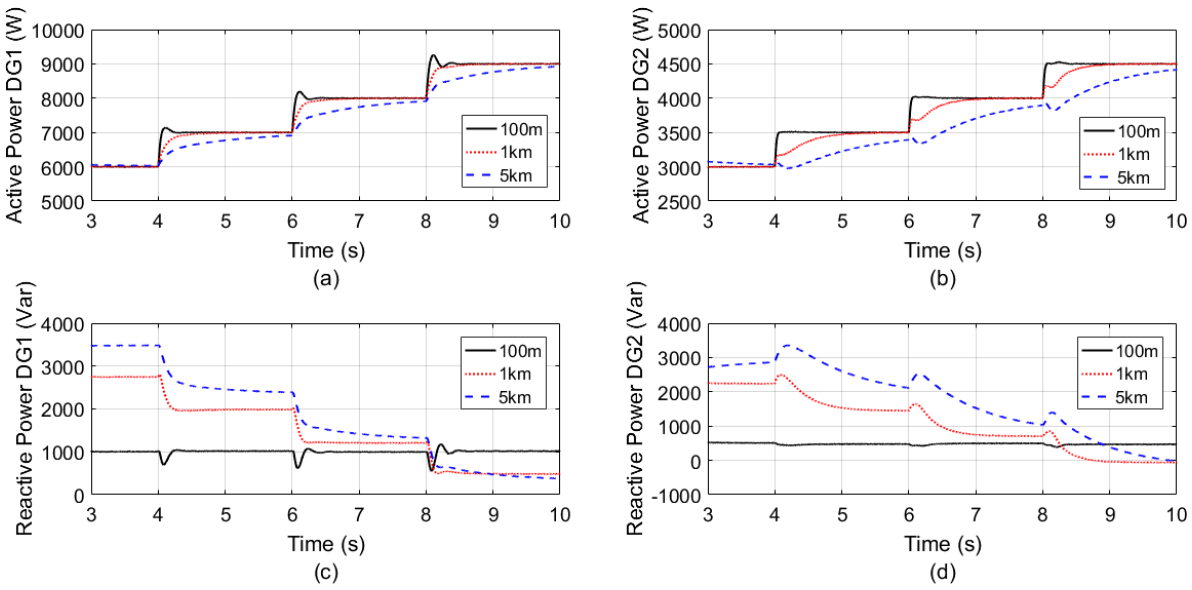

Figure 5. 11: (a) Active and (c) reactive power supplied by the DG unit 1, (b) Active and (d) reactive power supplied by the DG unit 2 (Sensitivity study 1)

It is evident that both DG units can adjust their active power supply accurately following the change in the active power set point in the VSG controller. However, if a longer line is used, it takes longer time for the active power supply to reach nominal values after each change. It is also observed that the active power of a smaller DG unit (DG2) is more impacted by the line length than that of a larger DG unit (DG1).

The adaptive virtual impedance loop is originally designed for a 100 m line length. It is found that the reactive power supply by DG units is maintained accurately under variation of active power supply when a 100 m line is used, but the same virtual impedance loop cannot ensure an acceptable performance when a different line length (i.e. 1 km, 5 km etc.) is used. The reason is that the transmission line impedance has effect on the overall system impedance, therefore, it is required to design virtual impedance values appropriately to ensure good reactive power sharing performance when a different line length is considered.

The dynamic response of the voltage and frequency at the PCC are shown in Fig. 5.12. If a shorter line is used, the voltage at the PCC remains closer to its nominal value; for a longer line the voltage does change at different operating points. It is found that a combination of a longer line and a larger active power set point lead to a higher PCC voltage. The frequency at the PCC shows a different fluctuation pattern compared to the voltage when the microgrid is subjected to operating point variations, and it takes a longer time for the frequency to return its nominal values for a longer transmission line.

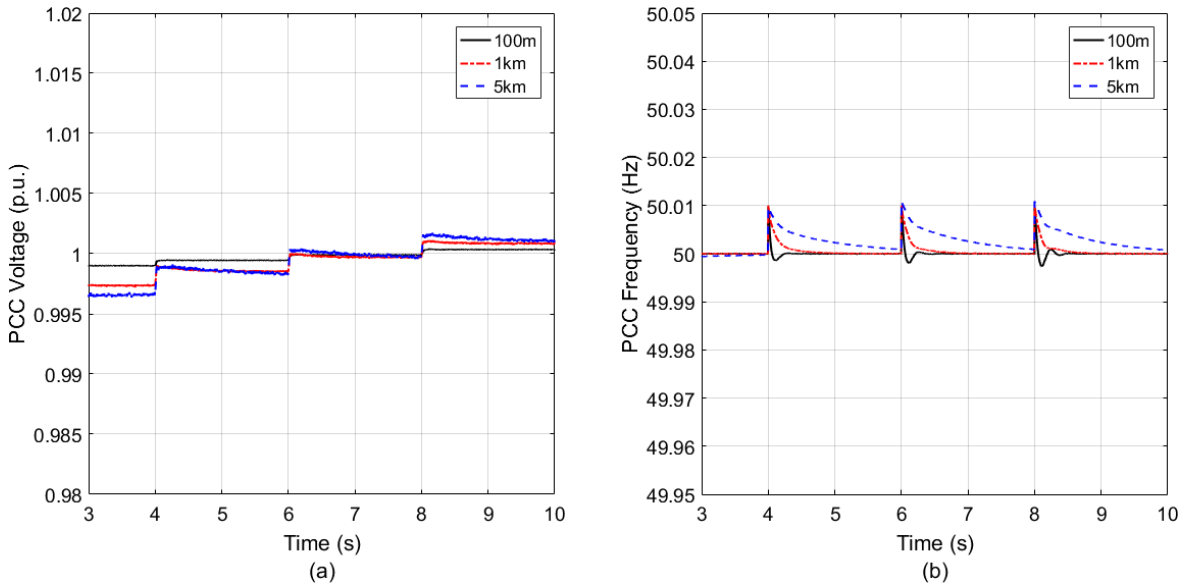

Figure 5. 12: (a) Voltage and (b) frequency at the PCC (Sensitivity study 1)

5.5.2 Sensitivity Study 2: Virtual Inductance Value

The inductance value (*Lv*) of a virtual impedance loop is an important parameter that can potentially affect dynamic performance of the proposed approach. In this study, the effect of *Lv* value is evaluated under the variation of PCC load in an islanded operation mode. The same microgrid and the specific event used in Case study 1 are adopted in this sensitivity study. Five different values of *Lv* are considered: L_{v1}= 0.01 mH, L_{v2} = 0.1 mH, L_{v3} = 1.2 mH, L_{v4} = 2 mH and L_{v5} = 5 mH. The virtual resistance value (*Rv*) is chosen adaptively from the 2-D lookup table based on the status of input parameters, as discussed before.

The dynamic response of active and reactive power supplied by the two DG units with an adaptive virtual impedance loop being incorporated in the VSG control scheme using various virtual inductance values are shown in Fig. 5.13.

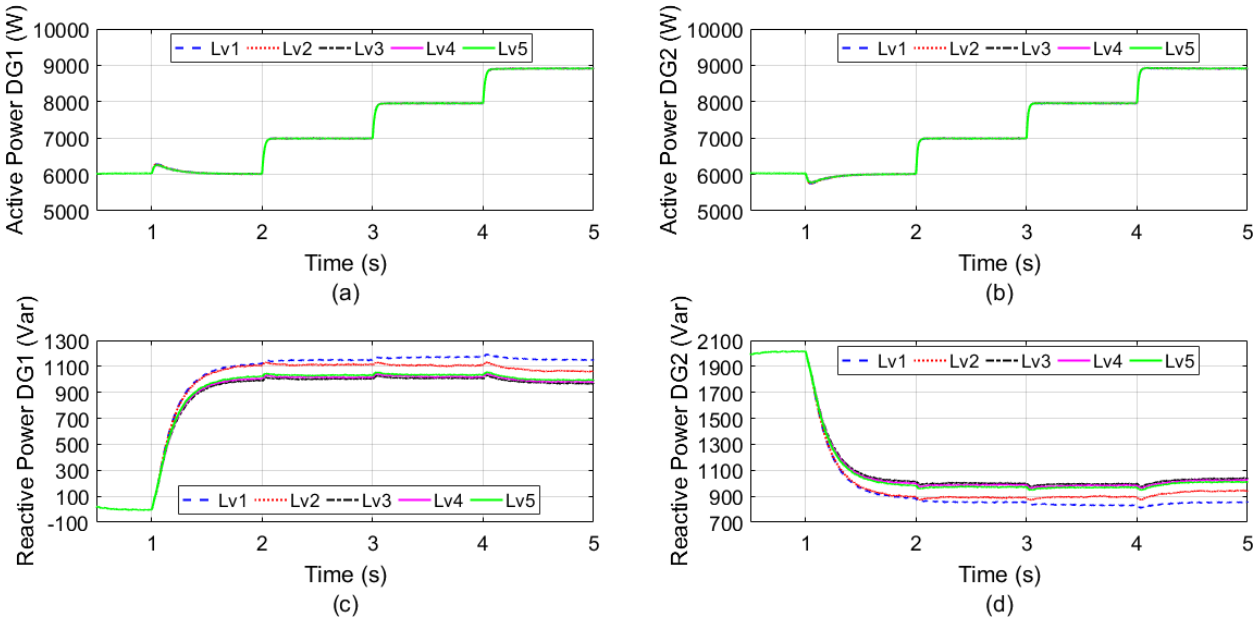

Figure 5. 13: (a) Active and (c) reactive power supplied by the DG unit 1, (b) Active and (d) reactive power supplied by the DG unit 2 (Sensitivity study 2)

It is found that for different values of *Lv* the active power is shared accurately between the two DG units when the load variation occurs. Therefore, *Lv* does not have significant influence on active power sharing performance. Both DG units share reactive power accurately (1 kVar equally) under the load variation when the virtual inductance value L_{v3} is chosen. For a lower values of *Lv*, such as L_{v1} and L_{v2}, reactive power sharing performance is deteriorated. Therefore, a sufficiently high value of *Lv* needs to be chosen, which is taken as 1.2 mH in this study. Any further increasing of the value of *Lv* does not offer significant improvement in the performance, rather it is observed that a very high value of *Lv* makes the system dynamic response slower. Significant effect of the *Lv* value on the voltage and frequency at the PCC cannot be observed based the study results.

6. Conclusion

In this paper, an adaptive virtual impedance method is proposed for reactive power sharing enhancement in a VSG controlled microgrid. A fuzzy secondary controller based VSG control

scheme developed by the authors previously is adopted as the base for implementation of the proposed virtual impedance approach. Several case and sensitivity studies are carried out to verify the effectiveness and robustness of the proposed approach.

Using the proposed adaptive virtual impedance method, 2-D look up tables are developed for both islanded and grid connected modes for a microgrid. Utilizing the 2-D lookup tables, virtual resistance values can be expressed as a function using a Polynomial 22 model. Sample virtual resistance values are determined and demonstrated for the case studies.

In the proposed approach, the virtual impedance consists of a virtual resistance and a virtual inductance. The virtual resistance is chosen to be variable while the virtual inductance is kept at a fixed value. In order ensure good reactive power sharing performance, a sufficiently large value of the virtual inductance must be chosen. Based on Sensitivity study 2, the minimum virtual inductance value of the test microgrid is recommended to be 1.2 mH.

It is found that the proposed approach can accurately regulate reactive power of DG units under operating point variations for microgrids. However, it is only functioning well for a fixed electrical system configuration of a microgrid. Further research is needed to establish a more generic method, through which the virtual impedance remains valid under alteration of a microgrid configuration.

References

[1] H. Xu, X. Zhang, F. Liu, R. Shi, C. Yu, and R. Cao, "A reactive power sharing strategy of VSG based on virtual capacitor algorithm," *IEEE Trans. Industrial Electronics*, 2017.

[2] H. Zhang, S. Kim, Q. Sun, and J. Zhou, "Distributed adaptive virtual impedance control for accurate reactive power sharing based on consensus control in microgrids," *IEEE Trans. Smart Grid*, vol. 8, no. 4, pp. 1749-1761, Jul 2017.

[3] A. Bouzid, P. Sicard, A. Yamane, and J. Paquin, "Simulation of droop control strategy for parallel inverters in autonomous AC microgrids," in *Proc. IEEE 8th Int. Conf. Modelling, Identification and Control*, 2016, pp. 701-706.

[4] N. Pogaku, M. Prodanovic, and T. C. Green, "Modeling, analysis and testing of autonomous operation of an inverter-based microgrid," *IEEE Trans. Power Electronics*, vol. 22, no. 2, pp. 613-625, Mar. 2007.

[5] C. Dou, Z. Zhang, D. Yue, and M. Song, "Improved droop control based on virtual impedance and virtual power source in low-voltage microgrid," *IET Generation, Transmission & Distribution*, vol.11, no. 4, pp. 1046-1054, 2017.

[6] Q. Zhong, "Robust droop controller for accurate proportional load sharing among inverters operated in parallel," *IEEE Trans. Industrial Electronics*, vol. 60, no. 4, pp. 1281-1290, Apr. 2013.

[7] J. He, Y. W. Li, and F. Blaabjerg, "An enhanced islanding microgrid reactive power, imbalance power, and harmonic power sharing scheme," *IEEE Trans. Power Electronics*, vol. 30, no. 6, pp. 3389-3401, Jun. 2015.

[8] J. Matas, M. Castilla, L. G. Vicuna, J. Miret, and J. C. Vasquez, "Virtual impedance loop for droop-controlled single-phase parallel inverters using a second-order general-integrator scheme," *IEEE Trans. Power Electronics,* vol. 25, no. 12, pp. 2993-3002, Dec 2010.

[9] U. Borup, F. Blaabjerg, and P. N. Enjeti, "Sharing of nonlinear load in parallel-connected three-phase converters," *IEEE Trans. Industry Applications,* vol. 37, no. 6, 1817-1823, Nov. 2001.

[10] X. Wu, C. Shen, and R. Iravani, "Feasible range and optimal value of the virtual impedance for droop-based control of microgrids," *IEEE Trans. Smart Grid,* vol. 8, no. 3, pp. 1242-1251, May 2017.

[11] Y. Zhu, F. Zhuo, F. Wang, B. Liu, R. Gou, and Y. Zhao, "A virtual impedance optimization method for reactive power sharing in networked microgrid," *IEEE Trans. Power Electronics,* vol. 31, no. 4, pp. 2890-2904, Apr 2016.

[12] Z. Liu, S. Ouyang, and W. Bao, "An improved droop control based on complex virtual impedance in medium voltage micro-grid," in *Proc. IEEE PES Asia-Pacific Power and Energy Engineering Conference,* 2013, pp. 1-6.

[13] M. C. Chandorkar, D. M. Divan, and R. Adapa, "Control of parallel connected inverters in standalone ac supply systems," *IEEE Trans. Industry Applications,* vol. 29, no. 1, pp. 136-143, Jan. 1993.

[14] Y. Sun, X. Hou, J. Yang, H. Han, M. Su, and J. M. Guerrero, "New Perspectives on Droop Control in AC Microgrid," *IEEE Trans. Industrial Electronics,* vol. 64, no. 7, pp. 5741-5745, Jul. 2017.

[15] J. M. Guerrero, L. G. Vicuna, J. Matas, M. Castilla, and J. Miret, "Output impedance design of parallel-connected UPS inverters with wireless load-sharing control," *IEEE Trans. Industrial Electronics,* vol. 52, no. 4, pp. 1126-1135, Aug 2005.

[16] J. M. Guerrero, J. Matas, L. G. Vicuna, M. Castilla, and J. Miret, "Decentralized control for parallel operation of distributed generation inverters using resistive output impedance," *IEEE Trans. Industrial Electronics,* vol. 54, no. 2 pp. 994-1004, Apr 2007.

[17] J. He, Y. W. Li, J. M. Guerrero, F. Blaabjerg, and J. C. Vasquez, "An islanding microgrid power sharing approach using enhanced virtual impedance control scheme," *IEEE Trans. Power Electronics,* vol. 28, no. 11, pp. 5272-5282, Nov 2013.

[18] C. Sao and P. W. Lehn, "Autonomous load sharing of voltage source converters," *IEEE Trans. Power Delivery,* vol. 20, no. 2, pp. 1009-1016, Apr 2005.

[19] H. Mahmood, D. Michaelson, and J. Jiang, "Accurate reactive power sharing in an islanded microgrid using adaptive virtual impedances," *IEEE Trans. Power Electronics,* vol. 30, no. 3, pp. 1605-1617, Mar 2015.

[20] C. Andalib-Bin-Karim, X. Liang, and H. Zhang, "Fuzzy Secondary Controller Based Virtual Synchronous Generator Control Scheme for Microgrids", in *Proc IEEE Industry Applications Society Annual Meeting*, 2017, pp. 1-14.

[21] H. P. Beck and R. Hesse, "Virtual synchronous machine," in *Proc. 9th Int. Conf. Electrical Power Quality and Utilisation*, 2007, pp. 1-6.

[22] S. D'Arco and J. A. Suul, "Equivalence of virtual synchronous machines and frequency-droops for converter-based microgrids," *IEEE Trans. Smart Grid,* vol. 5, no. 1, pp. 394-395, Jan. 2014.

[23] X. Liang, "Emerging power quality challenges due to integration of renewable energy sources," *IEEE Trans. Industry Applications,* vol. 53, no. 2, pp. 855-866, Mar. 2017.

[24] X. Liang and C. Andalib-Bin-Karim, "Virtual synchronous machine method in renewable energy integration," in *Proc. IEEE PES Asia-Pacific Power and Energy Engineering Conference, 2016*, pp. 364-368.

[25] Y. Chen, R. Hesse, D. Turschner, and H. P. Beck, "Dynamic properties of the virtual synchronous machine (VISMA)," in *Proc. Int. Conf. Renewable Energies and Power Quality*, 2011, pp. 1-6.

[26] H. Zhao, Q. Yang and H. Zeng, "Multi-loop virtual synchronous generator control of inverter-based DGs under microgrid dynamics," *IET Generation, Transmission & Distribution*, vol. 11, no. 3, pp. 795-803, 2017.

[27] Y. Chen, R. Hesse, D. Turschner, and H. P. Beck, "Improving the grid power quality using virtual synchronous machines," in *Proc. IEEE Int. Conf. Power engineering, energy and electrical drives*, 2011, pp. 1-6.

[28] Q. C. Zhong and G. Weiss, "Synchronverters: Inverters that mimic synchronous generators," *IEEE Trans. Industrial Electronics*, vol. 58, no. 4, pp. 1259–1267, April 2011.

[29] J. Alipoor, Y. Miura and T. Ise, "Power system stabilization using virtual synchronous generator with alternating moment of inertia," *IEEE Journal of Emerging and Selected Topics in Power Electronics*, vol. 3, no. 2, pp. 451-458, June 2015.

[30] Y. W. Li and C. Kao, "An accurate power control strategy for power-electronics-interfaced distributed generation units operating in a low-voltage multibus microgrid," *IEEE Trans. Power Electronics*, vol. 24, no. 12, pp. 2977-2988, Dec. 2009.

Chapter 6

Conclusion

This chapter consists of a summary of main contributions of this thesis, followed by an outlook on future work.

6.1 Summary

The main objective of this thesis is to develop advanced inverter control mechanisms for power quality improvement in microgrids. Several control techniques are proposed in this thesis and verified to be effective for microgrids: 1) voltage and frequency regulation, 2) active and reactive power control.

In Chapter 1, the importance of microgrids and renewable energy based DGs in modern power systems is explained. Different power quality challenges experienced by microgrids are briefly explored and importance of maintaining good power quality in microgrid is also outlined. Different devices and techniques conventionally used for power quality improvement are reviewed. It is identified that inverter control mechanism is the most efficient, reliable and cost effective way of satisfying power quality requirements in microgrids.

In Chapter 2, an advanced inverter control mechanism, VSG control, is introduced, which is considered to be a promising approach for inverter control in microgrids. Recent literatures are reviewed to gain a comprehensive knowledge about this control mechanism and its possible application in renewable energy source integration to power grids. The review of existing techniques is essential before making further effort for its improvement. Moreover, some state of

the art control mechanisms for harmonic mitigation in renewable energy system are also reviewed which will facilitate researchers to develop more advanced control methods in the future.

In Chapter 3, a data driven analytics approach is proposed for determination of Q-V curve in grid connected wind firms. The physical model of complex systems like wind firms is difficult to obtain, the data driven analytics is an effective approach to determine characteristics of such a system because it works solely based on measurement data. The determination of Q-V curve is essential because it can provide valuable indication on voltage stability of the system and offer useful information for voltage controllers design. The proposed approach is applied for two grid connected wind firms currently in operation at Newfoundland and Labrador, Canada as case studies. The *Gaussian* 2 model is determined as the best fitted model for both wind firms. A step by step approach is presented for determination of the best fitted model, similar approach can be used to determine Q-V curve of any grid connected wind farm. The work undertaken in this chapter can extensively facilitate voltage control actions in grid integrated wind farms.

In Chapter 4, a fuzzy secondary controller (FSC) is incorporated in VSG control scheme to improve voltage and frequency regulation and dynamic performance of microgrids under various disturbance conditions. The applicability of FSG in VSG controlled microgrid is analyzed for the first time in this work. One important advantage of FSC over conventional secondary control is that, it does not require to switch on an additional tertiary layer when a microgrid is subjected to a mode change. The proposed FSC based VSG control scheme is found to work effectively under both islanded and grid connected modes. The proposed FSC can operate based on less number of rules compared to existing methods in previous literatures, which makes it less complicated and enables it to operate faster. Critical parameters of FSC are identified, and systematic approaches for determination of those parameters are also outlined. The dynamic models of test system

incorporating the proposed control scheme is developed in MATLAB/Simulink, which will be useful for researchers to develop similar models and conduct further studies. A comparison study between conventional droop and conventional VSG in terms of their power quality improvement features under various disturbance conditions is also presented in this chapter, which has not been found in any previous literatures. These comparisons can facilitate better understanding of control approaches under study and can be identified as an important contribution of this work.

In Chapter 5, the incorporation of an adaptive virtual impedance loop in the fuzzy secondary controller based VSG control scheme is proposed to ensure accurate reactive power sharing in a microgrid. In a practical microgrid, feeder impedance mismatch and difference in rated capacity among DG units is a very common phenomenon which leads to inaccuracy in reactive power sharing. It is recognized that the virtual impedance method is a promising approach to solve this problem, however significant research efforts has not been found in previous literatures to offer effective ways to adaptively determine virtual impedance values under variation of operating points of a microgrid. In this work, an effort has been made to eliminate this research gap by proposing a new implementation approach of adaptive virtual impedance loop which is simple, easy to implement and does not require many measurements from external sources. The proposed approach has been verified applying on a test microgrid system. A two dimensional (2-D) function for the test microgrid system is developed based on which the virtual resistance value is adaptively tuned under the variation of operating points of a microgrid, and the designed values of virtual resistances under various operating points are also presented. A systematic approach of determining the 2-D function is discussed, same approach can be followed for designing an adaptive virtual impedance loop for any microgrids.

6.2 Future Works

- The Q-V curves determined in this thesis are based on measurement data of only one month. A whole year data can be analyzed in future to see if the proposed model remains valid, seasonal variations of Q-V characteristics can also be studied.
- Secondary control mechanisms based on other intelligent techniques can be developed to improve voltage and frequency regulation performance in microgrids.
- The adaptive virtual impedance method proposed in this thesis is system specific, an optimization algorithm based on behaviors of microgrids with different configurations can be developed and incorporated to make the proposed approach more generic and enable it to work effectively under any system configuration of a microgrid.
- Since it was not possible to validate the developed models experimentally, experimental set up can be done in future. Experimental results can explain the reliability of these models more clearly.